UCLA
UCLA Electronic Theses and Dissertations

Title
Factors Controlling Summertime Surface Ozone In The Western U.S.

Permalink
https://escholarship.org/uc/item/6m16n5vm

Author
Gao, Mei

Publication Date
2015

Peer reviewed|Thesis/dissertation

eScholarship.org Powered by the California Digital Library
University of California

University of California
Los Angeles

Factors Controlling Summertime Surface Ozone In The Western U.S.

A dissertation submitted in partial satisfaction
of the requirements for the degree
Doctor of Philosophy in Atmospheric and Oceanic Science

by

Mei Gao

2015

© Copyright by
Mei Gao
2015

Abstract of the Dissertation

Factors Controlling Summertime Surface Ozone In The Western U.S.

by

Mei Gao

Doctor of Philosophy in Atmospheric and Oceanic Science

University of California, Los Angeles, 2015

Professor Qinbin Li, Chair

In this dissertation we investigate different factors controlling summertime surface ozone (O_3) in the western U.S., including the impacts from increased wildfire emissions, the modulation by North American summer monsoon as well as long-range transport of O_3 and its precursors from outside of North America.

We first analyze the surface ozone observations from the Clean Air Status and Trend Network (CASTNet) using a global chemical transport model (GEOS-Chem) to investigate the impact of biomass burning on surface O_3 in the western U.S. (WUS) mountain ranges during the June-October fire season of 2007, one of the stronger fire years in the WUS in the past decade. GEOS-Chem O_3 captures the observed seasonal, synoptic and daily variations. Model daily afternoon average surface O_3 concentrations at the CASTNet sites are within 2 ppb of the observations, with correlation coefficients of 0.51-0.83 and Taylor scores of 0.64-0.92. Observed maximum daily 8-hour (MAD8) surface O_3 concentrations are 37-58 ppb at the sites, while the corresponding model results are higher by 6 ppb on average. Model results show July-September maximum surface O_3 enhancement of $\sim$9 ppb on average because of biomass burning. Peaks in fire-contributed surface O_3 correspond broadly with high levels of potassium (K), reaffirming a strong fire influence. We find a policy relevant background (PRB) O_3 of 45.6 ppb on average during July-September. Fire-contributed O_3

accounts for up to 30 % of the PRB O_3, highest in the intense fire region (Montana, Idaho, and Wyoming) with maxima in August and September.

We also examine an unexpected summertime surface O_3 minimum ($\sim$ 30-45 ppb) in July-August observed throughout the Southwestern U.S. (SWUS) by interpreting observations of O_3 and rainfall from the Clean Air Status and Trends Network (CASTNet) for 2000-11 with a global chemical transport model. The O_3 minimum reflects competing chemical and dynamic factors as well as anthropogenic and natural influences. Its occurrence corresponds to the interannual rainfall maximum in North American summer monsoon (NASM) -negative surface O_3 anomalies are accompanied by positive rainfall anomalies at the CASTNet sites (r = -0.5 to -0.7, p <0.05). Relative to June 15-July 15, 2007 (prior to the monsoon onset in the SWUS), increased cloudiness during the maximum rainfall in July 15-August 15 (after the onset) weakens photochemistry, reduces O_3 production from anthropogenic emissions, thereby depresses O_3 at the surface (-5 ppb at Chiricahua, AZ and -3 ppb on average across the SWUS) and throughout the lower troposphere. Largest relative changes (ΔO_3) are seen at rainfall maxima, particularly in the core of the Great Plains low-level jet. The corresponding enhancement in lightning (hence NO_x emissions) augments O_3 production in the middle troposphere and subsequent downward mixing in convective downdrafts, thus increases surface O_3 non-negligibly (+2 ppb at Chiricahua and +1 ppb averaged over the SWUS) and significantly throughout the tropospheric column. The resulting ΔO_3 is largest (+8 ppb) in the anti-cyclonic circulation associated with the upper-level high. Weaker photochemistry dominates the overall ΔO_3 near the surface, while enhanced lightning dominates in much of the free troposphere. Additionally, we find that transport leads to a net export of O_3 throughout the tropospheric column and the influence from stratospheric intrusion is vanishingly small. These competing effects suppress O_3 in the lower troposphere (ΔO_3 up to -5 ppb) while enhance O_3 at higher altitudes (ΔO_3 up to +7 ppb) across the SWUS during the monsoon.

Lastly we use the GEOS-Chem 3-D global tropospheric chemical transport model and

its adjoint to quantify the source contributions to O_3 pollution observed at Mt. bachelor Observatory (MBO) during the summer of 2008. The adjoint computes the sensitivity of O_3 concentration at the receptor site to O_3 production rates at $2^\circ \times 2.5^\circ$ resolution over the history of air parcels reaching the site. We found that MBO experienced distinct O_3 pollution episodes from Siberia wildfire emissions. During the O_3 pollution episode from June 30th to July 4th in year 2008, 7.5 ppb of MBO O_3 is produced over Siberia, comparable to the amount of O_3 (8 ppb) produced over North America. A significant amount of O_3 (18 ppb) production took place over the North pacific, with maxima just off the west coast of the U.S. where subsidence of air masses causes decomposition of PAN (peroxyacetylnitrate, a thermo-unstable NO_x reservoir species) and drives further ozone production. We also used the adjoint of GEOS-Chem to show the model O_3 at MBO is largely sensitive to NO_x emissions from biomass burning sources in Siberia and northern California, lightning sources over southwestern U.S. and Mexico, and anthropogenic sources in western U.S. and eastern Asia. For the CO emissions, the largest O_3 sensitivity is to the biomass burning sources in northern California and Siberia. The peak sensitivity to biomass burning CO emissions is comparable to the peak O_3 sensitivity to anthropogenic NO_x emissions.

The dissertation of Mei Gao is approved.

Stanley Sander

Jochen Stutz

Kuo-Nan Liou

Qinbin Li, Committee Chair

University of California, Los Angeles

2015

To my parents . . .

who have been with me every step of the way

through good times and bad

Table of Contents

List of Figures

List of Tables

Acknowledgments

My deepest gratitude goes to my advisor, Professor Qinbin Li, for his guidance, enormous help and patience in my research life. I can not thank him enough for his tremendous support along the way. He has taught me how to become an independent researcher, how to conduct critical thinking and how to overcome obstacles both in research and in life.

I also want to express my sincere thanks to my committee members, Professor Kuo-Nan Liou, Professor Jochen P. Stutz, and Professor Stanley Sander, for sharing with me their expertise and insights and provided me with constructive comments and help at every stage of my research.

I would also like to thank all my coauthors for their creative suggestions. Special thanks to Professor Lin Zhang for all the stimulating discussions. I would like to extend my appreciation to my fellow group members, Dr. Yuhao Mao, Dr. Li Zhang, Dr. Dan Chen, Dr. Bin Zhao, Ling Qi, Cenlin He, Rose Tseng for all the helpful discussions, and to my fellow colleagues, Ross Cheung, Catalina Tsai, Yue Chao, Wu Sun for all the help. I want to thank them for their company for the past a few years and for sharing all my happiness and sorrows.

Lastly I want to give my special thanks to my parents, who have been with me every step of the way, through good times and bad . I would not be here without their endless love, wholehearted support, and all the sacrifice they had made for me.

Vita

2006–2010	B.S. ∼(Mathematics) and B.A. ∼(Economics) , Peking University, Beijing, China.
2010–2012	M.S.∼(Atmospheric and Oceanic Science), UCLA.
2013–2015	M.S.∼(Statistics), UCLA.

CHAPTER 1

Overview

Ozone (O_3) is produced in the troposphere by oxidation of hydrocarbons and CO catalyzed by hydrogen oxide radicals ($HO_x \equiv OH + H +$ peroxy radicals) and nitrogen oxide radicals ($NO_x \equiv NO+NO_2$). In populated regions with large emissions of NO_x and hydrocarbons, high surface concentrations of O_3 are a major air pollution problem. Tropospheric O_3 is also of global interest as the primary source of OH, the main atmospheric oxidant, and as an effective greenhouse gas (*Change*, 2007). A fraction of tropospheric O_3 comes from the stratosphere. The major O_3 precursors, including NO_x, CO and VOCs, come from both anthropogenic sources, i.e. fuel combustion, and natural sources such as lightning, biomass burning and the biosphere.

O_3 itself is an air pollutant that is associated with a variety of adverse impacts on human health, including a decrease in lung function and exacerbation of respiratory illness (*Mickley*, 2007). Therefore, elevated concentrations of O_3 can have negative impacts on human health. Primary and secondary National Ambient Air Quality Standards (NAAQS) for O_3 have been established to protect public health and public welfare (*McDonald-Buller et al.*, 2011). The Environmental Protection Agency (EPA) established primary and secondary O_3 in March 2008: annual 4th highest daily maximum 8-hour average (MDA8) concentration not to exceed 75 ppb. There are currently 227 counties, home to 123 million people, classified as not having attained the 75 ppb standard (`www.epa.gov/airquality/greenbook/index.html`). In 2015, a new standard proposed by the EPA was issued, further lowering it from 75 to 70 ppb. As the O_3 standard becomes increasingly stringent, to accurately determine the background O_3 levels becomes more imperative. Background O_3 concentrations used to

inform decisions about setting the NAAQS are referred to as Policy Relevant Background (PRB) O_3 concentrations. The U.S. EPA defines PRB O_3 concentrations as those that would occur in the U.S. in the absence of anthropogenic emissions in continental North America (*EPA*, 2006). The PRB O_3 represents the O_3 concentration that is not amenable to reduction under current policy frameworks and provides a baseline for assessing risk from exposure to O_3 pollution. It is important for regulatory decisions as it sets the maximum O_3 reduction and relative health benefits that can be achieved through North American emission controls. Processes that contribute to PRB O_3 include photochemistry associated with biogenic emissions, wildfires, lightning, the long-range transport of O_3 and its precursors from outside of North America, and stratospheric-tropospheric exchange (STE) (*EPA*, 2006). From both scientific and regulatory points of view, a lower O_3 standard will motivate air quality-control planners to see more accurate and precise attribution of the background O_3 to determine how much domestic emissions must be reduced in order to attain that standard (*Cooper et al.*, 2014).

While summertime surface O_3 levels have been decreasing throughout the U.S., the western U.S. (WUS) has seen an upward trend in the past two decades (*Cooper et al.*, 2014, 2012). The U.S. Environmental Protection Agency (EPA) reported a decrease of 15% in emissions of NO_x and 40% in emissions of non-methane hydrocarbons (NMHCs) in the U.S. between 1983 and 2002 (*EPA*, 2003). Changes in these factors strongly influence the O_3 concentrations in the atmosphere. In most urban areas in the U.S., there have been reductions in peak O_3 concentrations, because of decreasing emissions of NO_x and NMHCs (*Lin et al.*, 2001; *EPA*, 2003, 2004). However, non-urban surface O_3 in the WUS has seen a significant increase over the past two decades. Jaffe et al. (*Jaffe and Ray*, 2007), for example, evaluated surface O_3 data for 1987-2004 from several sites in the WUS. They found that at seven out of the nine sites examined, there is a statistically significant increase in O_3, with a mean trend of 0.26 ppb per year. This corresponds to an increase of approximately 5 ppb over the 18 years of observations. Several hypotheses were put forward to explain this trend,

including changing global background O_3 concentrations, changing climate and increasing emissions associated with fires (*Jaffe and Ray*, 2007; *Cooper et al.*, 2012). Our focus here is the increasing trend in wild fire activities in the region. The hot, dry summer of the WUS make the region susceptible to large forest fires. Wildfire emissions can become important source of O_3 precursors. Fires in the WUS have increased in both frequency and duration in the WUS in recent decade (*Westerling et al.*, 2006; *Spracklen et al.*, 2009, 2007; *Jaffe et al.*, 2008) due to several factors related to climate change: increased spring and summer temperatures, earlier spring snowmelt, and dryer conditions. The modeling study by (*Spracklen et al.*, 2009) showed that the annual mean area burned in the WUS could increase by 54% by the 2050s relative to the present under future warming. An analysis of more than 20 years of fire and air quality data has shown clear positive correlations of O_3 levels with total area burned and biomass consumed by fires in the WUS (*Jaffe et al.*, 2008). It is conceivable that fires will be an even larger contributor to surface O_3 in the WUS for years to come.

In Chapter 2 we investigate the impact of biomass burning on the surface O_3 in the WUS and quantify its contribution to PRB O_3. Our approach is to apply a global three-dimensional (3-D) chemical transport model (CTM) GEOS-Chem to analyze surface O_3 observations over the WUS. We conduct model simulations for 2006 and 2007, two of the stronger fire years during the past decade (*Giglio et al.*, 2006). We calculated an average of $\sim$9 ppb in the maximum surface O_3 enhancement that was attributed to biomass burning emissions during July-September 2007; the corresponding value was $\sim$4 ppb for 2006, reflecting the less intense burning in that year. The enhancements varied considerably across individual Clean Air Status and Trends Network (CASTNet) sites. The maximum surface O_3 enhancements were largest ($\sim$30 ppb) at Glacier, MT, in the middle of the intense fire region. Peaks in fire-contributed surface O_3 correlated strongly with high concentrations of potassium (K), a tracer for biomass burning, at the CASTNet sites, supporting a strong fire influence at the sites. The observed and model simulated maximum daily 8-hour (MAD8) O_3 in the remote WUS are in the range of 37.4-58.2 and 42.0-66.2. Our results show that the model simulated

PRB O_3 is 45.6 ppb on average for July-September 2007. Fire-contributed O_3 accounts for up to 30% of the PRB O_3, highest in Montana, Idaho and Wyoming during August and September.

In the WUS, a region of particular interest is the southwestern U.S. (SWUS). Many counties in the SWUS are often close to violating the national O_3 air quality standards (*Wise and Comrie*, 2005; *EPA*, 2008). PRB O_3 is especially high over the intermountain SWUS regions due to the arid terrain, high elevations, and large-scale subsidence in the region citepzhang2011improved. PRB O_3 in the SWUS is impacted by many factors including biomass burning (*Jaffe et al.*, 2008; *Jaffe*, 2010), lightning (*Zhang et al.*, 2014) and trans-Pacific transport of Asian pollution (*Parrish et al.*, 2009; *Cooper et al.*, 2010). Meteorological conditions also have large impacts on the variations of surface O_3 air quality in this region [Wise and Comrie, 2005, and references therein]. Increasing baseline O_3 from trans-Pacific emissions, more frequent wildfire activities during summer fire season, and deep stratospheric intrusions during spring are factors that may prevent the SWUS region from attaining the new EPA O_3 standard (*Cooper et al.*, 2012; *Lin et al.*, 2015)

A defining meteorological event in the SWUS is the recurring North American summer monsoon (NASM). NASM brings 50% of the annual rainfall in New Mexico and Arizona, two states in the SWUS where the monsoonal precipitation is most pronounced in the form of thunderstorms during July-September (*Carleton et al.*, 1990; *Sheppard et al.*, 1999; *Harrington Jr et al.*, 1992). Thunderstorms produced from the monsoon moisture often extend into the Mojave Desert to the west and the lower Colorado River valley to the north (*Adams and Comrie*, 1997). More broadly, the monsoon influence spans an expanded region from the Sierra Nevada in the west to the Wyoming Rockies and Colorado in the east and reaches as far north as Oregon, the Idaho-Utah border, and Wyoming (*Tang and Reiter*, 1984). The influence of future climate change on both timing and strength of the NASM activities will also conceivably lead to significant impacts on the seasonal and interannual variations of background O_3.

In Chapter 3 we seek to probe the impacts of the NASM on the surface and tropospheric O_3 in the SWUS mountain ranges. Previous studies have analyzed the influence of monsoon on surface O_3 air quality and meteorological conditions at urban sites (*Wise and Comrie*, 2005; *Agel et al.*, 2011) or in other regions (*Yang et al.*, 2014). To our knowledge, no previous studies have systematically examined such impacts. We focus here on regional to continental scales. We examine an unexpected summertime surface O_3 minimum (∼30-45 ppb) in July-August observed throughout the SWUS by interpreting observations of O_3 and rainfall from CASTNet for 2000-11 with GEOS-Chem. The O_3 minimum reflects competing chemical and dynamic factors as well as anthropogenic and natural influences associated with the NASM. We also investigated the O_3 change during NASM associated with each of these factors both at surface and across the troposphere.

Long-range transport of air pollution is becoming another major issue as counties at northern mid-latitude strive to meet increasingly stringent air quality standards. Elevated air pollutants levels have been observed in the U.S due to long range transport of Canadian forest fire emission (*Wotawa and Trainer*, 2000), Siberian biomass burning emission (*Jaffe et al.*, 2004; *Oltmans et al.*, 2010) and Asian emission (*Zhang et al.*, 2009). A number of studies have investigated the impact of transpacific pollution on surface O_3 in the WUS. O_3 has a lifetime of days in the boundary layer but weeks in the free troposphere (*Wang et al.*, 1998), enabling transport on the intercontinental scale. Eurasian pollution is typically exported to the Pacific by front lifting in warm conveyor belts (WCBs), convection, and orographic lifting (*Liu et al.*, 2003; *Brock et al.*, 2004; *Liang et al.*, 2004; *Dickerson et al.*, 2007). The transport is most rapid and frequent in spring due to active cyclonic activity and strong westerly winds (*Forster et al.*, 2004; *Liang et al.*, 2004). *Jaffe et al.* (2004) found that the fires in Siberia, 2003 resulted in enhancements in summer background O_3 of 5-9 ppbv at sites in Alaska, Canada and the Pacific Northwest. Zhang et al., 2008 used an ensemble of aircraft, satellite, sonde, and surface observations during the INTEX-B campaign (April-May 2006) to quantify the transpacific transport of Asian pollution. They concluded that Asian

anthropogenic emission increased surface O_3 concentrations by 5-7 ppb in WUS during the INTEX-B period.

Most of the previous studies on the influence of long range transport on surface O_3 have run sensitivity simulations with perturbed emissions using a chemical transport model (*Jacob et al.*, 1999; *Yienger et al.*, 2000; *Wild and Akimoto*, 2001; *Derwent et al.*, 2008; *Duncan et al.*, 2008; *Fiore et al.*, 2009). This source-oriented method is computationally limited in the spatial resolution of the source region that they can achieve. The adjoint method is a much more computationally efficient approach for the receptor-oriented problem, for example, to calculate the source attribution of O_3 concentration at a given site. A single run of the adjoint model can compute the sensitivity of ozone concentrations at a given location and time (or an average over a spatial domain and time interval) to the global distribution of sources over the spatial and temporal resolution of the model (*Zhang et al.*, 2009). The adjoint method has been applied in previous studies to investigate long range transport of aerosol to the U.S. (*Henze et al.*, 2009), pollutant transport to Hawaii island (*Vukićević and Hess*, 2000; *Hess and Vukicevic*, 2003) as well as regional sensitivity analyses for O_3 pollution episodes (*Elbern and Schmidt*, 2001; *Hakami et al.*, 2006; *Nester and Panitz*, 2006).

In Chapter 4, we used the adjoint model of GEOS-Chem to quantify the impacts of the long-range transport of the Siberian wildfire emissions during the summer of 2008 on surface O_3 on the U.S. west coast. We interpreted model results with the observation at site MBO (Mt. Bachelor Observatory, Oregon). It's a standard reference site for background air entering the United States (*Goldstein et al.*, 2004; *Jaffe et al.*, 2005; *Oltmans et al.*, 2008). It's particularly sensitive to long range influences due to its exposure to the free troposphere (*Jaffe et al.*, 2005; *Weiss-Penzias et al.*, 2006; *Wolfe et al.*, 2007). We have shown that an adjoint model analysis can provide detailed geographical and temporal information on intercontinental pollution influences at specific receptor sites. Such information can be used to better determine the sources of this intercontinental pollution, down to the scale of individual source countries and urban areas. We also used the GEOS-Chem adjoint model

to calculate the sensitivity of O_3 concentration at a receptor site to emission estimates of O_3 precursors (NO_x, CO) from different sources (anthropogenic, biomass burning, lightning, soil, aircraft). For policy purposes it will be important to attribute the long range transport of O_3 pollution to the actual emissions of O_3 precursors, taking advantage of the fine resolution enabled by the adjoint model. This requires us to resolve the non-linearity of the O_3 production in the chemical mechanism in the model, and hence a more elaborate calculation than was presented in this study.

CHAPTER 2

The impact of biomass burning on the surface ozone in the Western U.S. mountain ranges

Abstract

We analyze the surface ozone observations from the Clean Air Status and Trend Network (CASTNet) using a global chemical transport model (GEOS-Chem) to investigate the impact of biomass burning on surface O_3 in the western U.S. (WUS) mountain ranges during the June-October fire season of 2007, one of the stronger fire years in the WUS in the past decade. GEOS-Chem O_3 captures the observed seasonal, synoptic and daily variations. Model daily afternoon average surface O_3 concentrations at the CASTNet sites are within 2 ppb of the observations, with correlation coefficients of 0.51-0.83 and Taylor scores of 0.64-0.92. Observed maximum daily 8-hour (MAD8) surface O_3 concentrations are 37-58 ppb at the sites, while the corresponding model results are higher by 6 ppb on average. Model results show July-September maximum surface O_3 enhancement of $\sim$9 ppb on average because of biomass burning. Peaks in fire-contributed surface O_3 correspond broadly with high levels of potassium (K), reaffirming a strong fire influence. We find a policy relevant background (PRB) O_3 of 45.6 ppb on average during July-September. Fire-contributed O_3 accounts for up to 30% of the PRB O_3, highest in the intense fire region (Montana, Idaho, and Wyoming) with maxima in August and September.

2.1 introduction

Ozone (O_3) is produced in the troposphere by oxidation of hydrocarbons and CO catalyzed by hydrogen oxide radicals ($HO_x \equiv OH + H +$ peroxy radicals) and nitrogen oxide radicals ($NO_x \equiv NO+NO_2$). In populated regions with large emissions of NO_x and hydrocarbons, high surface concentrations of O_3 are a major air pollution problem. Tropospheric O_3 is also of global interest as the primary source of OH, the main atmospheric oxidant, and as an effective greenhouse gas (*Change*, 2007). A fraction of tropospheric O_3 comes from the stratosphere. The major O_3 precursors, including NO_x, CO and VOCs, come from both anthropogenic sources, i.e. fuel combustion, and natural sources such as lightning, biomass burning and the biosphere.

O_3 itself is an air pollutant that is associated with a variety of adverse impacts on human health, including a decrease in lung function and exacerbation of respiratory illness (*Mickley*, 2007). Primary and secondary National Ambient Air Quality Standards (NAAQS) for O_3 have been established to protect public health and public welfare (*McDonald-Buller et al.*, 2011). In March 2008, the Environmental Protection Agency (EPA) established primary and secondary NAAQS of 75 ppb for ground-level O_3: annual 4th highest daily maximum 8-hour average (MAD8) concentration not to exceed 75 ppb. In 2010, EPA proposed to change the standard to a value in the range of 60-70 ppb (*Zhang et al.*, 2011). As the standard becomes more stringent, the accurate determination of background O_3 levels above which risks to human health can be assessed has become increasingly imperative. Background O_3 concentrations used to inform decisions about setting the NAAQS are referred to as Policy Relevant Background (PRB) O_3 concentrations. The U.S. EPA defines PRB O_3 concentrations as those that would occur in the U.S. in the absence of anthropogenic emissions in continental North America (*EPA*, 2006). The PRB O_3 represents the O_3 concentration that is not amenable to reduction under current policy frameworks and provides a baseline for assessing risk from exposure to O_3 pollution. It is important for regulatory decisions as it sets the maximum O_3 reduction and relative health benefits that can be achieved through

North American emission controls. Processes that contribute to PRB O_3 include photochemistry associated with biogenic emissions, wildfires, lightning, the long-range transport of O_3 and its precursors from outside of North America, and stratospheric-tropospheric exchange (STE) (*EPA*, 2006).

While summertime surface O_3 levels have been decreasing throughout the U.S., the western U.S. (WUS) has seen an upward trend in the past two decades (*Cooper et al.*, 2014, 2012). The U.S. Environmental Protection Agency (EPA) reported a decrease of 15% in emissions of NO_x and 40% in emissions of non-methane hydrocarbons (NMHCs) in the U.S. between 1983 and 2002 (*EPA*, 2003). Changes in these factors strongly influence the O_3 concentrations in the atmosphere. In most urban areas in the U.S., there have been reductions in peak O_3 concentrations, because of decreasing emissions of NO_x and NMHCs (*Lin et al.*, 2001; *EPA*, 2003, 2004). However, non-urban surface O_3 in the WUS has seen a significant increase over the past two decades. *Jaffe and Ray* (2007), for example, evaluated surface O_3 data for 1987-2004 from several sites in the WUS. They found that at seven out of the nine sites examined, there is a statistically significant increase in O_3, with a mean trend of 0.26 ppb per year. This corresponds to an increase of approximately 5 ppb over the 18 years of observations. Several hypotheses were put forward to explain this trend, including changing global background O_3 concentrations, changing climate and increasing emissions associated with fires (*Jaffe and Ray*, 2007; *Cooper et al.*, 2012). Our focus here is the increasing trend in wild fire activities in the region. The hot, dry summer of the WUS make the region susceptible to large forest fires. Wildfire emissions can become important source of O_3 precursors. Fires in the WUS have increased in both frequency and duration in the WUS in recent decade (*Westerling et al.*, 2006; *Spracklen et al.*, 2009, 2007; *Jaffe et al.*, 2008) due to several factors related to climate change: increased spring and summer temperatures, earlier spring snowmelt, and dryer conditions. The modeling study by (*Spracklen et al.*, 2009) showed that the annual mean area burned in the WUS could increase by 54% by the 2050s relative to the present under future warming. An analysis of more than 20 years of fire and

air quality data has shown clear positive correlations of O_3 levels with total area burned and biomass consumed by fires in the WUS (*Jaffe et al.*, 2008). It is conceivable that fires will be an even larger contributor to surface O_3 in the WUS for years to come.

We intend to investigate the impact of biomass burning on the surface O_3 in the WUS and to quantify its contribution to PRB O_3. Our approach is to apply a global three-dimensional (3-D) chemical transport model (CTM) to analyze surface O_3 observations over the WUS. We conduct model simulations for 2006 and 2007, two of the stronger fire years during the past decade (*Giglio et al.*, 2006). We give a brief description of the observations in Sect.2. Sect. 3 describes the GEOS-Chem model and simulations. Model evaluation is shown in Sect. 4. We present our simulation results and related discussions in Sect. 5 and 6. Conclusions are given in Sect. 7.

2.2 CASTNet surface O_3

Surface O_3 observations for our analysis come from the Clean Air Status and Trends Network (CASTNet: `http://www.epa.gov/castnet`; *Clarke et al.* (1997)). The CASTNet was developed by the U.S. Environmental Protection Agency (EPA) in order to establish an effective, rural monitoring and assessment network at locations away from pollutant emission sources and heavily populated areas (*EPA*, 2008; *Baumgardner*, 1998). Monitoring locations were selected according to strict siting criteria designed to avoid undue influence from point sources, area sources and local activities. As a result, most CASTNET sites are located in rural or remote locations away from pollutant emission sources and heavily populated areas. The CASTNet is spatially designed to be regionally representative of rural conditions (*EPA*, 2008) and therefore more suitable to compare with coarse horizontal resolution (in this case, roughly 200×250 km^2). The CASTNet measures O_3 and other pollutants. We use hourly surface O_3 measured with ultra-violet absorbance (accuracy and precision, 10%) (*EPA*, 2010). The hourly values are more relevant to evaluating model O_3 responses to syn-

optic and diurnal variability. Also used here is maximum daily 8-hour average (MAD8) O_3 calculated from hourly observations. CASTNet O_3 data has been widely used in previous studies, for instance, the investigation of subgrid segregation on O_3 production efficiency in a chemical model (*Liang and Jacobson*, 2000), the variability in surface background O_3 throughout the U.S. (*Lefohn et al.*, 2001; *Fiore et al.*, 2003), and the positive trend in O_3 in the WUS (*Jaffe and Ray*, 2007).

In polluted regions, anthropogenic emissions of NO_x, VOC and CO would lead to high O_3 concentrations. While in remote troposphere, O_3 is generally thought to be in a steady state between chemical sources and sinks (*Ramaswamy et al.*, 2001). At each CASTNet site, there is a continuous O_3 analyzer, which measures hourly average concentrations using Ultraviolet (UV) absorption and follows consistent calibration procedures using National Institute of Standards and Technology (NIST) traceable standard photometers. The data records were screened to ensure that only reasonable values were included in the analysis. Unrealistic O_3 values in CASTNet data are removed prior to model evaluation. These were identified by extended periods (>6h) when O_3 mixing ratios remained unchanged to three significant figures at either very high or very low values (<10 ppb or >100 ppb). We choose sites with missing data less than 15 days per year and exclude the coastal sites, yielding 12 sites in the WUS for year 2007 and 10 sites for 2006. Fig. 2.1 shows the locations of the sites. Table 2.1 lists the geographic information (latitude, longitude and elevation) for each site. Most of the sites are elevated mountainous sites, scattered across the Sierra Nevada/Cascades Mountains and the Rocky Mountains. Surface elevation typically is in excess of 1.5 km in the region. As a result, background O_3 there is higher than in the eastern U.S. (*Lefohn et al.*, 2001; *Fiore et al.*, 2002; *Jaffe*, 2010). Positive correlations have been observed between O_3 and regional fires (*Jaffe et al.*, 2008; *Jaffe*, 2010). Also shown in Fig. 2.1 is Terra and Aqua Moderate Resolution Imaging Spectrometer (MODIS) active fire counts in the WUS summed over the summer (July, August and September) fire season of 2007. Several of the sites are adjacent to regions with high frequencies of fire activities -it is thus conceivable that

the surface O_3 concentrations at the sites would be influenced by biomass burning emissions in the surrounding regions.

2.3 Model description and simulations

We use the GEOS-Chem global 3-D model (v8-02-03; `http://acmg.seas.harvard.edu/geos/`) in simulation of tropospheric O_3. Meteorological input is from NASA Goddard Earth Observing System (GEOS-5) assimilated observation data with a temporal resolution of 6 hours (3 hours for surface variables and mixing depths), a horizontal resolution of 0.5° latitude by 0.667° longitude and 47 vertical levels between the surface and 0.01 hpa. The lowest model levels are centered at approximately 60, 200, 200, 300, 450, 600, 700, 850, 1000, 1150, 1300, 1450, 1600, 1800 m in GEOS-5. GEOS-Chem includes a detailed simulation of O_3-NO_x-hydrocarbon-aerosol chemistry with 120 species simulated explicitly. A general description of the model is first given by (*Bey et al.*, 2001) with many updates (*Zhang et al.*, 2011). Evaluations of the model simulations for O_3 and related species over the U.S. with measurements are presented by (*Wang et al.*, 2009; *Zhang et al.*, 2010; *Walker et al.*, 2010; *Parrington et al.*, 2008).

We use both a global horizontal resolution of 2°×2.5° and a 0.5°×0.667° nested domain over North America and the adjacent oceans (140°-40°W, 10°-70°N). We first conduct the global GEOS-Chem simulation at 2°×2.5° resolution, and then use the output archived at 3-hour temporal resolution as dynamic boundary conditions for the nested simulation. The one-way nesting capability in GEOS-Chem is described by (*Wang et al.*, 2004), and application of the nested model to O_3 simulations over China has been presented by (*Wang et al.*, 2011).

Tracer advection is computed every 15 minutes with a flux-form semi-Lagrangian method (*Lin and Rood*, 1996). Tracer moist convection is computed using the GEOS convective, entrainment, and detrainment mass fluxes as described by (*Allen et al.*, 1996a,b). The deep

convection scheme of GEOS-4 is based on (*Zhang and McFarlane*, 1995), and the shallow convection treatment follows (*Hack et al.*, 1994). GEOS-5 convection is parameterized using the relaxed Arakawa-Schubert scheme (*Moorthi and Suarez*, 1992).

Biomass burning emissions are from Global Fire Emission Database version 2 (GFEDv2) (*van der Werf et al.*, 2006; *Randerson et al.*, 2006). GFEDv2 is derived using satellite observations including active fire counts and burned areas in conjunction with the Carnegie-Ames-Stanford-Approach (CASA) biogeochemical model. Carbon emissions are calculated as the product of burned area, fuel loading and combustion completeness. Burned area is derived using the active fire and 500-meter burned area datasets from MODIS as described by (*Giglio et al.*, 2006). Fig. 2.2 shows the monthly mean total carbon emissions in the WUS (100°-125°W, 30°-50°N) for 2006 and for 2007. The fire season started in April, peaked in July-September, and lasted through November in both years. The emissions are larger in 2007 than those in 2006 for much the year, especially during summer months. The overall larger emissions in 2007 than in 2006 are consistent with the higher active fire count numbers in 2007 than in 2006, based on the MODIS fire products. The GFEDv2 inventory has a multitude of temporal resolutions from monthly, 8-day, to 3-hourly with diurnal cycles, as reported previously by (*Chen et al.*, 2009). The original GFED v2 inventory has a spatial resolution of 1°(latitude)×1°(longitude) and a monthly temporal resolution. The emissions are re-sampled to 2°(latitude)×2.5°(longitude) grids and 0.5°(latitude)×0.667°(longitude) grids nested over North America for use in our GEOS-Chem simulations. Forest fires typically last from several days to weeks as seen in MODIS active fires *Giglio et al.* (2006). Therefore, the GFEDv2 monthly emissions were resampled to an 8-day time step according to MODIS 8-day active fire counts (*Chen et al.*, 2009). In our model simulations, the GFEDv2 8-day emissions are used.

Lightning NO_x emissions in the model are computed locally in deep convection events following the scheme of (*Price and Rind*, 1992) that relates flash rates to convective cloud top heights. The NO_x emissions are vertically distributed following the profile from (*Pickering*

et al., 1998) where 55-75% of the emissions are above 8 km. Implementation of the lightning source in GEOS-Chem is as described by (*Wang et al.*, 1998) with some recent updates (*Hudman et al.*, 2007; *Sauvage et al.*, 2007a; *Nassar et al.*, 2009; *Jourdain et al.*, 2010; *Murray et al.*, 2012). To improve the spatial distribution of lightning in the model, the spatial distribution of lightning is scaled to reproduce seasonal mean lightning flash rates to match the climatological satellite observations of lightning flashes from the Optical Transient Detector and Lightning Imaging Sensor (OTD/LIS) High Resolution Monthly Climatology (HRMC) v2.2 product (*Christian et al.*, 2003). Globally the lightning NO_x source is scaled to 6 Tg N/yr (*Martin et al.*, 2007; *Hudman et al.*, 2007; *Sauvage et al.*, 2007b). In this work, we use the higher density National Lightning Detection Network data (*Christian et al.*, 2003) for the continental U.S. to constrain lightning flash rates, following (*Zhang et al.*, 2014). NLDN observes cloud-to-ground lightning flashes only, and intra-cloud flashes are estimated to be three times that amount (*Boccippio et al.*, 2001). The constraint largely corrects excessive lightning flash rates and consequently high bias of surface O_3 in the SWUS in previous GEOS-Chem simulations (*Zhang et al.*, 2011, 2014).

Anthropogenic emissions used here are as described by (*Zhang et al.*, 2011) unless stated otherwise. Global anthropogenic emissions are from the Emission Database for Global Atmospheric Research (EDGAR) inventory for 2000, superseded by regional emission inventories from the U.S. EPA 2005 National Emission inventory (NEI-05) for the U.S., the European Monitoring and Evaluation Program (EMEP) for Europe, the Canada Criteria Air Contaminates (CAC) emission inventory for Canada, and the Big Ben Regional Aerosol and Visibility Observational (BRAVO) emission inventory for Mexico. Biogenic emissions are based on the Model of Emissions of Gases and Aerosols from Nature (MEGAN) inventory (*Guenther et al.*, 2006).

We conducted GEOS-Chem simulations for 2006 and 2007, driven by GEOS-5 meteorological data. All simulations presented here were conducted for 12 months (January-December) using standard GEOS-Chem model output as initial conditions. The first three

months were used for initialization, and we focus our attention on results for April - December. We also conducted model simulations with: (1) zero biomass burning emissions, (2) zero lightning NO_x emissions and (3) zero North American anthropogenic emissions (North American background or PRB). Detailed discussions and justifications for these model simulations are provided in the following sections where appropriate. The difference between the standard simulation and (1) represents the contribution to surface O_3 from biomass burning emissions. The difference between the standard simulation and (2) represents O_3 enhancement from lightning NO_x emissions. Sensitivity simulation (3) would provide us with am estimation of the PRB O_3 concentrations. As pointed out by (*Fiore et al.*, 2002), comparison of model results with surface observations is most appropriate in the afternoon when the observations are representative of a relatively deep mixed layer. Therefore all surface O_3 concentrations presented here are afternoon mean values (13:00-17:00 local time) unless stated elsewhere. For comparison with CASTNet observations, we extracted model results at the time and location of the observations and applied the same temporal averaging as we did for the observations.

2.4 Surface O_3 in the western U.S.

2.4.1 Statistic evaluation of model performance

We compare our model results with the observed surface O_3 concentrations from the CASTNet. Fig. 3 shows the observed versus simulated daily afternoon mean O_3 concentrations from April-December of 2007 (Fig. 2.3a) and of 2006 (Fig. 2.3b) at four selected sites. We excluded the first three months of the year from our analysis because it is typically not a period of strong biomass burning impact, surface O_3 is at its annual minimum in almost each site and the exceedances of the national O_3 standard are rare. Mean values, correlation coefficients and root mean square (RMS) differences for simulated vs. observed O_3 time series at all sites for both year 2006 and 2007 are summarized in Table 2.2.

We found that the average afternoon mean O_3 concentrations in the model are generally within 5 ppb of the CASTNet observations for global simulation, and within 2 ppb for nested grid simulation. The Pearson correlation coefficients between model simulations and observations are generally in the range of 0.5-0.8 for both global and NA nested grid resolution. At most sites, correlation coefficient is larger for nested grid simulation, with an average of 0.67 for 12 sites in 2007 and 0.62 for 10 sites in 2006, compared to an average of 0.63 in 2007 and 0.58 in 2006 for global simulation. For only a few sites, the correlation coefficients are only around 0.3, this may reflect the small dynamic range of variability in the observations. We also compared the RMS difference in both global and nested model simulation. As shown in the table, the RMS difference is smaller for nested simulation at most sites than that for global simulation. The correlation coefficient and the RMS difference provide complementary statistical information quantifying the correspondence between two patterns. We use Taylor's diagram (Fig. 2.4) to summarize statistically how well each simulation compares with the observation at different CASTNet sites. On the diagram the correlation coefficient and the RMS difference between simulation and observation, along with the ratio of the standard deviation of the two patterns, are all indicated by a single point on the two-dimensional (2-D) plot (*Taylor*, 2000). Different color in Fig. 2.4 denotes simulations at different CASTNet sites. Solid and hollow circles represent results of the global and nested simulation, respectively. The red asterisk is the reference field, representing the observed O_3 concentration. As shown in Fig. 2.4, at most of the sites, nested simulation perform relatively better than global simulation as they lie relatively closer to the reference point. We also evaluate model skill by calculating Taylor's score derived from the equation:

Where and are the standard deviations of simulation and observation, and R is the correlation coefficient between them. is the maximum correlation attainable (here we use = 1). As the model variance approaches the observed variance (i.e., as 1) and as the Taylor's score approaches unity. Nested simulation has a higher Taylor's score at eight out of the twelve sites analyzed in this study. At one site, both nested and global simulation have the

same Taylor's score. Only three sites have a higher Taylor's score for the global simulation than that for the nested simulation. The comparison results indicate that the nested model generally performs better than the global model in capturing daily variation of surface O_3 concentrations.

2.4.2 Seasonal variation of surface O_3

Fig. 3 also indicates very significant seasonal variation of surface O_3. O_3 concentration is the highest during spring-summer. In spring, a longer O_3 lifetime and more efficient ventilation of pollution from the Asian continent result in a peak in global background O_3. In summer, high temperatures accelerate the photochemical O_3 production from regional NO_x emissions, especially for those sites that are adjacent to metropolitan regions. Surface O_3 concentration is the lowest during winter due to the lower temperature and less efficient trans-pacific transportation of air pollution. The afternoon mean (13:00-17:00 LT) surface O_3 concentration among all the 12 CASTNet sites in the WUS averages 42-59 ppb during spring, 43-58 ppb during summer, and 29-46 ppb during winter, respectively. Comparison results are generally consistent with the previous GEOS-Chem simulations presented by (*Zhang et al.*, 2011). Meanwhile, much of the variability in observation is on a daily basis. The model simulations (especially the nested model) generally well reproduce this variability. However, the 6-h temporal resolution of the GEOS-5 meteorological data may limit the ability of the model to reproduce this variability.

2.5 Impacts of biomass burning on surface O_3

2.5.1 Fire-contributed O_3 in the WUS

To quantify the influence of biomass burning emission on surface O_3 in the WUS, we conducted GEOS-Chem sensitivity simulations where biomass burning emissions were shut off for both the global ($2^\circ \times 2.5^\circ$) and NA nested grid ($0.5^\circ \times 0.667^\circ$) resolution. The difference

between sensitivity and standard simulation thus represents the impact of biomass burning emissions on surface O_3, which we define as fire-contributed O_3 concentration. Fig. 2.5 shows the time series of the fire-contributed O_3 at four selected sites in the WUS for both global and NA nested simulation for year 2006 and 2007. Fire contribution to surface O_3 mainly occurs during July to September, which is the main fire season in WUS. O_3 enhancement could reach to a maximum of more than 30 ppb. Fig. 2.6 and Table 2.3 summarize the mean, median, maximum and minimum fire contribution to surface O_3 at each CASTNet site during July to September in 2007 and 2006. The average increase in O_3 concentration due to biomass burning emissions ranges from 0.5 to only a few ppb during summer. However, since fire activities usually last for just a few days, we would like to investigate the maximum fire contribution to surface O_3, which is a better indicator of how the emission of an individual fire activity may influence O_3 concentration. Averaging among all the CASTNet sites used in our study, the maximum increase in surface O_3 is about 9 ppb in 2007 and 4 ppb in 2006. Based on MODIS active fire product (`ftp://fuoco.geog.umd.edu`), fire activity in 2007 is very intensive while that in 2006 is about 20% weaker. This is consistent with our simulation results of fire contribution to surface O_3, which show a much larger increase in O_3 concentration due to biomass burning emissions in 2007 than that in 2006. The negative values of minimum fire-contributed O_3 at a few sites indicate the non-linearity of O_3-NO_x-hydrocarbon-aerosol chemistry.

2.5.2 Correlation with Potassium

Surface concentrations of potassium (K) are shown to increase significantly during wildfire episodes (*Tanner et al.*, 2001)and therefore are a good tracer of biomass burning. CASTNet observations of weekly average K are used in this paper to identify fire influence. In this section we examined the correlations between fire-contributed O_3 and surface K to further verify the large influence of biomass burning on surface O_3 concentrations in the WUS during the fire season. Fig. 2.7 shows the time series of observed surface concentrations of K and

fire-contributed O_3 at four selected CASTNet sites. The peak in K concentrations during July to September also corresponds to the high concentrations of fire-contributed surface O_3 during the same period, which is the fire season at most of the mountainous CASTNet sites. However the peaks are not perfectly correlated with each other, and a time lag about half a month exits between the two peaks. This is very likely due to the fact that as a fire tracer, potassium is directly emitted and the maximum impacts occur right over the source region. O_3, however, is chemically produced from the fire-emitted precursors. The time needed for this O_3 production may result in the difference in the occurrence of maximum value for K concentration and fire-contributed O_3 concentration. We found similar patterns during the fire season at most of the CASTNet sites in WUS. These correlations suggest that biomass burning emissions to a great extent contribute to the enhancement in surface O_3 concentrations at sites in the WUS, and the time lag between the peaks in K and fire-contributed O_3 suggested the time needed for O_3 production from fire emissions.

2.5.3 Seasonal variation of fire-contributed O_3

Fig. 2.8 shows the spatial distribution of monthly averaged fire-contributed surface O_3 concentration for July-October 2007, as a result from NA nested grid ($0.5^\circ \times 0.667^\circ$) simulations. It indicates strong geographic and temporal variations of the fire-contributed O_3 across the WUS. Red regions indicate areas where the fire contribution to surface O_3 could reach up more than 20 ppb. The largest enhancement occurs in the Pacific Northwest, where most wildfires in the lower 48 states took place. The maximum increase could reach to more than 40 ppb. We can also observe a relatively large enhancement in O_3 concentration due to biomass burning in Southern California. Wildfires periodically burn large areas of chaparral and woodlands in summer and autumn in Southern California. These fires often occur in conjunction with Santa Ana weather events. Dry Santa Ana winds promote the ignition and rapid spread of wildfires by drying fuels and fanning the flames of fires once they are started (*Westerling et al.*, 2004). Enhancement in surface O_3 due to wildfire emission in South-

ern California could also be as much 20 ppb during August. Across the WUS, the largest fire contributions to surface O_3 occur in August, and then the enhancements decrease in September and October as wildfires abate.

2.6 Implications for PRB O_3

2.6.1 The PRB O_3 in the WUS

We also estimated the PRB (North American background) O_3 in 2007 using GEOS-Chem model to determine the relative fraction of background O_3 that is contributed by biomass burning emissions. We conducted sensitivity simulations where the North American anthropogenic emissions are turned off in the model. Fig. 2.9 shows the simulated PRB O_3 from the nested model at four selected sites during summer fire season, from July to September 2007. Also shown are model simulated surface O_3 and fire-contributed O_3 concentrations. Values here are maximum daily 8-hour averaged (MAD8) O_3. We switched from afternoon mean O_3 (13:00-17:00 local time) to MAD8 O_3 because the U.S. NAAQS is defined with MAD8 O_3. Mean values of model simulated MAD8 surface and PRB O_3 during summer fire season, as well as observed surface MAD8 O_3 at CASTNet sites in the WUS are summarized in Table 2.4.

The PRB (North American background) O_3 averages between 33 to 52 ppb during summer fire season in 2007 for the ensemble of CASTNet sites in the intermountain West and drives a large part of the day-to-day variability in the model. This relatively high PRB O_3 in the mountain ranges in the WUS is due to high elevations, arid terrain, and large-scale subsidence. There is also evidence showing that O_3 inflow from the Pacific to the WUS has been increasing over the past decades (*Cynthia Lin et al.*, 2000; *Jaffe and Ray*, 2007; *Parrish et al.*, 2009; *Cooper et al.*, 2010). The difference between standard and PRB simulations averages between 9 to 20 ppb among these sites. This indicates the impact on surface O_3 from North American anthropogenic emissions. In the estimation from (*Zhang et al.*, 2011),

the 2006 PRB averages 35-45 ppb during summer for sites in the intermountain West. Our simulation results in 2007 are comparatively higher, due to the fact that the year 2007 has experienced stronger wild fire activities. Stronger fire emissions would then lead to an increase in background O_3 levels. Fire contribution to surface O_3 also strongly correlates with PRB O_3 during summer, while most wildfire activities are taking place. At site Glacier, the peak in fire-contributed O_3 drives the peaks in both PRB and surface O_3 during the mid of August (Fig. 2.9).

2.6.2 Contribution of biomass burning emission to the PRB O_3

Fig. 2.8 indicates the largest enhancement in O_3 concentration caused by fire emission occurs in the Pacific Northwest. We selected three sites located within this region: Glacier, MT (49°N, 114°W, 1.0 km), Pinedale, WY (43°N, 110°W, 2.4 km) and Yellowstone, WY (45°N, 110°W, 2.4 km). Among all the CASTNet sites analyzed in this study, these three sites are the most adjacent to wildfire activities in Pacific Northwest regions and therefore should have the most significant influence from fire emissions. Fig. 2.10 shows the fraction of fire-contributed O_3 to PRB O_3 on each day during summer fire season for each of the three sites. Also shown are the number of days on which the fire-contributed O_3 accounts for more than 20%, 10% and 5% of the PRB O_3, respectively. At site Glacier, there are 17 days during summer fire season with the fraction exceeding 20%, 28 days exceeding 10% and 54 days exceeding 5%. During the strongest fire event, O_3 enhancement caused by fires could contribute up to 40% of the PRB O_3. This is strong evidence that photochemical production of O_3 from biomass burning emissions is a major process that contributes to the PRB O_3, At Pinedale and Yellowstone, the fire-contributed O_3 also reaches up to 30% of the PRB O_3. The number of days when the fraction exceeding 20%, 10% and 5% are less then that in Glacier because the locations of these two sites are further away from active fire regions, compared to Glacier.

2.7 Summary and conclusions

We used a global 3-D chemical transport model driven by assimilated meteorological data (GEOS-Chem) to examine the impacts of biomass burning on surface O_3 in the western United States (WUS) mountain ranges. We conducted GEOS-Chem simulations at ($2^\circ \times 2.5^\circ$) (globally) and ($0.5^\circ \times 0.667^\circ$) (one-way nested over North America) horizontal resolutions for 2006 and 2007, two of the stronger (in terms of burned area and emissions) fire years in the WUS in the past decade. We focused our analysis primarily on 2007. We evaluated our model results with observed surface O_3 concentration data from the CASTNet. Sensitivity simulations were used to estimate the contribution from biomass burning emissions to surface O_3.

GEOS-Chem O_3 simulated at the two resolutions captured the observed seasonal, synoptic and daily variations at the CASTNet sites. Model results from the nested simulations offered considerably better agreements with the observations as evidenced in the higher Taylor scores. Daily afternoon average O_3 concentrations from the nested simulations were within 2 ppb of the observations, with correlation coefficients of 0.51-0.83 and Taylor scores of 0.64-0.92 at the individual sites.

We calculated an average of $\sim$9 ppb in the maximum surface O_3 enhancement that was attributed to biomass burning emissions during July-September 2007; the corresponding value was $\sim$4 ppb for 2006, reflecting the less intense burning in that year. The enhancements varied considerably across individual CASTNet sites. The maximum surface O_3 enhancements were largest ($\sim$30 ppb) at Glacier, MT, in the middle of the intense fire region. Peaks in fire-contributed surface O_3 correlated strongly with high concentrations of potassium (K), a tracer for biomass burning, at the CASTNet sites, supporting a strong fire influence at the sites. The observed and model simulated maximum daily 8-hour (MAD8) O_3 in the remote WUS are in the range of 37.4-58.2 and 42.0-66.2. Our results show that the model simulated PRB O_3 is 45.6 ppb on average for July-September 2007. Fire-contributed O_3 accounts for

up to 30% of the PRB O_3, highest in Montana, Idaho and Wyoming during August and September.

Acknowledgements. This research was supported in part by NASA grants NNX09AF07G and NNX08AF64G from the Atmospheric Chemistry Modeling and Analysis Program (ACMAP) and from the Interdisciplinary Science Program (IDS). The GEOS-Chem model is managed by the Atmospheric Chemistry Modeling group at Harvard University with support from the NASA ACMAP program.

Table 2.1: CASTNet sites used in this study (see also Fig. 2.1).

Site	**Latitude** (°N)	**Longitude** (°W)	**Elevation (km)**
Canyonlands, UT (**CAN**)	38.46	109.82	1.8
Centennial, WY (**CNT**)	41.36	106.24	3.18
Chiricahua, AZ (**CHA**)	32.01	109.39	1.57
Glacier, MT (**GLR**)	48.51	113.99	0.98
Great Basin, NV (**GRB**)	39.01	114.22	2.06
Grand Canyon, AZ (**GRC**)	36.06	112.18	2.07
Gothic, CO (**GTH**)	38.96	106.99	2.93
Mesa Verde, CO (**MEV**)	37.2	108.49	2.17
Petrified Forest, AZ (**PET**)	34.82	109.89	1.72
Pinedale, WY (**PND**)	42.93	109.79	2.39
Rocky Mtn, CO (**ROM**)	40.28	105.55	2.74
Yellowstone, WY (**YEL**)	44.56	110.4	2.4

Table 2.2: Annual averages and standard deviations of observed and simulated daily, afternoon (13:00-17:00 local time) O_3 concentrations (unit: ppb) at the 12 CASTNet sites (see Table 1 and Fig. 2.1) for 2006 and 2007. The Pearson correlation coefficients (R) and the root mean square differences (RMS) are also shown. *Petrified Forest (PET) and Pinedale (PND) each had more than 20 days of missing data during July-September 2006.

CASTNet Site	Year	Obs.	Model		R	
			2°×2.5°	0.5°×0.667°	2°×2.5°	0.5°×0.667°
CAN	2007	52.0±9.9	50.6±9.0	51.9±10.0	0.72	0.78
	2006	51.3±10.3	49.3±8.3	50.7±9.4	0.72	0.72
CNT	2007	51.0±7.1	45.1±12.3	49.2±8.7	0.63	0.67
	2006	48.3±11.6	43.6±12.6	48.2±8.5	0.57	0.65
CHA	2007	49.5±9.7	53.6±10.1	49.7±9.7	0.59	0.63
	2006	49.9±12.1	53.4±9.8	51.5±8.4	0.37	0.51
GLR	2007	37.9±10.1	38.9±9.9	37.8±7.0	0.72	0.59
	2006	37.0±12.1	38.3±11.1	37.7±6.9	0.72	0.66
GRB	2007	49.4±10.1	47.3±10.4	49.9±10.1	0.69	0.83
	2006	48.2±12.5	46.2±10.6	48.6±10.0	0.49	0.55
GRC	2007	53.5±8.0	53.4±10.4	51.8±8.9	0.67	0.72
	2006	52.3±9.6	52.3±10.2	51.1±8.2	0.56	0.62
GTH	2007	50.7±9.4	53.4±12.5	49.8±7.4	0.45	0.54
	2006	49.2±12.9	52.0±12.1	49.1±6.0	0.54	0.58
MEV	2007	52.8±10.2	53.4±12.5	54.3±13.0	0.75	0.77
	2006	52.5±11.6	52.0±12.1	53.5±13.8	0.67	0.65
PET*	2007	52.6±10.2	54.7±11.3	53.5±10.7	0.69	0.71
	2006	NA	NA	NA	NA	NA
PND*	2007	49.0±11.8	46.4±9.5	47.7±8.8	0.42	0.38
	2006	NA	NA	NA	NA	NA
ROM	2007	52.1±11.9	48.1±12.3	52.0±10.6	0.61	0.63
	2006	51.5±11.0	46.7±12.3	51.1±10.1	0.58	0.66
YEL	2007	47.4±8.4	43.0±9.8	44.6±7.9	0.67	0.73
	2006	48.6±11.5	41.2±10.0	42.9±6.9	0.58	0.61

Table 2.3: Taylor's scores for GEOS-Chem simulations (at both 2°×2.5°and 0.5°×0.667° horizontal resolutions) of surface O_3 concentrations in comparison with observations at the 12 CASTNet sites (see Table 1 and Fig. 2.1).

CASTNet site	Taylor score	
	2°×2.5°	0.5°×0.667°
CAN	0.85	0.89
CNT	0.61	0.82
CHA	0.79	0.81
GLR	0.86	0.7
GRB	0.85	0.92
GRC	0.78	0.85
GTH	0.67	0.73
MEV	0.84	0.84
PET	0.84	0.85
PND	0.68	0.64
ROM	0.81	0.8
YEL	0.82	0.86

Table 2.4: GEOS-Chem simulated mean, median, maximum and minimum biomass burning contributions to surface O_3 concentrations (unit: ppb) at the 12 CASTNet sites (see Table 1 and Fig. 2.1) during July-September of 2006 and 2007. Values from simulations at horizontal resolutions $2^\circ \times 2.5^\circ$ and at $0.5^\circ \times 0.667^\circ$ (nested over North America) are shown. Values for 2006 are in parentheses. *Petrified Forest (PET) and Pinedale (PND) each had more than 20 days of missing data during July-September 2006.

CASTNet Site	Mean		Maximum		Minimum	
	2°×2.5°	0.5°×0.667°	2°×2.5°	0.5°×0.667°	2°×2.5°	0.5°×0.667°
CAN	1.1 (0.4)	1.2 (0.9)	4.0 (0.8)	7.9 (3.1)	0.0 (0.1)	0.5 (0.4)
CNT	2.2 (0.6)	1.3 (1.3)	14.7 (2.0)	7.0 (6.3)	-0.3 (0.1)	0.0 (0.4)
CHA	0.7 (2.4)	0.7 (0.6)	1.4 (15.6)	1.2 (1.9)	0.1 (0.3)	0.5 (0.3)
GLR	3.0 (1.1)	3.7 (1.9)	20.4 (3.7)	32.4 (6.7)	0.2 (0.4)	0.7 (0.5)
GRB	2.0 (0.6)	1.4 (1.1)	10.2 (1.2)	15.6 (3.2)	-0.8 (0.4)	0.6 (0.6)
GRC	0.9 (0.6)	0.9 (0.8)	3.1 (1.7)	2.4 (2.1)	-0.3 (0.2)	0.4 (0.3)
GTH	1.1 (0.4)	1.1 (1.0)	3.5 (1.3)	5.8 (3.7)	-0.1 (0.1)	0.5 (0.4)
MEV	1.0 (0.4)	1.0 (0.9)	3.7 (0.9)	4.4 (2.5)	-0.2 (0.1)	0.4 (0.3)
PET*	0.7 (NA)	0.9 (NA)	2.0 (NA)	3.1 (NA)	0.0 (NA)	0.5 (NA)
PND*	2.8 (NA)	1.9 (NA)	15.3 (NA)	8.9 (NA)	0.3 (NA)	0.4 (NA)
ROM	1.6 (0.5)	1.2 (1.1)	8.5 (1.6)	7.6 (4.0)	-0.2 (0.2)	0.5 (0.4)
YEL	4.5 (1.3)	3.0 (2.3)	15.0 (4.8)	16.3 (8.1)	0.5 (0.3)	0.3 (0.5)

Table 2.5: Observed maximum daily 8-hour averaged (MAD8) surface O_3 concentrations and GEOS-Chem simulated MAD8 and policy relevant background (PRB) surface O_3 concentrations during July-September 2007 at the 12 CASTNet sites (see Table 1 and Fig. 2.1). Model results are from the simulation at the $0.5° \times 0.667°$ horizontal resolution (nested over North America). Unit: ppb.

CASTNet Site	Surface O_3 (MAD8)		PRB O_3
	Obs.	Model	
CAN	56.9±6.5	60.1±7.4	43.7±8.3
CNT	56.8±6.0	60.6±9.5	48.7±9.8
CHA	47.0±12.3	61.0±10.4	46.3±11.9
GLR	37.4±10.2	42.0±8.7	33.2±9.4
GRB	53.3±10.8	60.3±8.8	44.9±8.1
GRC	55.8±5.8	61.9±9.2	47.1±11.5
GTH	52.3±6.2	63.2±10.5	52.2±11.5
MEV	56.0±10.5	66.2±9.3	45.8±11.0
PET	53.5±10.2	63.8±10.0	46.4±12.0
PND	55.2±5.5	57.1±8.6	45.7±8.9
ROM	58.2±10.2	61.4±9.5	47.6±9.7
YEL	49.4±6.1	55.3±8.8	45.9±9.7

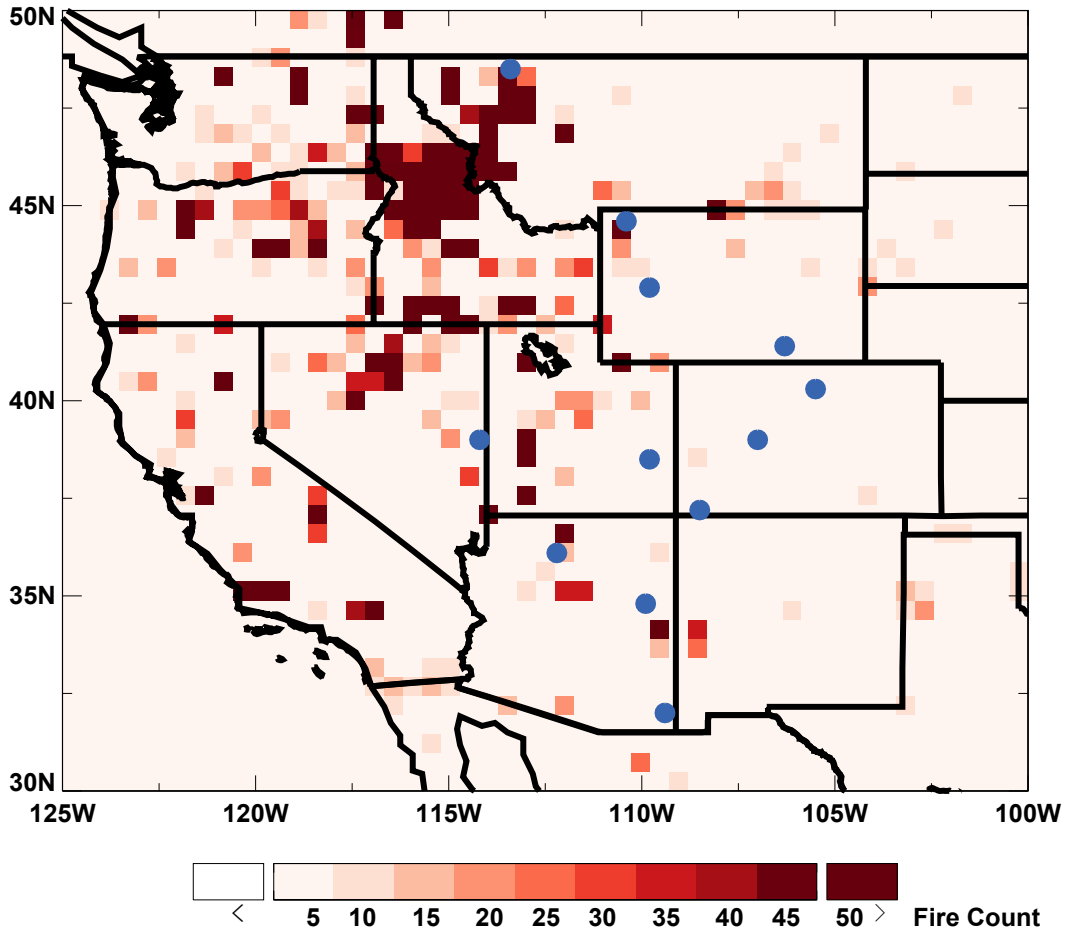

Figure 2.1: CASTNet sites used in this study (see also Table 1). Also shown are MODIS total active fire counts for July-September 2007 over the western U.S. (MODIS data from `ftp://fuoco.geog.umd.edu`).

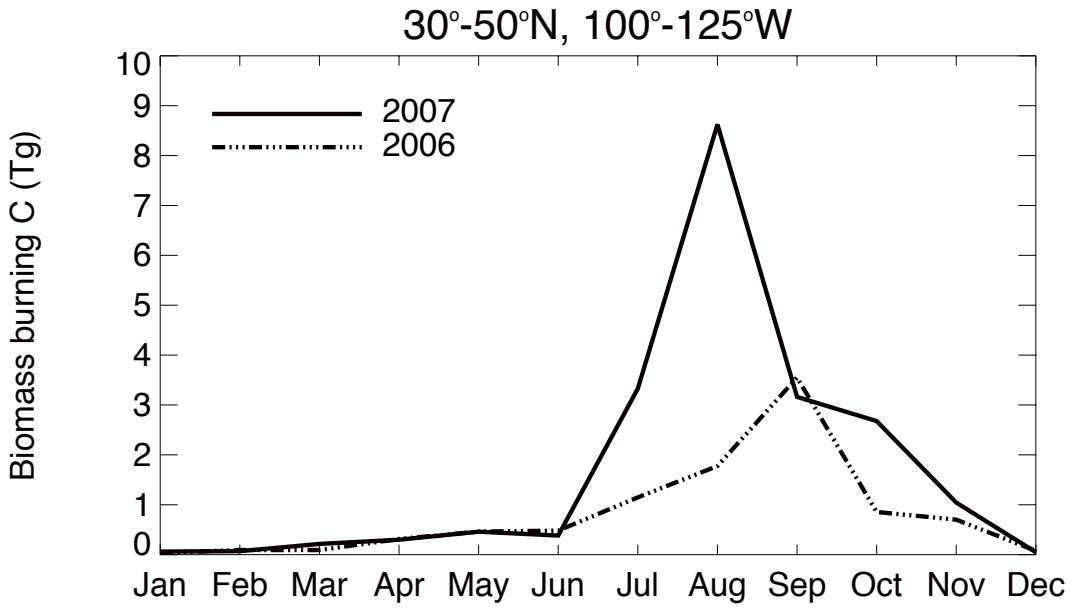

Figure 2.2: Monthly total carbon emissions from biomass burning in the western U.S (100°-125°W, 30°-50°N) for 2006 (dashed line) and 2007 (solid line). Data is from the Global Fire Emissions Database (GFED) version 2 (`http://www.globalfiredata.org/Data`).

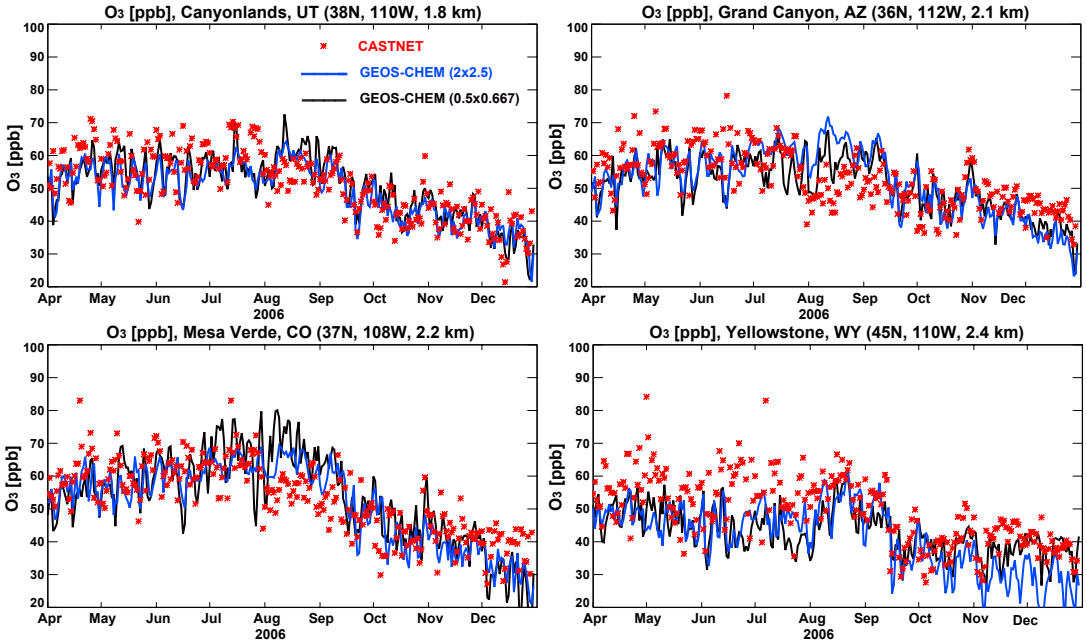

(a) 2006

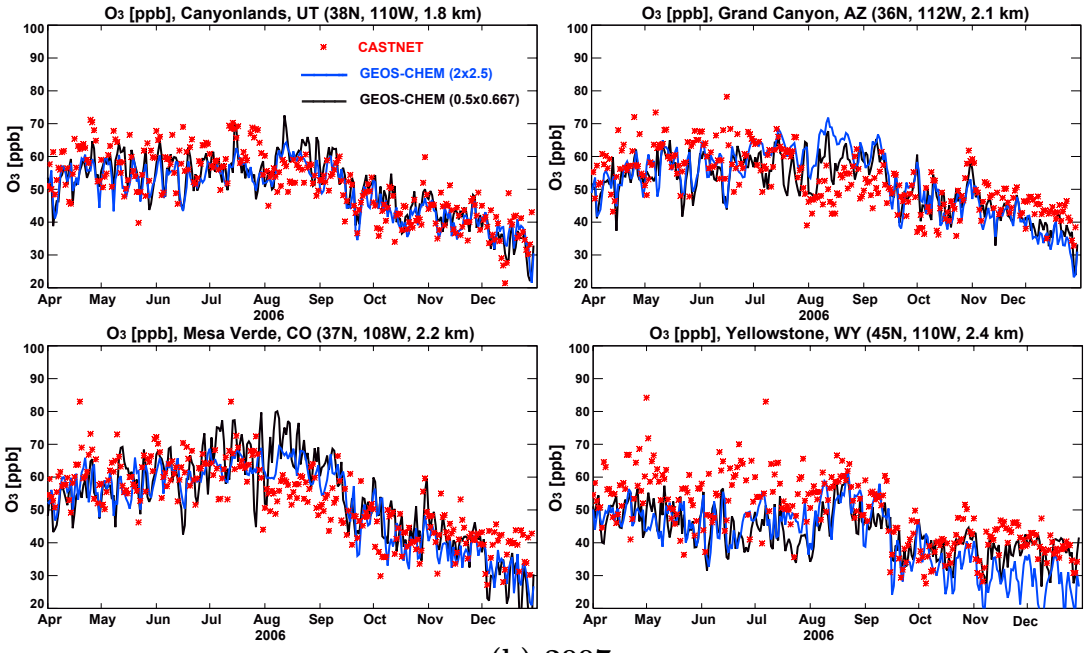

(b) 2007

Figure 2.3: (a) Observed (red dots) and GEOS-Chem simulated (blue line: 2°×2.5°; black line: 0.5°×0.667° nested over NA) surface O_3 concentrations for April-December 2006 at four CASTNet sites: Canyonlands, UT (138°N, 110°W, 1.8 km), Grand Canyon, AZ (36°N, 112°W, 2.1 km), Mesa Verde, CO (37°N, 108°W, 2.2 km) and Yellowsone WY (45°N, 110°W, 2.4 km). Values are averages for 13:00-17:00 local time. (b) Same as 3a, but for 2007.

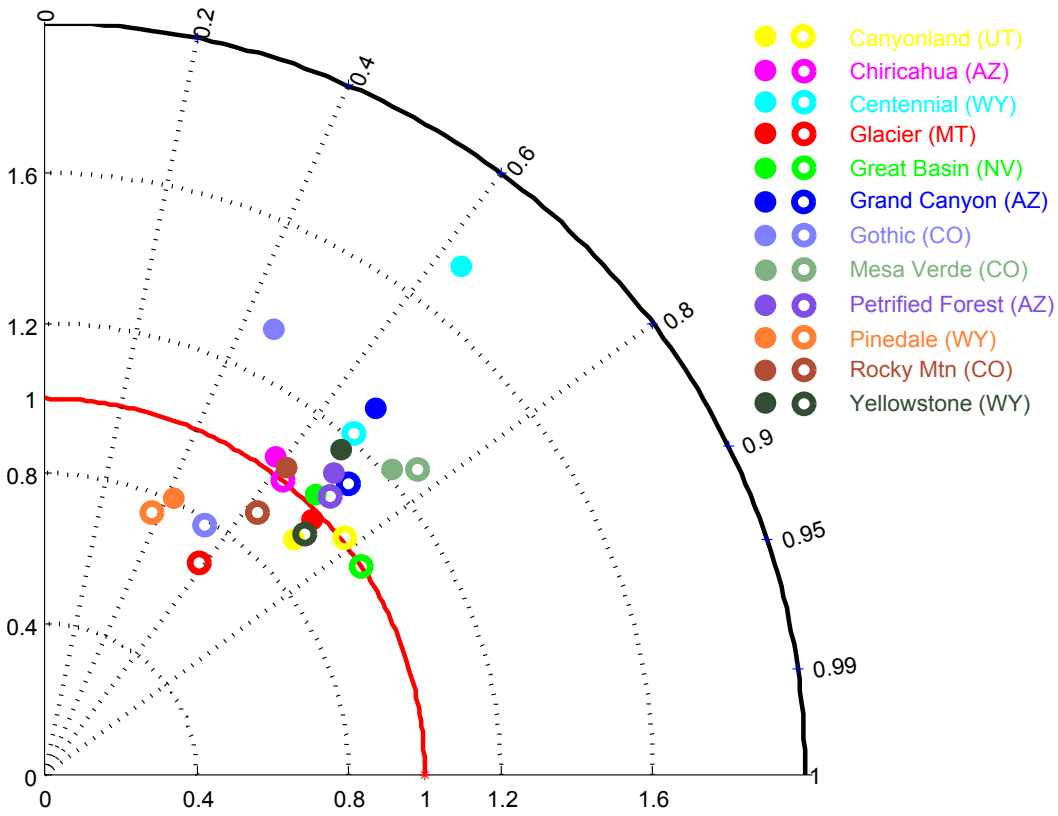

Figure 2.4: Taylor's diagram of pattern statistics describing the surface O_3 concentration at 12 CASTNet sites in the WUS simulated by global ($2°\times2.5°$, solid circle) and nested ($0.5°\times0.667°$, hollow circle) model compared with observations. The radial distance from the origin is proportional to the standard deviation of a pattern. The centered RMS difference between simulation and observation is proportional to their distance apart. The correlation between them is given by the azimuthal position of the simulation field.

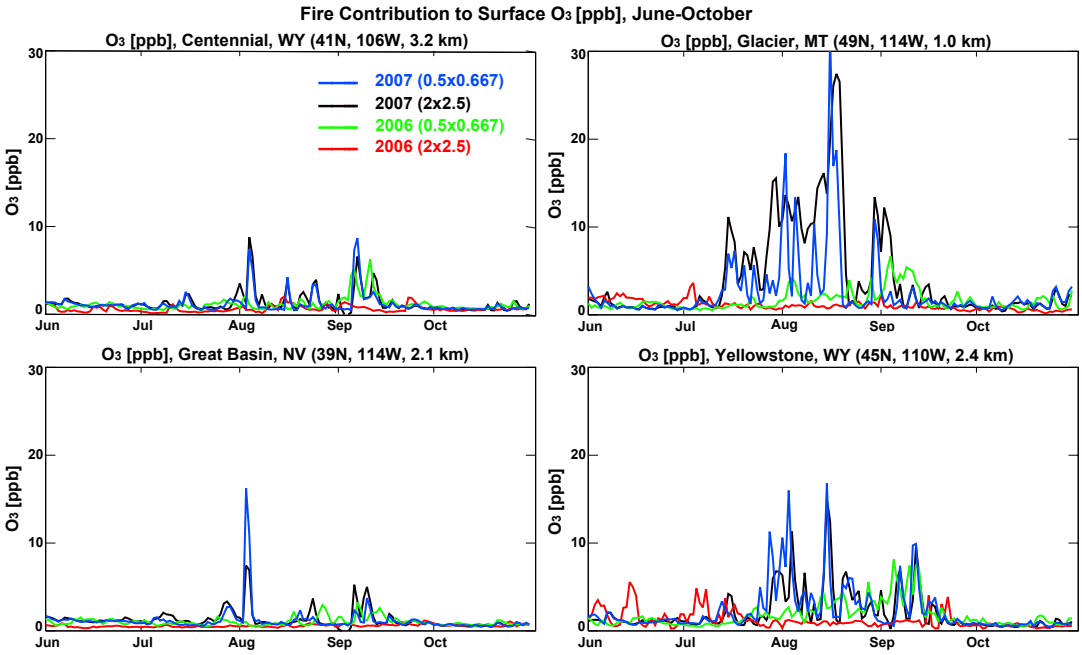

Figure 2.5: GEOS-Chem simulated surface O_3 enhancements from biomass burning emissions for April-December 2006 and 2007 at four CASTNet sites: Centennial, WY (41°N, 106°W, 3.2 km), Glacier, MT (49°N, 114°W, 1.0 km), Great Basin, NV (39°N, 114°W, 2.1 km), Yellowstone, WY (45°N, 110°W, 2.4 km). Values from the simulations with horizontal resolutions 2°×2.5° (black line: 2007; red line: 2006) and with 0.5°×0.667° nested over North America (blue line: 2007; green line: 2006) are shown.

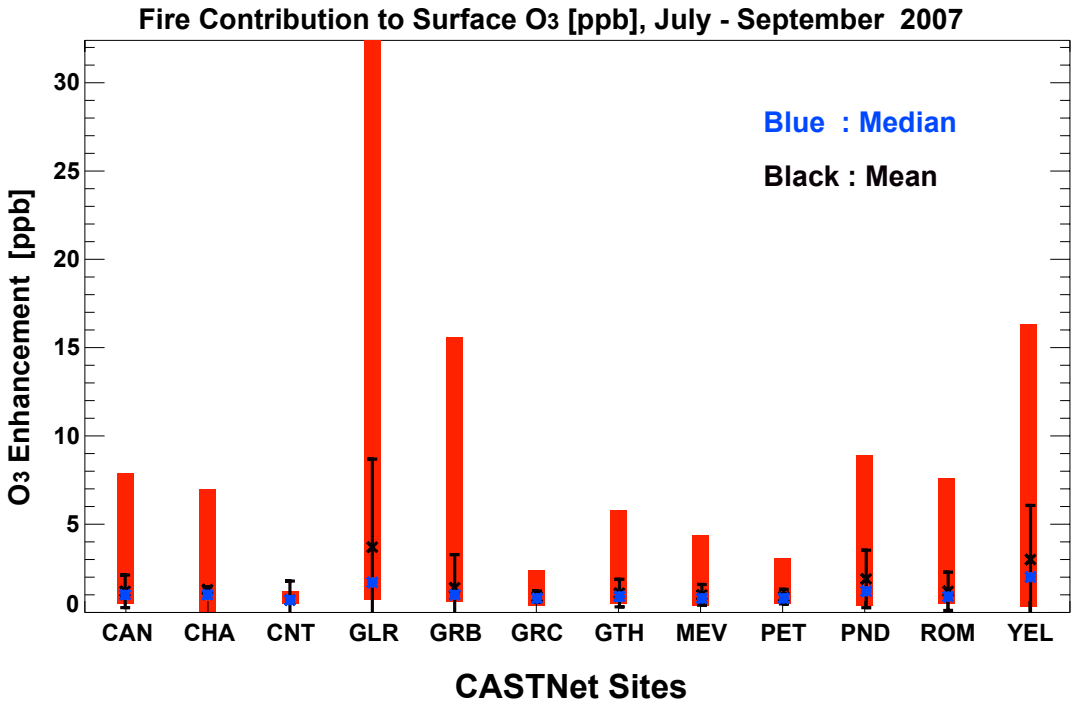

Figure 2.6: GEOS-Chem simulated mean, median, maximun and minimum biomass burning contributions to daily surface O_3 at the CASTNet sites (Fig. 1 and Table 1) for 2007 averaged over July through September. Values from the simulation with $0.5° \times 0.667°$ horizontal resolutions nested over North America are shown.

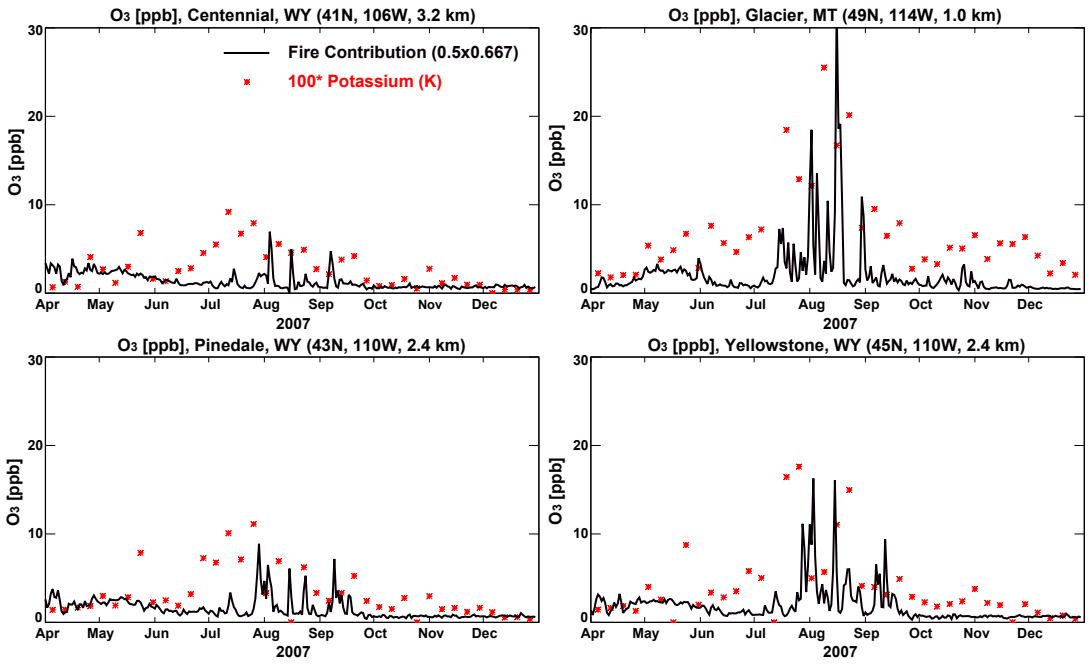

Figure 2.7: GEOS-Chem simulated fire-contributed surface O_3 (lines) and observed potassium (asterisks, values multiplied by 100 for clarity) for April-December 2007 at four CASTNet sites: Centennial, WY (41°N, 106°W, 3.2 km), Glacier, MT (49°N, 114°W, 1.0 km), Great Basin, NV (39°N, 114°W, 2.1 km), Yellowstone, WY (45°N, 110°W, 2.4 km). Model results from the 2°×2.5° model (red line) and the 0.5°×0.667° nested model (blue line) simulations are shown. Unit: ppb.

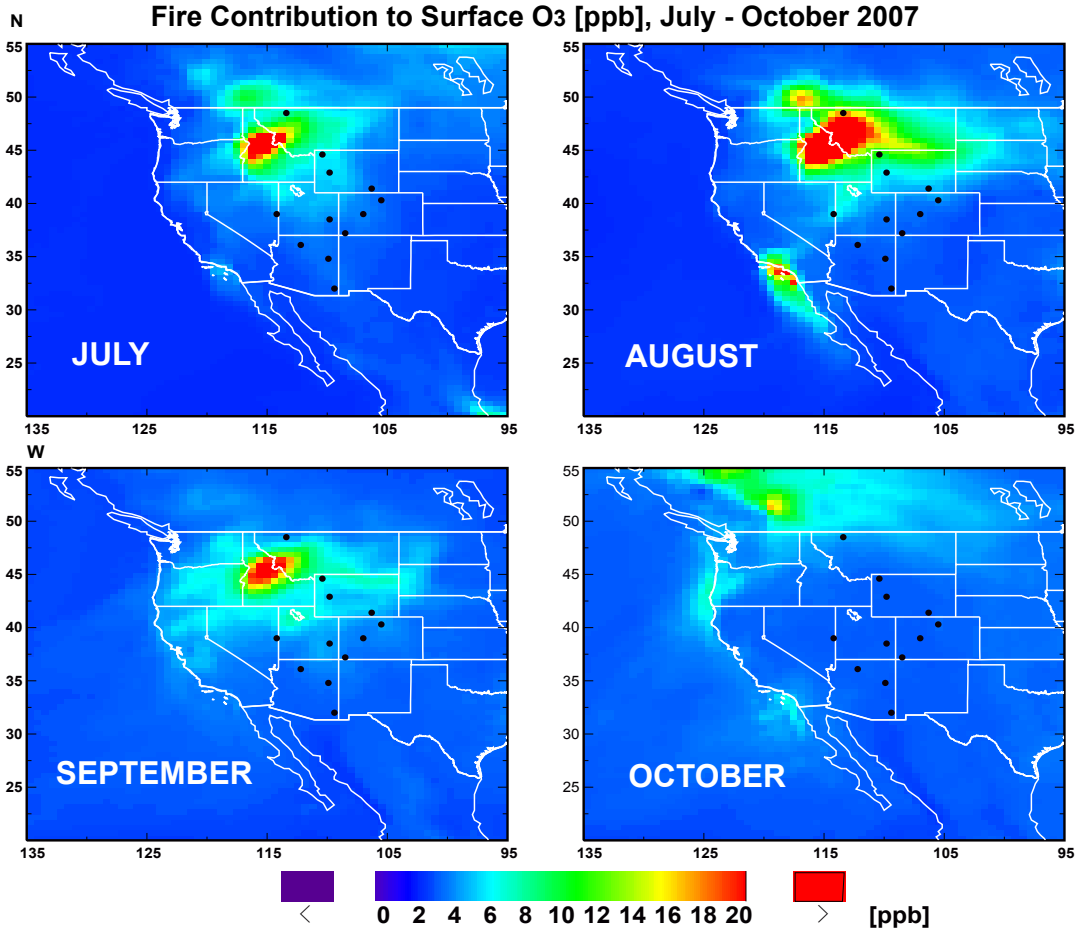

Figure 2.8: GEOS-Chem simulated surface O_3 enhancements from North American biomass burning emissions for July, August, September and October 2007, as determined by difference with sensitivity emissions where North American biomass burning emissions are shut off. Results are from the nested simulations (see text for details). Black dots indicate the 12 CASTNet sites (Fig. 1 and Table 1).

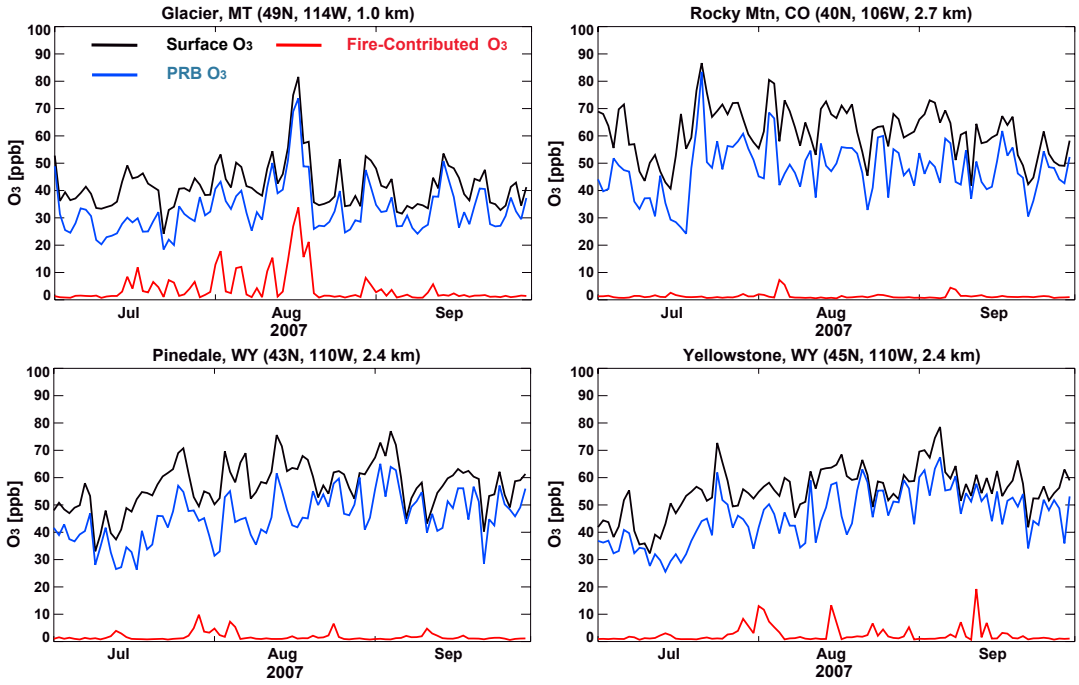

Figure 2.9: GEOS-Chem simulated policy relevant background (PRB) O_3 averaged over the 2007 summer fire season (July through September) at four CASTNet sites: Glacier, MT (49°N, 114°W, 1.0 km), Rocky Mtn, CO (40°N, 106°W, 2.7 km), Pinedale, WY (43°N, 110°W, 2.4 km), Yellowstone, WY (45°N, 110°W, 2.4 km). Also shown are the model simulated surface O_3 and fire-contributed O_3 concentrations. Results are from the nested simulations (see text for details) and values are maximum daily 8-hour averages (MAD8).

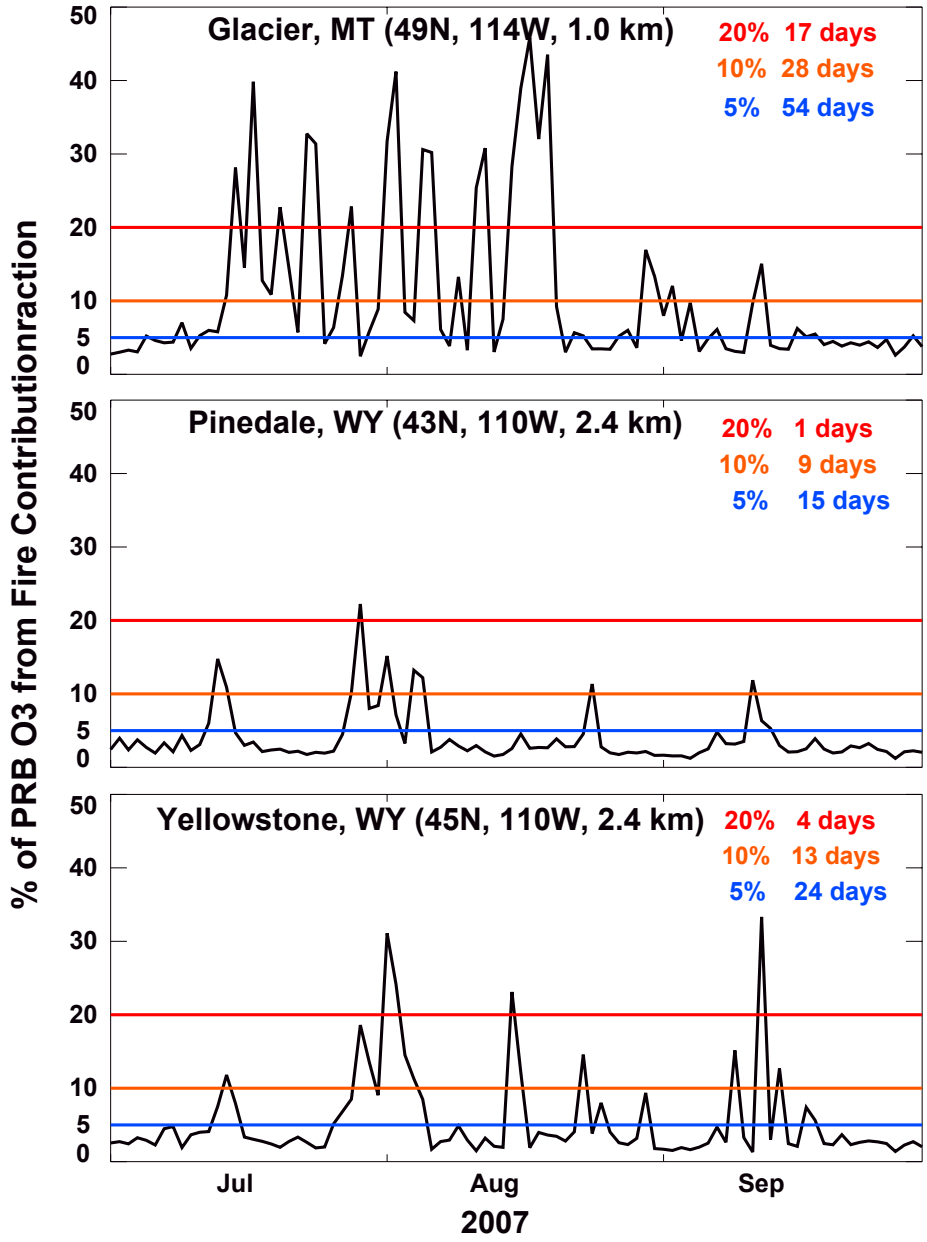

Figure 2.10: Fraction of GEOS-Chem simulated daily fire-contributed O_3 to PRB O_3 during summer fire season (July to September) at three CASTNet sites: Glacier, MT (49°N, 114°W, 1.0 km), Pinedale, WY (43°N, 110°W, 2.4 km), Yellowstone, WY (45°N, 110°W, 2.4 km).Values are maximum daily 8-hour averages (MAD8). Also shown are the number of days when the fire-contributed O_3 accounts for more than 20%, 10% and 5% of the PRB O_3, respectively.

CHAPTER 3

The North American monsoon modulation on summertime ozone in the Southwest

Abstract

We examine an unexpected summertime surface O_3 minimum (∼30-45 ppb) in July-August observed throughout the Southwestern U.S. (SWUS) by interpreting observations of O_3 and rainfall from the Clean Air Status and Trends Network (CASTNet) for 2000-11 with a global chemical transport model. The O_3 minimum reflects competing chemical and dynamic factors as well as anthropogenic and natural influences. Its occurrence corresponds to the interannual rainfall maximum in North American summer monsoon (NASM) -negative surface O_3 anomalies are accompanied by positive rainfall anomalies at the CASTNet sites (r = -0.5 to -0.7, p <0.05). Relative to June 15-July 15, 2007 (prior to the monsoon onset in the SWUS), increased cloudiness during the maximum rainfall in July 15-August 15 (after the onset) weakens photochemistry, reduces O_3 production from anthropogenic emissions, thereby depresses O_3 at the surface (-5 ppb at Chiricahua, AZ and -3 ppb on average across the SWUS) and throughout the lower troposphere. Largest relative changes (ΔO_3) are seen at rainfall maxima, particularly in the core of the Great Plains low-level jet. The corresponding enhancement in lightning (hence NO_x emissions) augments O_3 production in the middle troposphere and subsequent downward mixing in convective downdrafts, thus increases surface O_3 non-negligibly (+2 ppb at Chiricahua and +1 ppb averaged over the SWUS) and significantly throughout the tropospheric column. The resulting ΔO_3 is largest (+8 ppb) in the anti-cyclonic circulation associated with the upper-level high. Weaker photochemistry

dominates the overall ΔO_3 near the surface, while enhanced lightning dominates in much of the free troposphere. Additionally, we find that transport leads to a net export of O_3 throughout the tropospheric column and the influence from stratospheric intrusion is vanishingly small. These competing effects suppress O_3 in the lower troposphere (ΔO_3 up to -5 ppb) while enhance O_3 at higher altitudes (ΔO_3 up to +7 ppb) across the SWUS during the monsoon.

3.1 Introduction

Tropospdsdfsheric ozone (O_3) is formed by the oxidation of hydrocarbons and carbon monoxide catalyzed by nitrogen oxide radicals ($NO_x \equiv NO_2 + NO$) and hydrogen oxide radicals ($HO_x \equiv H + OH +$ peroxy radicals). High surface concentrations of O_3 in populated regions, where emissions of both NO_x and hydrocarbons are large, are a serious air pollution problem. O_3 in the troposphere is also of global interest as a main atmospheric oxidant, a primary source of OH and an effective greenhouse gas OH and an effective greenhouse gas (*Change*, 2007). A fraction of tropospheric O_3 comes from the stratosphere. The major sources of O_3 precursors are anthropogenic (fuel combustion) and natural such as lightning and biomass burning.

The variability in background surface O_3 is a critical issue in the decision making of air quality policy (*McDonald-Buller et al.*, 2011). During the past decades, the U.S. National Ambient Air Quality Standards (NAAQS) for ground-level O_3 have become increasingly stringent. The Environmental Protection Agency (EPA) established primary and secondary NAAQS for ground-level O_3 in March 2008: annual 4th highest daily maximum 8-hour average (MDA8) concentration not to exceed 75 ppb. There are currently 227 counties, home to 123 million people, classified as not having attained the 75 ppb standard (`www.epa.gov/airquality/greenbook/index.html`). In 2015, a new standard proposed by the EPA was issued, further lowering it from 75 to 70 ppb. As the O_3 standard becomes increasingly

stringent, to accurately determine the background O_3 levels becomes more imperative. Policy Relevant Background (PRB) O_3 is the maximum O_3 reduction that can be achieved through controls of North American emissions alone (*EPA*, 2006). From both scientific and regulatory points of view, a lower O_3 standard will motivate air quality-control planners to see more accurate and precise attribution of the background O_3 to determine how much domestic emissions must be reduced in order to attain that standard (*Cooper et al.*, 2014).

Surface O_3 in the western U.S. has trended up (0.19-0.51 ppb yr^{-1}) during the past two decades even though surface O_3 in the eastern U.S. has gone down (*Jaffe and Ray*, 2007; *Cooper et al.*, 2014, 2012). Free tropospheric O_3 in the western U.S. has been steadily increasing (0.41 ± 0.27 ppb yr^{-1}) during the same time period (*Cooper et al.*, 2010). A region of particular interest is the southwestern U.S. (SWUS). Many counties in the SWUS are often close to violating the national O_3 air quality standards (*Wise and Comrie*, 2005; *EPA*, 2006). PRB O_3 is especially high over the intermountain SWUS regions due to the arid terrain, high elevations, and large-scale subsidence in the region (*Zhang et al.*, 2011). PRB O_3 in the SWUS is impacted by many factors including biomass burning (*Jaffe et al.*, 2008; *Jaffe*, 2010), lightning (*Zhang et al.*, 2014) and trans-Pacific transport of Asian pollution (*Parrish et al.*, 2009; *Cooper et al.*, 2010). Meteorological conditions also have large impacts on the variations of surface O_3 air quality in this region [*Wise and Comrie* (2005), and references therein]. Increasing baseline O_3 from trans-Pacific emissions, more frequent wildfire activities during summer fire season, and deep stratospheric intrusions during spring are factors that may prevent the SWUS region from attaining the new EPA O_3 standard (*Cooper et al.*, 2012; *Lin et al.*, 2015).

A defining meteorological event in the SWUS is the recurring North American summer monsoon (NASM). NASM brings 50% of the annual rainfall in New Mexico and Arizona, two states in the SWUS where the monsoonal precipitation is most pronounced in the form of thunderstorms during July-September (*Carleton et al.*, 1990; *Sheppard et al.*, 1999; *Harrington Jr et al.*, 1992). Thunderstorms produced from the monsoon moisture often extend

into the Mojave Desert to the west and the lower Colorado River valley to the north (*Adams and Comrie*, 1997). More broadly, the monsoon influence spans an expanded region from the Sierra Nevada in the west to the Wyoming Rockies and Colorado in the east and reaches as far north as Oregon, the Idaho-Utah border, and Wyoming (*Tang and Reiter*, 1984). The influence of future climate change on both timing and strength of the NASM activities will also conceivably lead to significant impacts on the seasonal and interannual variations of background O_3.

In this study we seek to probe the impacts of the NASM on the surface and tropospheric O_3 in the SWUS mountain ranges. In our analysis we focus on a smaller region, the Four Corners states (114°-104°W and 30°-42°N), which is the core of the SWUS. We would be referring to the Four Corners states (114°-104°W and 30°-42°N) when discussing SWUS in the following sessions. Previous studies have analyzed the influence of monsoon on surface O_3 air quality and meteorological conditions at urban sites (*Wise and Comrie*, 2005; *Agel et al.*, 2011) or in other regions (*Yang et al.*, 2014). To our knowledge, no previous studies have systematically examined such impacts. We focus here on regional to continental scales.

3.2 Observations

We use surface O_3 observations from the Clean Air Status and Trends Network (CASTNet: `http://www.epa.gov/castnet`; *Clarke et al.* (1997)). CASTNet was developed by the U.S. EPA in order to establish an effective, rural monitoring and assessment network at locations away from pollutant emission sources and heavily populated areas (*EPA*, 2008; *Baumgardner*, 1998). Monitoring sites were selected according to strict siting criteria designed to avoid undue influence from point sources, area sources and local activities. CASTNet is spatially designed to be regionally representative of rural conditions (*EPA*, 2008), and the measurements are thus suitable for comparison with regional and global models. O_3 was measured with ultra-violet absorbance (accuracy and precision, 10%) (*EPA*, 2010). CASTNet O_3 data

has been widely used in previous studies of subgrid segregation on O_3 production efficiency in a chemical model (*Liang and Jacobson*, 2000), the variability in surface background O_3 throughout the U.S. (*Lefohn et al.*, 2001; *Fiore et al.*, 2003), and the positive trend in O_3 in the western US (*Jaffe and Ray*, 2007). We use the hourly values that are relevant to evaluating model O_3 responses to synoptic and diurnal variability. We also calculate MDA8 O_3 from the hourly data. We choose sites with missing data less than 15 days per year and exclude the coastal sites, yielding 12 sites in the western US (seven of which are in the SWUS) for year 2007 (Table 3.1). Most of the sites are elevated mountainous sites, scattered across the Sierra Nevada/Cascades Mountains and the Rocky Mountains.

CASTNet also provides meteorological data such as precipitation. Precipitation is recorded to the nearest 0.01 inch. The hourly values are pertinent to examining synoptic and diurnal variabilities. Additionally, precipitation data from the Global Precipitation Climatology Project (GPCP, 1°×1°) (*Adler et al.*, 2003) and the Climate Prediction Center merged Analysis of Precipitation (CMAP, 2.5°×2.5°) (*Xie et al.*, 2003) are examined.

3.3 Model description and simulations

We use a global 3-D chemical transport model (GEOS-Chem, v8-02-03, available at `http://geos-chem.org`) [*Bey et al.* (2001); many updates thereafter] to interpret the CASTNet observations. The model is driven by GEOS-5 data assimilation system (DAS) meteorological fields from the NASA Global Modeling and Assimilation Office (GMAO) with a temporal resolution of 6-hour (3-hour for surface variables and mixing depths) and consists of 47 levels in the vertical up to 0.01 hPa. The lowest model levels are centered at approximately 60, 200, 200, 300, 450, 600, 700, 850, 1000, 1150, 1300, 1450, 1600, 1800 m in GEOS-5. We run the model at 2°×2.5° globally and at 0.5°×0.667° nested resolution over North America (140°-40°W, 10°-70°N). Description of the nested model was first provided by citepwang2011seasonal.

Tracer advection is calculated using a flux-form semi-Lagrangian method (*Lin and Rood*, 1996)every 15 minutes. Following (*Allen et al.*, 1996a,b), tracer moist convection is computed using GEOS-5 convective, entrainment, and detrainment mass fluxes. Treatment for shallow convection is using citephack1994climate and parameterization of deep convection follows the relaxed Arakawa-Schubert scheme (*Moorthi and Suarez*, 1992).

GEOS-Chem includes detailed ozone-NO_x-hydrocarbon-aerosol chemistry. Tropospheric O_3 is simulated with about 80 species and over 300 chemical reactions (*Bey et al.*, 2001). Photolysis rates are computed using the fast-J algorithm (*Wild et al.*, 2000). The O_3 simulation over the U.S. has been extensively evaluated (*Wang et al.*, 2009; *Zhang et al.*, 2010; *Walker et al.*, 2010; *Parrington et al.*, 2008). Anthropogenic emissions are as described by (*Zhang et al.*, 2011). Global anthropogenic emissions are from the Emission Database for Global Atmospheric Research (EDGAR) inventory for 2000, superseded by regional emission inventories from the U.S. EPA 2005 National Emission inventory (NEI-05) for the U.S., the European Monitoring and Evaluation Program (EMEP) for Europe, the Canada Criteria Air Contaminates (CAC) emission inventory for Canada, and the Big Ben Regional Aerosol and Visibility Observational (BRAVO) emission inventory for Mexico. Biogenic emissions are based on the Model of Emissions of Gases and Aerosols from Nature (MEGAN) inventory (*Guenther et al.*, 2006).

Lightning NO_x emissions are computed locally in deep convection events (*Price and Rind*, 1992), where flash rates are related to convective cloud top heights. NO_x yields per flash are 260 moles in the tropics and 500 moles in the extra-tropics (*Huntrieser et al.*, 2007, 2008; *Hudman et al.*, 2007; *Ott et al.*, 2010). The vertical distribution of lightning emissions follow (*Pickering et al.*, 1998). In this work, we use the higher density National Lightning Detection Network data (*Christian et al.*, 2003) for the continental U.S. to constrain lightning flash rates, following (*Zhang et al.*, 2014). NLDN observes cloud-to-ground lightning flashes only, and intra-cloud flashes are estimated to be three times that amount (*Boccippio et al.*, 2001). The constfeferaint largely corrects excessive lightning flash rates and consequently high bias

of surface O_3 in the SWUS in previous GEOS-Chem simulations (*Zhang et al.*, 2011, 2014).

Biomass burning emissions are from the daily Global Fire Emission Database version 3 (GFEDv3) (*Giglio et al.*, 2013; *van der Werf et al.*, 2006). GFEDv3 is derived using satellite observations including active fire counts and burned areas in conjunction with the Carnegie-Ames-Stanford-Approach (CASA) biogeochemical model. Carbon emissions are calculated as the product of burned area, fuel loading and combustion completeness. Burned area is derived using the active fire and 500-meter burned area datasets from the Moderate Resolution Imaging Spectroradiometer (MODIS) as described by (*Giglio et al.*, 2013). The NO_x emission factors for extra-tropical forest fires are updated following (*Alvarado et al.*, 2010).

We conduct model simulations for 2006, 2007, and 2008 and focus our analysis on 2007. Justifications are provided where appropriate in subsequent sections. We first conduct a global simulation at $2^\circ \times 2.5^\circ$, and then use the output archived at 3-hour temporal resolution as dynamic boundary conditions for the nested model at $0.5^\circ \times 0.667^\circ$ resolution. A three-month initialization is used in all cases. We find that the results from the simulations at $2^\circ \times 2.5^\circ$ and $0.5^\circ \times 0.667^\circ$ are rather comparable and the results presented hereinafter are from the $2^\circ \times 2.5^\circ$ simulations. Additionally, we conduct two separate model simulations with lightning NO_x emissions shut off and with anthropogenic emissions turned off. The difference between these and the standard simulations thus represents the contributions to surface O_3 from lightning and from anthropogenic emissions. We also conduct a tagged O_3-tracer simulation (*Zhang et al.*, 2014) to compute stratospheric downward flux of O_3. Discussions and justifications for these simulations are provided where appropriate. We extract model results at the location and time of CASTNet observations and apply the same temporal averaging for both observed and simulated O_3 concentrations. Results presented here are daily MAD8 O_3 concentrations unless stated otherwise.

3.4 Impacts of NASM on summertime surface O_3 in the SWUS

Fig. 3.1 shows observed and simulated O_3 concentrations during June-October 2007 at Chiricahua, AZ (32°N, 109°W, 1.6 km), Petrified Forest, AZ (35°N, 110°W, 1.7 km), Gothic, CO (39°N, 107°W, 3.0 km) and Mesa Verde, CO (37°N, 108°W, 2.2 km), four CASTNet sites in the SWUS. Model results are generally within 2 ppb of the observations (r = 0.5-0.73, p <0.001, Fig. 3.2) and largely reproduce the observed day-to-day variations. The sharp decreases in late July-early August at all four sites, however, are surprising in the middle of summer when peak O_3 levels are typically expected (*Trainer et al.*, 1993; *Jaffe and Ray*, 2007; *Parrish et al.*, 2013; *Cooper et al.*, 2014). The decreases are evident in both the observations and in the model results. Such decreases are also apparent in the modeling study of (*Zhang et al.*, 2014). We find that these decreases are unique to the SWUS - surface O_3 anomalies, calculated as the deviation from the annual mean, during late July-early August are much more pronounced (∼4 ppb lower on average) at the seven SWUS sites than at the other western U.S. sites (not shown here).

The distinct decreases in surface O_3 coincide with the maximum intensity of the NASM, a period characterized by enhanced rainfall maxima over western Mexico and throughout much of the SWUS. The typical onset of the monsoon is in early July in Arizona and New Mexico. It reaches maturity in July and August with the development of a 'monsoon high' at the jet stream altitude (∼10 km above sea level) (*Adams and Comrie*, 1997) before decaying in September and October (*Sheppard et al.*, 1999). We use here precipitation as a proxy to examine both the seasonal and interannual variability of the monsoon, because one of the most recognizable features of the NASM is the associated rainfall pattern. The strongest July-August precipitation during 2000-2011 is in 2007 at Chiricahua (Fig. 3.3, left and Fig. 3.5) and in 2006 at Gothic (Fig. 3.3 right). The onset and the duration of the peak monsoon activities vary from year to year. Precipitation is strongest during late July-early August of 2007 at Chiricahua and during early July-mid August in 2006 at Gothic (Fig. 3.3), a manifestation of the peak monsoon activities. The sharp decreases in surface O_3

concentrations correspond to the maximum precipitation at both sites (Fig. 3.3). The anti-correlation between O_3 and precipitation is seen not only at these two sites but also at the other seven SWUS sites (r = -0.38 $\sim$ -0.67). These results clearly point toward a strong modulating effect of the NASM on the surface O_3 in the SWUS.

Since the typical onset of the NASM in the SWUS region is usually in July [`http://www.cpc.ncep.noaa.gov`], here we loosely defined a monsoon season as July 15-August 15, 2007 and a pre-monsoon season as June 15-July 15, 2007. They are used in this study more as a contrast to investigate the effect of monsoon modulation. In order to investigate the impacts of NASM on O_3 concentration in the continental SWUS, we show in Fig. 3.4 (left) the simulated spatial distribution of MAD8 surface O_3 concentrations changes between monsoon period and pre-monsoon period. Values are calculated by subtracting the simulated surface O_3 concentration averaged over June 15-July 15, 2007 from the surface O_3 concentration averaged over July 15-August 15, 2007. Region in rectangle is the Four Corners states (114°-104°W and 30°-42°N), which is loosely referred to as SWUS in the following analysis. Relative to the concentrations during pre-monsoon period, surface O_3 levels during monsoon period are generally lower across the SWUS. The decreases are most visible in Arizona and New Mexico, where surface O_3 concentration could decrease by more than 8 ppb. The decrease also extends to the lower and middle part of Utah and Colorado, where we observe a reduction around 2-4 ppb. Both the Great plains low-level jet (GPLLJ) and the Gulf of California low-level jet (GCLLJ) are important part of the North American monsoon circulation and are responsible for the convective activities associated with the circulation (*Helfand and Schubert*, 1995; *Higgins et al.*, 1997). The GPLLJ transports moisture from the Gulf of Mexico to the Great Plains and the GCLLJ transports moisture through the Gulf of California to northwestern Mexico and the SWUS region (*Mo et al.*, 2005). The combined effect of these low level jets in the monsoon circulation produced a pronounced increase in rainfall over large areas of northwestern Mexico and the SWUS during the summer monsoon season (*Bordoni et al.*, 2004). As indicted in Fig. 3.4 (left), the region with decreasing

O_3 in the SWUS is consistent with the northern part of the core regions of the North American monsoon circulation (*Adams and Comrie*, 1997). On average, the decrease in surface O_3 across the SWUS region during monsoon period is about 5 ppb, compared to the pre-monsoon period. Fig. 3.4 (right) is pressure -longitude plots of the O_3 changes averaged over the latitude range of 30°-42°N. From surface to about 600 hPa, O_3 concentrations during July 15-August 15, 2007 are lower across the SWUS than during June 15-July 15, 2007. While at 600 hPa levels and above, the changes in O_3 exhibit increases during the monsoon period. We will provide a detailed analysis of different factors controlling the O_3 change during NASM in the following sections.

3.5 Impacts of NASM on the interannual variations of summertime O_3 in the SWUS

We analyze here CASTNet surface O_3 and precipitation anomalies at Chiricahua for July-August 2000-2011 (Fig. 3.5, left). The anomalies are 5-day averages relative to the respective 12-year means. We choose 5-day averages to be temporally consistent with the pentad GPCP data. Positive precipitation anomalies are largest in 2006, 2007, and 2008, reflecting stronger monsoon activities in those years. Maximum (minimum) precipitation anomaly is consistently accompanied by minimum (maximum) surface O_3 anomaly. The anti-correlation is most significant in 2006 (r = -0.70, p <0.05), 2007 (r = -0.47, p <0.05) and 2008 (r = -0.71, p <0.05), when both precipitation and O_3 anomalies are largest, as shown in further details in Fig. 3.5 (right panels).

We now focus our analysis on 2006, 2007, and 2008. First, we determine the strongest monsoon activities in the SWUS using GPCP and CAMP precipitation data. Specifically, we calculate the precipitation anomalies relative to the 5-day moving averages of 2000-2011 during June-September (not shown). We find that the summer monsoon is strongest during July 20-August 15 in 2006, July 20-August 5 in 2007 and August 1-20 in 2008. The

corresponding CASTNet O_3 and precipitation anomalies at Chiricahua are shown in Fig. 3.5 (lower right). Linear regressions yield negative slopes for all three years with 2007 being the strongest. We find similar negative correlations at other CASTNet sites in the SWUS (not shown), indicating that the modulation is regional throughout the SWUS region.

Previous studies have noted the marked variability of the NASM (*Carleton et al.*, 1990). The interannual variability results in part from the latitudinal shift of the middle level subtropical ridge over the SWUS hence is strongly associated with the Madden-Julian Oscillation (MJO), Pacific-North American (PNA) teleconnection and El Nino-Southern Oscillation (ENSO) (*Adams and Comrie*, 1997). As the hottest and driest region in the U.S., the SWUS has and will face great challenges from climate change with increased heat, sustained drought and changes in rainfall and snowpack pattern (*Pachauri et al.*, 2014). It is well known that climate change driven by rising greenhouse gases will cause a reduction of winter precipitation in the SWUS (*Seager and Vecchi*, 2010). (*Cook and Seager*, 2013) used a suite of models from the Coupled Model Intercomparison Project version 5 (CMIP5) (*Taylor et al.*, 2012) and predicted significant declines in early monsoon season precipitation (June-July) and increases in late monsoon season (September-October) precipitation. This shift in seasonality toward delayed onset and withdrawal of the NASM is caused by the change in vertical stability and moisture convergence associated with the future climate. We thus further examine the interannual variability of the NASM using precipitation data over the SWUS. We use GPCP precipitation data here because CMAP data shows interannual variability that is broadly consistent with that from the GPCP data. Specifically, we analyze GPCP precipitation anomaly during June-September for 2000-2011, averaged over the SWUS (Fig. 3.6, left). The anomaly is calculated as the deviation of the total pentad precipitation from the 12-year average. The strongest positive precipitation anomaly is in 2006 and to a lesser degree in 2004, 2007 and 2008. Such interannual variability is seen not only in the precipitation anomaly but also in the total precipitation (Fig. 3.6, right). The NASM index (NASMI) proposed by (*Jianping and Qingcun*, 2003) affirms such interannual

variability, with negative indices indicating strong monsoon years (Fig. 3.6, right). This is consistent with the observed interannual variations of precipitation anomaly at individual CASTNet sites. At Chiricahua, for example, strong positive precipitation anomalies are also in 2006, 2007 and 2008 (Fig. 3.5).

3.6 Processes controlling summertime surface O_3 in the SWUS

(*Zhang et al.*, 2014) quantified the contribution from different processes controlling surface O_3 in the western U.S. including lightning, stratospheric intrusion and wildfires using GEOS-Chem. They found that lightning increased surface O_3 by 6-8 ppbv on average in the Intermountain West. They concluded that the highest observed O_3 concentrations in the region (>75 ppb) in spring were associated with stratospheric intrusions. Their model results showed high O_3 events (in excess of 80 ppb) associated with wildfire emissions, though such events were not seen in the observations. In this section we focus on the processes controlling surface O_3 in the SWUS, particularly the effects of the NASM. It is conceivable that the NASM modulates surface O_3 directly or indirectly through reducing O_3 photochemistry because of increased cloudiness and enhancing lightning emissions of NO_x and subsequent O_3 production followed by vertical mixing in convective updrafts and downdrafts. Widespread cloudiness prevailing during the monsoon season greatly attenuates the solar radiation reaching the surface, likely resulting in substantially reduced photochemical production of surface O_3 (*Garreaud and Wallace*, 1997; *Xu and Small*, 2002). Lightning is known to be a predominant source of NO_x hence O_3 production in the middle and upper troposphere over most regions in the U.S. (*Pickering et al.*, 1998; *Martin et al.*, 2007; *Hudman et al.*, 2007). (*Kaynak et al.*, 2008) found a 1.7 ppb enhancement due to lightning to the 8-hour background surface O_3 concentration averaged over the continental U.S., less than the 6-8 ppb enhancement in the Intermountain West estimated by (*Zhang et al.*, 2014). Convective downdrafts are known to transport lightning NO_x emissions downward thereby increasing surface NO_x concentrations (*Murazaki and Hess*, 2006). (*Pickering et al.*, 1998) shows that the convective

downdrafts that descend and flow near the surface would bring a portion of the lightning emitted NO_x and therefore lead to O_3 formation in the boundary layer. On the other hand, when this lightning-derived NO_x is found later in the afternoon or into the evening, it may result in depressed surface O_3 due to both nighttime chemistry and direct titration, which further reduces O_3 and result in much NO_x depletion (*Kaynak et al.*, 2008; *Russell et al.*, 1986).

To delineate the various factors determining the surface O_3 during the monsoon, we examine the pertinent parameters including cloud optical depth, shortwave radiation, NO_2 photolysis rate and net O_3 production. Model results capture the sharp decreases in surface O_3 at Chiricahua during late July-early August 2007 while the monsoon is at its maximum strength as indicated by the maximum rainfall (Fig. 3.7, left). The abrupt decreases coincide with maxima in cloud optical depth, reflecting increased cloudiness hence weaker photochemistry. The weaker photochemistry is further borne out by the large reductions in downward solar radiation at the surface hence substantially lower photolysis rates of NO_2 (13:00-17:00 pm local time averages). The lower photolysis rates result in significantly lower net O_3 production (up to $\sim$10 ppb reduction per day).

Additionally, we decompose the major contributions to surface O_3 from anthropogenic emissions, lightning NO_x emissions and stratospheric intrusions. The results are shown in Fig. 3.7 (right). On average, the contribution from anthropogenic emissions is $\sim$20 ppb during June-August, while that from lightning is from a few ppb to about 10 ppb. This is broadly consistent with previous studies (*Pfister et al.*, 2008; *Hudman et al.*, 2009). (*Hudman et al.*, 2009), for example, showed that the boundary layer O_3 enhancement in the U.S. was mainly anthropogenic, but the free troposphere has roughly equal enhancements from anthropogenic emissions and lightning NO_x. Fig. 3.7 shows that the contribution from anthropogenic emissions to surface O_3 is significantly suppressed ($\sim$5 ppb reduction on average) during late July-early August as a result of weaker O_3 photochemistry. There is a $\sim$2 ppb contribution from lightning NO_x emissions and subsequent O_3 production followed

by downward transport in the downdrafts of deep convective events (*Pickering et al.*, 1998; *Murazaki and Hess*, 2006; *Lelieveld and Crutzen*, 1994). The influence of stratospheric intrusion is vanishingly small. Previous studies have identified about 20-30% increases in upper tropospheric O_3 and 2% increase in middle troposphere at northern mid-latitude due to stratosphere-troposphere-exchange, the increases are mostly in winter and spring (*Langford*, 1999; *Zeng and Pyle*, 2005; *Koumoutsaris et al.*, 2008; *Neu et al.*, 2014). (*Lin et al.*, 2015) also showed that O_3 enhancements due to stratospheric intrusion did not reach the surface in the Western U.S. in summer.

3.7 The impact on summertime tropospheric O_3 in the SWUS

It is conceivable that the aforementioned processes effect changes on summertime O_3 not only at the surface but also in the free troposphere in the SWUS. We examine here the changes to O_3 before the monsoon onset (June 15-July 15, 2007) and after (July 15-August 15, 2007). The results are shown in Fig. 3.4, both at the surface and averaged over the latitudes 30°-42°N over the SWUS (the rectangle in Fig. 3.4). Reduction in O_3 is seen throughout much of the lower troposphere up to 500 hPa, with largest changes between the surface and 750 hPa. Largest changes in O_3 (Fig. 3.4, left) are collocated with maximum rainfall as inferred from both GPCP and GEOS-5 precipitation (figures not shown). The core of the largest changes is between 110°W and 115°W, corresponding to the core regions of the GCLLJ [*Mo and Berbery* (2004), and references therein]. The absolute changes in O_3 ($|\Delta O_3|$) increases from the east to the west, following the increasing amount of rainfall (Fig. 3.4, right).

To understand how different factors may influence the O_3 concentration at different altitudes during NASM, we examine the vertical profile of ΔO_3 associated with anthropogenic emissions and lightning NO_x emissions. The results, both at the surface and in the free troposphere (averaged over the SWUS), are shown in Fig. 3.8. As a result of increased

cloudiness and therefore reduced O_3 photochemistry during NASM, we observe a decrease in anthropogenic contribution to O_3 concentrations at the surface. The largest O_3 reduction region is located in New Mexico and Arizona, where O_3 decrease reaches up to 6 ppb. The decrease in surface O_3 also extends to lower part of Colorado and Utah, with smaller magnitude. On average, ΔO_3 associated with anthropogenic contribution is about 3ppb across the SWUS region at surface. From surface to about 500 hPa, O_3 production from anthropogenic emissions is lower during the NASM period. The decrease peaks at 600 hPa. It is also interesting to note that anthropogenic contribution to O_3 increases during NASM at levels above 500hPa. This increase is likely caused by two processes. The first is the higher temperature in the middle and upper troposphere during monsoon period compared to pre-monsoon period. The second is the increase in actinic flux in the middle and upper troposphere resulted from the increased cloudiness and therefore increased albedo from clouds below. A more detailed analysis of the impacts from these two processes needs to be conducted in future researches.

O_3 production from lightning NO_x associated with the monsoon is predominantly in the middle and upper troposphere (*Wang et al.*, 2013; *DeCaria et al.*, 2005; *Pickering et al.*, 1993). (*Cooper et al.*, 2006, 2007) estimated that ∼11-13 ppb O_3 was produced due to lightning NO_x above Eastern North America at middle latitudes during the summer of 2004. Fig. 3.8 (bottom) shows the changes in lightning contribution to O_3 during monsoon period in the SWUS at surface (Fig. 3.8 bottom left) and across the troposphere (Fig. 3.8 bottom right, pressure-longitude plot averaged over 30°-42°N). Again values in the figure are calculated by subtracting the averaged lightning contribution to O_3 concentration during pre-monsoon period from the averaged lightning contribution to O_3 concentration during monsoon period. Due to the enhanced lightning NO_x emission in the convection activities during NASM, O_3 production due to lightning NO_x emissions increased from surface all the way up to the upper troposphere. The average increase of surface O_3 concentration is about 1.2 ppb across SWUS. This is consistent with the study by (*Kaynak et al.*, 2008). They

found a 1.7 ppb enhancement to background surface O_3 concentration averaged over the continental U.S. The maxima of the increase in lightning NO_x induced O_3 production occurs at about 550 hPa (+9 ppb), corresponding to the level of the 'Four-corners' High in the anticyclone circulation associated with NASM. This mid-level high pressure system forms over northeastern Arizona and can help guide mid-level moisture in around the high from the northeast and east that may be in place from monsoon thunderstorm activity over the SWUS region (*Crimmins*, 2006). As we discussed earlier, (*Cooper et al.*, 2006) estimated 11-13 ppb of O_3 produced due to lightning NO_x emission. Our result of 9 ppb here is the increase in lightning production of O_3 during the monsoon period compared to the pre-monsoon period defined in this study, instead of the absolute value of O_3 production from lightning, as calculated in (*Cooper et al.*, 2006). The other reason contributing to the difference is that, the lightning NO_x emissions is most predominant along a band stretching along the northern coast of the Gulf of Mexico, extending across Florida and into the westernmost North Atlantic Ocean off the southeastern U.S. The lightning NO_x emission over the Sierra Madre Mountains is also prevalent but is less than the eastern U.S. region (*Cooper et al.*, 2006).

We analyze transport, deposition, and net production of O_3 in determining the budget of tropospheric O_3 over SWUS (from the surface to 500 hPa), focusing on July 15-August 15, 2007. The model results, averaged for the aforementioned period, are summarized in Fig. 3.9. The prevailing winds in the region are westerlies and southerlies during the monsoon (*Barlow et al.*, 1998). The widespread convective activities during the monsoon produces a net upward export of O_3 (213 kg s^{-1}) out of the domain, which is a stark contrast to the net import (downward transport) associated with the typical large-scale subsidence over the SWUS prior to the monsoon onset (*Barlow et al.*, 1998). In total, transport reduces tropospheric O_3 over the SWUS (an overall net export of 53 kg s^{-1}). Deposition accounts for a large fraction of O_3 loss (343 kg s^{-1}), smaller than but comparable to the net O_3 production (430 kg s^{-1}). It is informative to examine the changes in these terms before and after the

onset of the monsoon by contrasting June 15 -July 15 and July 15-August 15. The net production of O_3 is substantially lower (by 78 kg s^{-1}) in the later because of the increased cloudiness hence weaker photochemistry. A large change in the net export of O_3 (-227 kg s^{-1}) reflects primarily the contrasting subsidence over the SWUS pre-onset and the upwelling after the onset of the monsoon. Deposition remains relatively unchanged.

The combined effects of transport and the O_3 production associated with anthropogenic emissions and lightning on the tropospheric O_3 over the SWUS are summarized in Fig. 3.10. The results shown are again the changes, i.e., ΔO_3, between June 15-July 15 and July 15-August 15 and averaged for the tropospheric column over the region. Increased lightning NO_x emissions during the monsoon elevate O_3 (relative to pre-onset levels) throughout the tropospheric column, with a maximum enhancement at ∼550 hPa. The weaker photochemistry post-onset depresses O_3 production from anthropogenic emissions for much of the lower troposphere (up to 500 hPa), with a maximum reduction at 600 hPa. The combined effect of the two processes is reducing O_3 at the surface and throughout the lower troposphere but increasing O_3 at higher altitudes (above 750 hPa). The decrease in O_3 production from anthropogenic emissions is the leading factor in the O_3 change in the lower troposphere, while the increase in lightning NO_x emissions induced O_3 production is dominant at higher altitudes. Transport reduces O_3 at all vertical levels over the SWUS. At the surface, net export accounts for about two thirds of the ΔO_3, while the combined effect of anthropogenic and lightning accounts for the rest. The change in dry deposition (not shown) is negligibly small.

3.8 Summary and conclusions

We investigated the seasonal and inter-annual variations of the modulation of NASM on surface O_3 concentrations in the SWUS by examining the relationship between observed surface O_3 anomalies and precipitation anomalies for multiple years. Results showed a strong

anti-correlation (r = -0.5 to -0.7) in strong monsoon years, indicating stronger negative impacts on surface O_3 levels induced by higher intensity of precipitation and convective activities during the monsoon.

We used GEOS-Chem simulations to analyze the primary processes closely related to the monsoon that may cause the variations in surface O_3: the reduced photochemistry resulted from cloud coverage increase and the enhanced NO_x from lightning emissions. We found that the sudden decrease in surface O_3 is mainly caused by the reduction in O_3 photochemistry associated with the increase in cloud coverage in the convective activities during the monsoon. The increase in lightning emission during the monsoon periods caused an average of $\sim$2 ppb increase in surface O_3, but this is not sufficient to offset the reduction due to less photolysis.

We also investigated the O_3 change during NASM at different vertical levels associated with these processes. In lower troposphere, the decrease in O_3 production from anthropogenic emission is the leading factor in O_3 concentration change. As altitude increases, the increase in lightning NO_x induced O_3 production becomes the leading factor. These competing effects suppress O_3 in the lower troposphere (ΔO_3 up to -5 ppb) while enhance O_3 at higher altitudes (ΔO_3 up to +7 ppb) across the SWUS during NASM. Additionally, we find that transport leads to a net export of O_3 throughout the tropospheric column and the influence from stratospheric intrusion is vanishingly small.

The future climate may lead to changes in both the spatial and seasonal pattern, as well as strength of the NASM. Since the 2015 new O_3 standard is just adopted, to understand the modulation of NASM on the surface and tropospheric O_3 over the SWUS may have important implication on how to more accurately estimating the background O_3 in the context of future climate change.

Acknowledgement: This study was funded by NASA grants NNX09AF07G, NNX08AF64G from the Atmospheric Chemistry Modeling and Analysis Program (ACMAP). We thank all the contributors to the CASTNet observation, GPCP and CMAP data. Users can access the data from this paper via the authors without any restrictions.

Table 3.1: Selected sites from the Clean Air Status and Trends Network (CASTNet, `http://www.epa.gov/castnet`).

Site	**Latitude** (°N)	**Longitude** (°W)	**Elevation (km)**
Canyonlands, UT (**CAN**)	38.46	109.82	1.8
Centennial, WY (**CNT**)	41.36	106.24	3.18
Chiricahua, AZ (**CHA**)	32.01	109.39	1.57
Glacier, MT (**GLR**)	48.51	113.99	0.98
Great Basin, NV (**GRB**)	39.01	114.22	2.06
Grand Canyon, AZ (**GRC**)	36.06	112.18	2.07
Gothic, CO (**GTH**)	38.96	106.99	2.93
Mesa Verde, CO (**MEV**)	37.2	108.49	2.17
Petrified Forest, AZ (**PET**)	34.82	109.89	1.72
Pinedale, WY (**PND**)	42.93	109.79	2.39
Rocky Mtn, CO (**ROM**)	40.28	105.55	2.74
Yellowstone, WY (**YEL**)	44.56	110.4	2.4

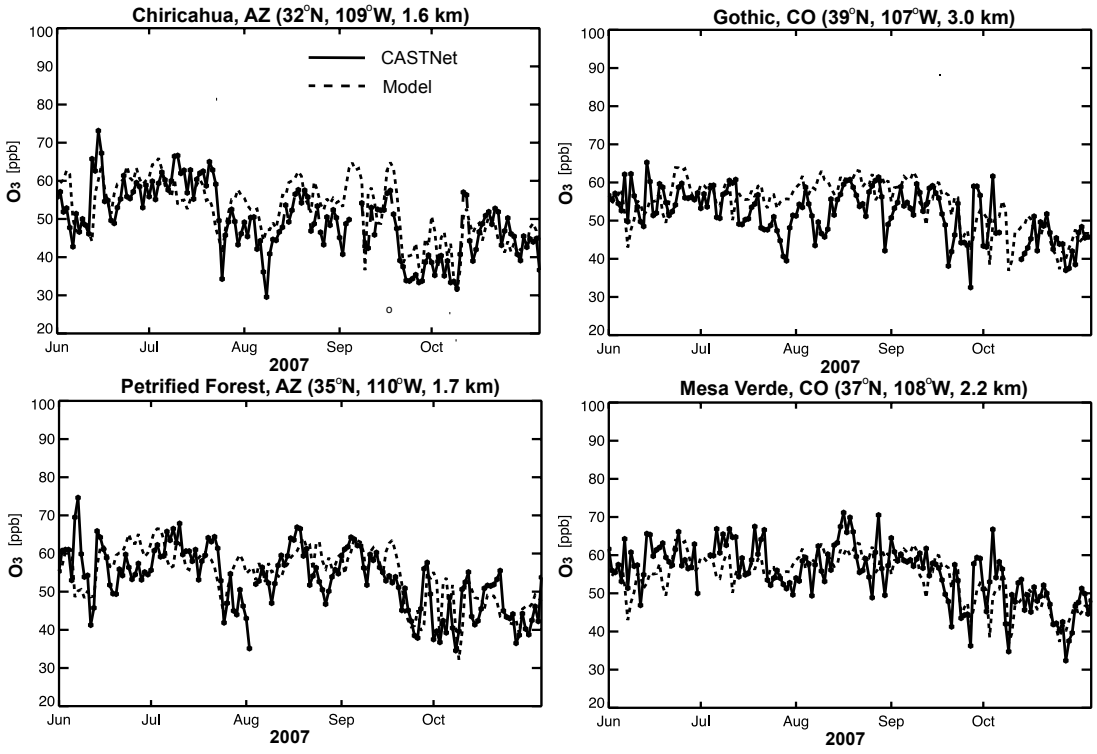

Figure 3.1: Observed (solid line) and GEOS-Chem simulated (dotted line) surface O_3 (ppb) for June-October 2007 at Chiricahua, AZ (32°N, 109°W, 1.6 km), Gothic, CO (39°N, 107°W, 3.0 km), Petrified Forest, AZ (35°N, 110°W, 1.7 km), and Mesa Verde, CO (37°N, 108°W, 2.2 km). Observations from the Clean Air Status and Trends Network (CASTNet, available at `http://www.epa.gov/castnet`). Values are maximum daily 8-hour averages (MDA8).

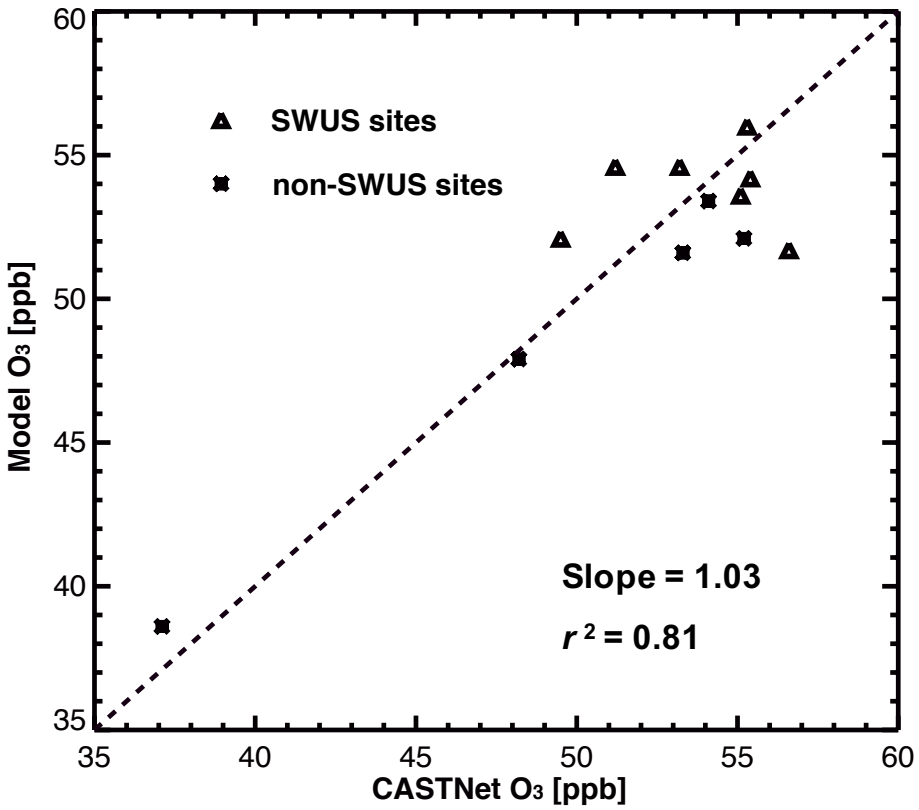

Figure 3.2: Observed and GEOS-Chem simulated surface O_3 (MDA8, ppb), averaged for June-October 2007, at selected CASTNet sites (Table 1). Correlation coefficients range from 0.50 to 0.73 for individual sites.

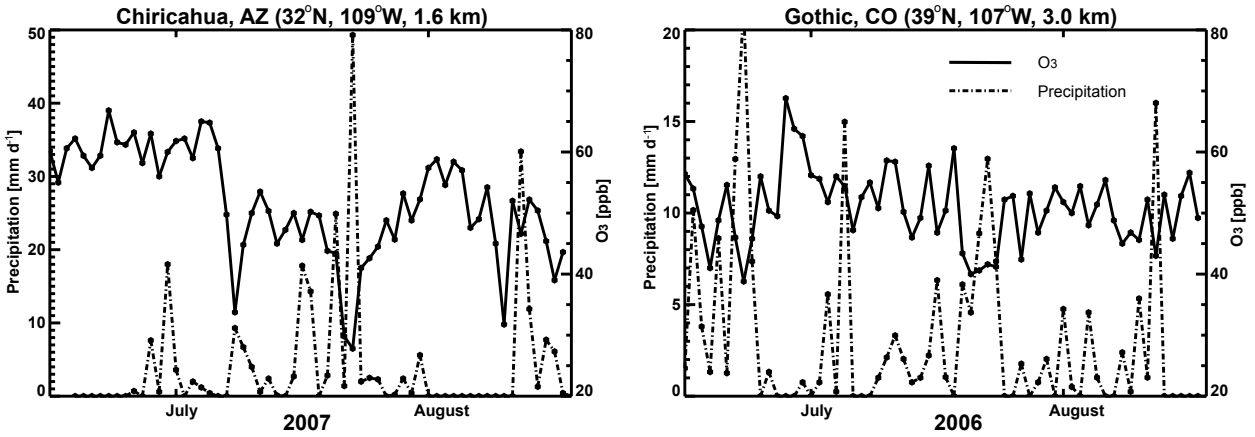

Figure 3.3: CASTNet O_3 (solid line, MDA8, ppb) and daily precipitation (dashed line, mm d^{-1}): (left) July-August 2007 at Chiricahua, AZ (32°N, 109°W, 1.6 km), and (right) July-August 2006 at Gothic, CO (39°N, 107°W, 3.0 km).

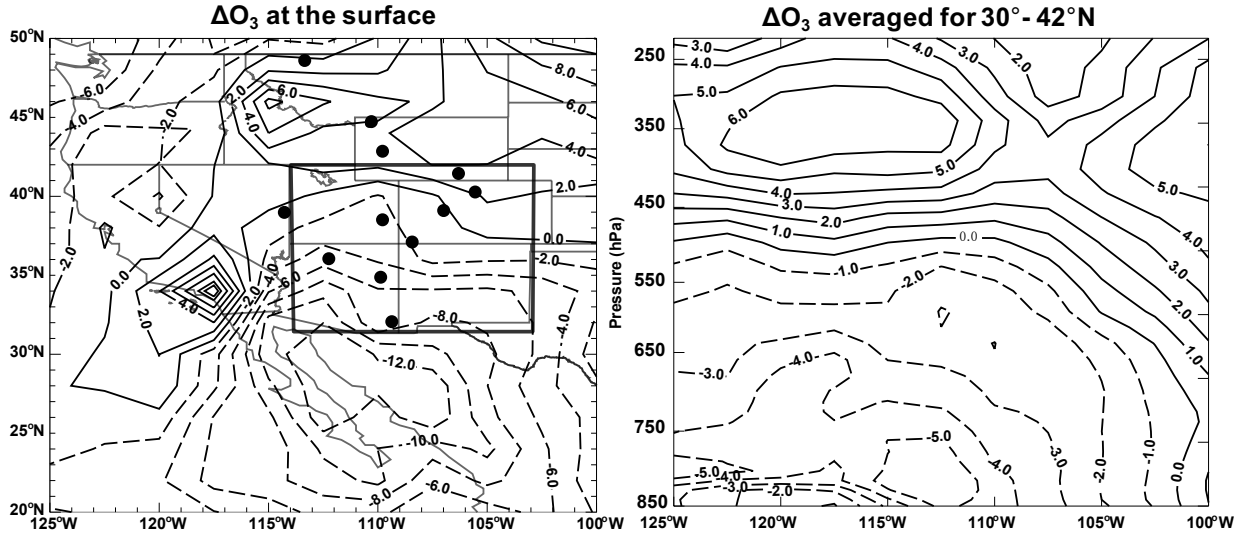

Figure 3.4: GEOS-Chem simulated changes in tropospheric O_3 (O_3, ppb, contour) from June 15-July 15 to July 15-August 15, 2007 (left) at the surface and (right) averaged over the latitudes 30°-42°N over the Four Corners states (the rectangle). Solid circles are CASTNet sites (Table 3.1).

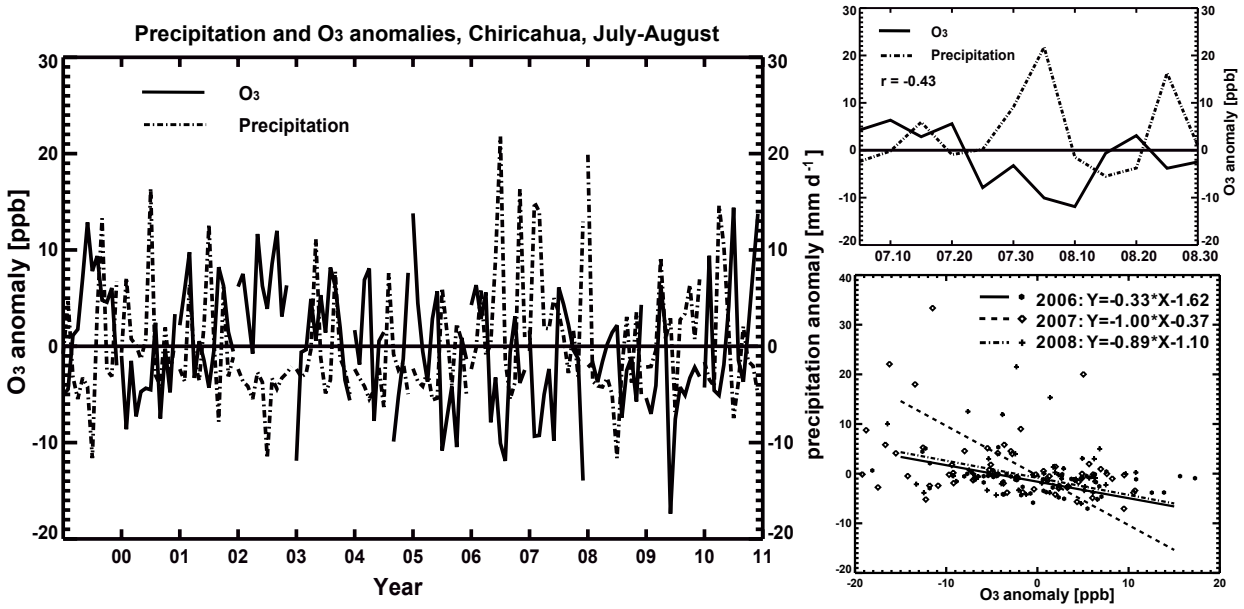

Figure 3.5: CASTNet O_3 (solid line, MDA8, ppb) and daily precipitation (dashed line, mm d^{-1}) anomalies at Chiricahua, AZ (32°N, 109°W, 1.6 km) for (left) July-August 2000-2011, (top right) July-August 2007, and (lower right) July 20-August 15, 2006 (solid circle), July 20-August 5, 2007 (open diamond), and August 1-20, 2008 (cross).

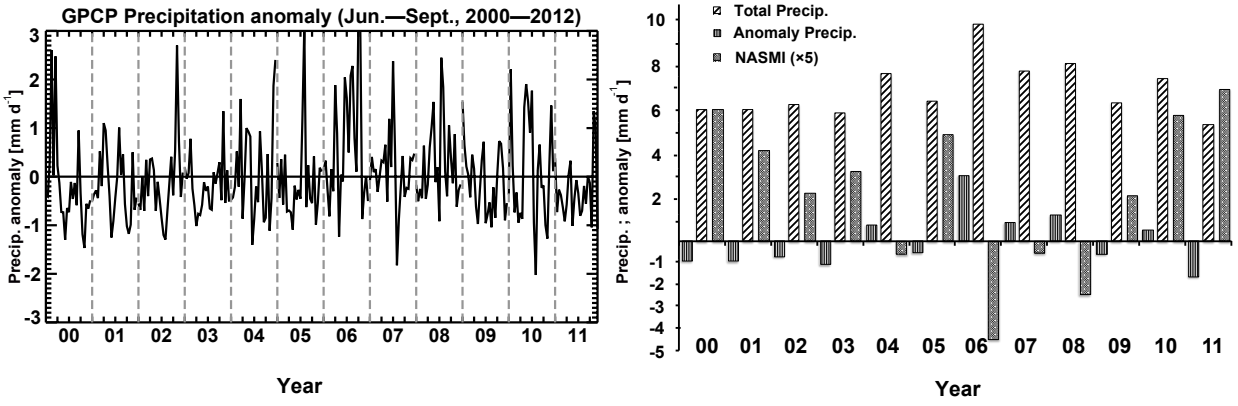

Figure 3.6: (Left) Precipitation anomaly (5-day average, mm d^{-1}) during June-September of 2000-2011 and (right) June-September mean monthly precipitation (mm d^{-1}) and the associated anomaly (mm d^{-1}), averaged over the Southwest U.S. (as defined by the rectangle in Fig. 4). Precipitation data is from the Global Precipitation Climatology Project (GPCP, $1^{\circ}\times1^{\circ}$, available at `http://precip.gsfc.nasa.gov/`). Also shown is the normalized North American summer monsoon index (NASMI, Li and Zeng, 2002). See text for details.

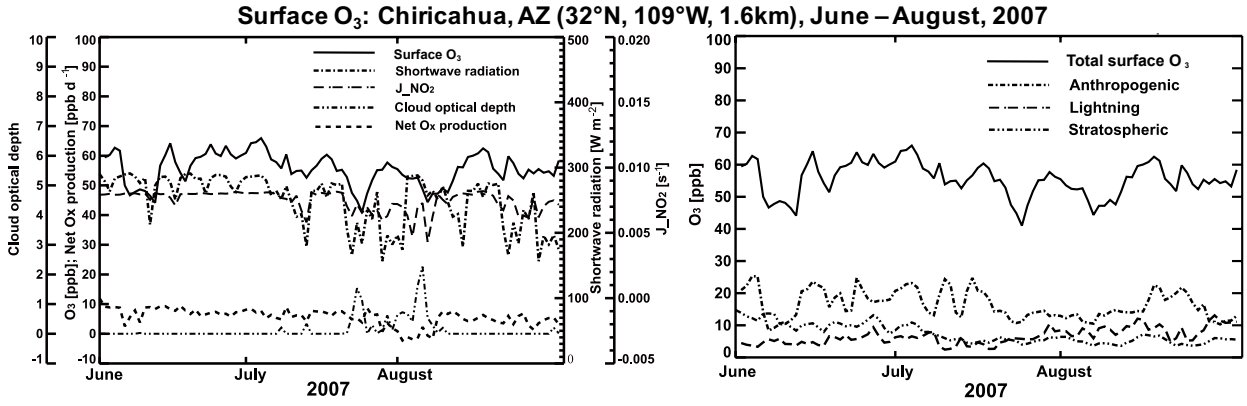

Figure 3.7: GEOS-Chem simulated (left) surface O_3 concentration (solid line, MDA8, ppb) at Chiricahua, AZ (32°N, 109°W, 1.6 km) for June-August 2007 and (right) the relative contributions from anthropogenic emissions (dashed dotted line), lightning NO_x emissions (long dashed line), and stratospheric intrusion (dashed dotted dotted line). Also shown are shortwave radiation at the surface (dashed dotted line, W m^{-2}), afternoon (13:00-17:00 local time) NO_2 photolysis rate (long dashed line, s^{-1}), GEOS-5 daily cloud optical depth (dashed dotted dotted line), and daily net O_x production rate (dashed line, ppb d^{-1}).

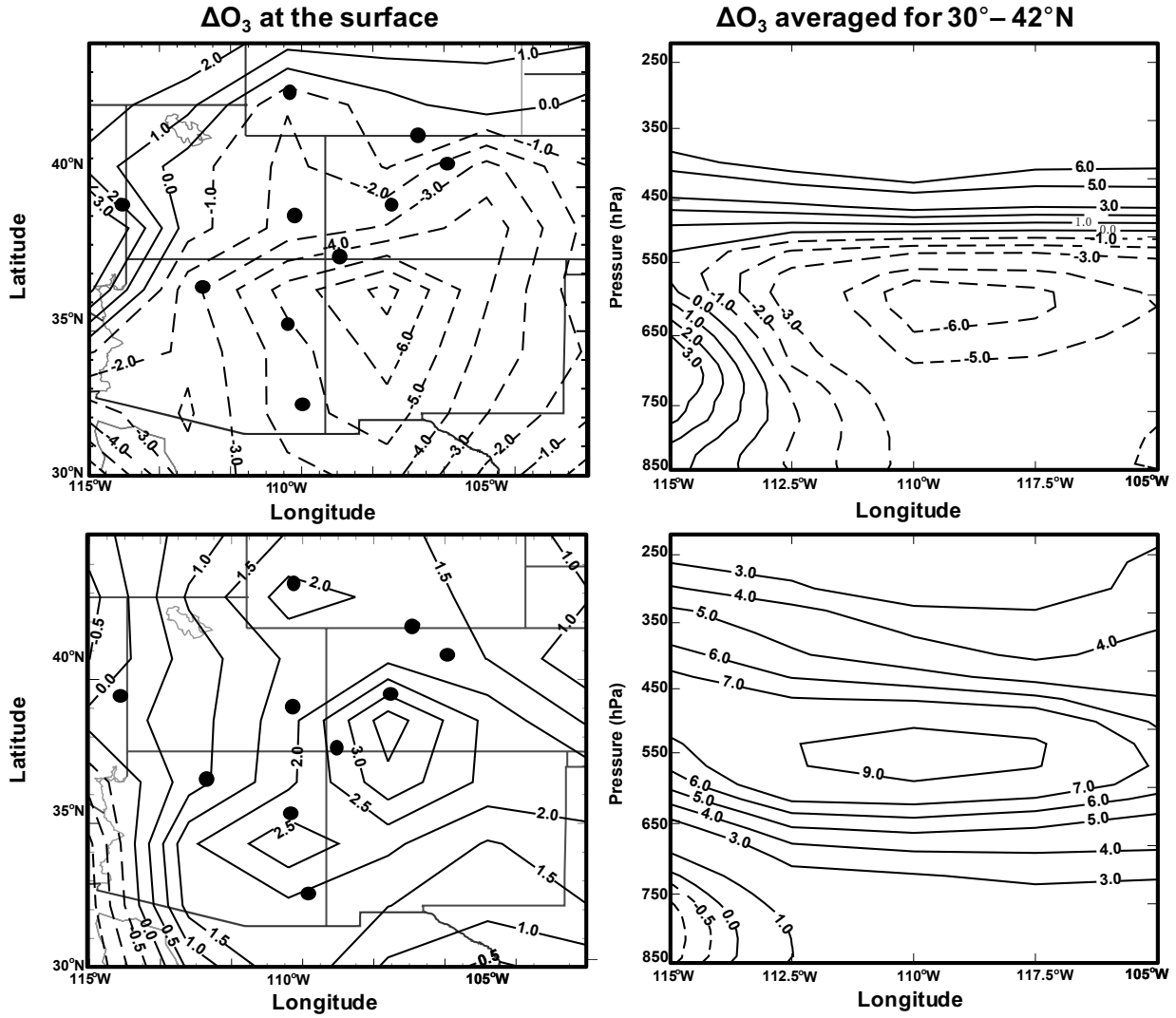

Figure 3.8: GEOS-Chem simulated changes in tropospheric O_3 (O_3, ppb, contour) from June 15-July 15 to July 15-August 15, 2007: contributions from (top panels) anthropogenic and (bottom panels) lightning NO_x emissions, (left panels) at the surface and (right panels) averaged over the latitudes 30°-42°N over the Southwest U.S. (rectangle in Fig. 4). Solid circles are CASTNet sites (Table 3.1).

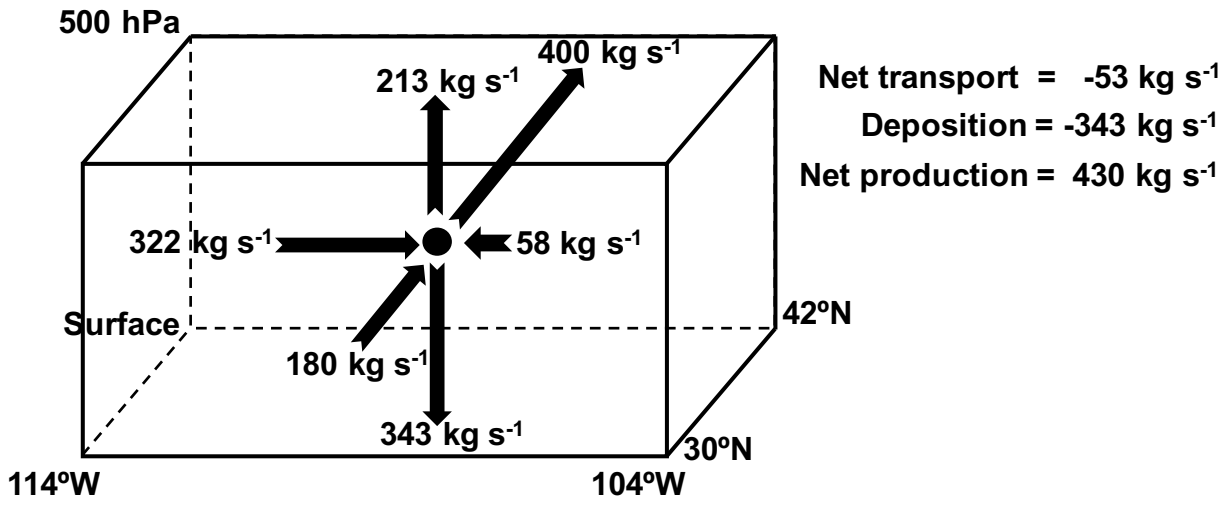

Figure 3.9: GEOS-Chem simulated budget of tropospheric O_3 over the Southwest U.S. (rectangle in Fig. 4), from the surface to 500 hPa, for July 15-August 15, 2007. Arrows are O_3 transport and deposition fluxes (kg s^{-1}), with lengths proportional to the magnitudes of the flux.

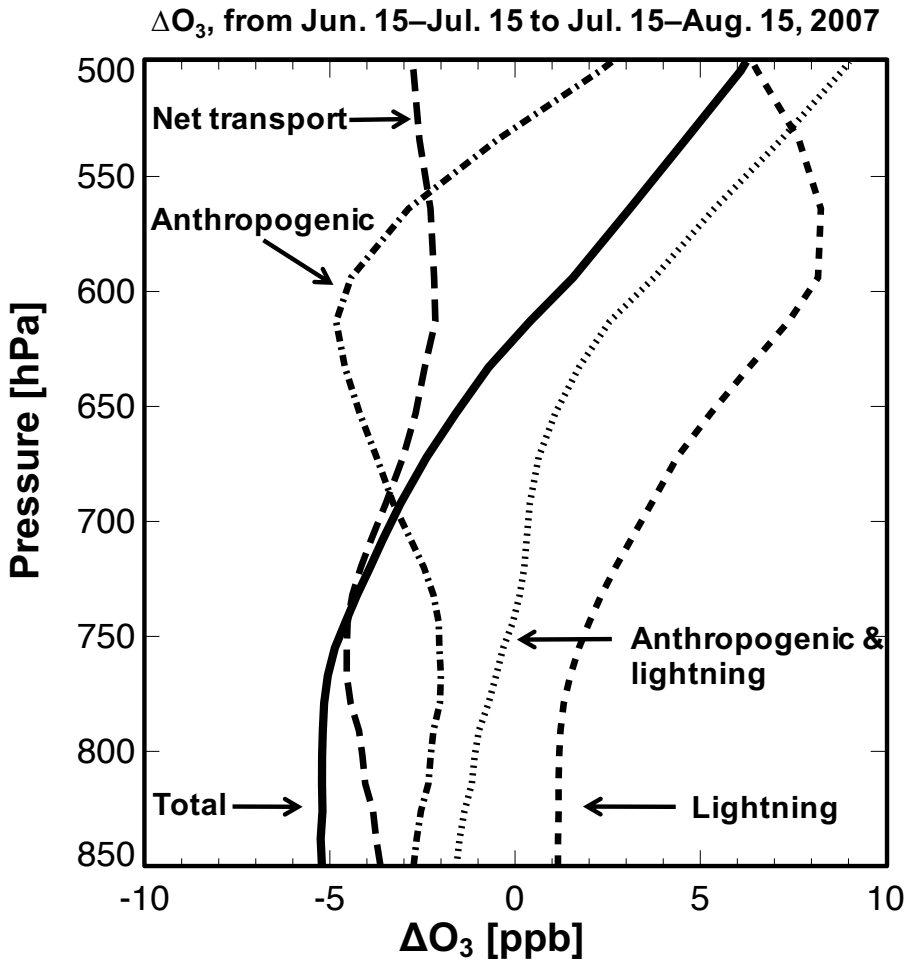

Figure 3.10: GEOS-Chem simulated changes in tropospheric O_3 (O_3, ppb, solid line) from June 15-July 15 to July 15-August 15, 2007, averaged over the Southwest U.S. (rectangle in Fig. 4). Also shown are the corresponding changes in the relative contributions from anthropogenic (dash-dotted), lightning (dashed), both anthropogenic and lightning (dotted), and net transport (long-dashed).

CHAPTER 4

Quantifying the impacts of long range transport of wildfires emissions on surface ozone at coastal Western U.S. sites using an adjoint method

Abstract

We use the GEOS-Chem 3-D global tropospheric chemical transport model and its adjoint to quantify the source contributions to O_3 pollution observed at Mt. bachelor Observatory (MBO) during the summer of 2008. The adjoint computes the sensitivity of O_3 concentration at the receptor site to O_3 production rates at $2^\circ \times 2.5^\circ$ resolution over the history of air parcels reaching the site. We found that MBO experienced distinct O_3 pollution episodes from Siberia wildfire emissions. During the O_3 pollution episode from June 30th to July 4th in year 2008, 7.5 ppb of MBO O_3 is produced over Siberia, comparable to the amount of O_3 (8 ppb) produced over North America. A significant amount of O_3 (18 ppb) production took place over the North pacific, with maxima just off the west coast of the U.S. where subsidence of air masses causes decomposition of PAN (peroxyacetylnitrate, a thermo-unstable NO_x reservoir species) and drives further ozone production. We also used the adjoint of GEOS-Chem to show the model O_3 at MBO is largely sensitive to NO_x emissions from biomass burning sources in Siberia and northern California, lightning sources over southwestern U.S. and Mexico, and anthropogenic sources in western U.S. and eastern Asia. For the CO emissions, the largest O_3 sensitivity is to the biomass burning sources in northern California and Siberia. The peak sensitivity to biomass burning CO emissions is comparable to the

peak O_3 sensitivity to anthropogenic NO_x emissions.

4.1 Introduction

Tropospheric ozone (O_3) is formed by the oxidation of hydrocarbons and carbon monoxide catalyzed by nitrogen oxide radicals ($NO_x \equiv NO_2 + NO$) and hydrogen oxide radicals ($HO_x \equiv H + OH +$ peroxy radicals). High surface concentrations of O_3 in populated regions, where emissions of both NO_x and hydrocarbons are large, are a serious air pollution problem. O_3 in the troposphere is also of global interest as a main atmospheric oxidant, a primary source of OH and an effective greenhouse gas OH and an effective greenhouse gas (*Change*, 2007). A fraction of tropospheric O_3 comes from the stratosphere. The major sources of O_3 precursors are anthropogenic (fuel combustion) and natural such as lightning and biomass burning.

The variability in background surface O_3 is a critical issue in the decision making of air quality policy (*McDonald-Buller et al.*, 2011). During the past decades, the U.S. National Ambient Air Quality Standards (NAAQS) for ground-level O_3 have become increasingly stringent. The Environmental Protection Agency (EPA) established primary and secondary NAAQS for ground-level O_3 in March 2008: annual 4th highest daily maximum 8-hour average (MDA8) concentration not to exceed 75 ppb. There are currently 227 counties, home to 123 million people, classified as not having attained the 75 ppb standard (`www.epa.gov/airquality/greenbook/index.html`). In 2015, a new standard proposed by the EPA was issued, further lowering it from 75 to 70 ppb. As the O_3 standard becomes increasingly stringent, to accurately determine the background O_3 levels becomes more imperative. Policy Relevant Background (PRB) O_3 is the maximum O_3 reduction that can be achieved through controls of North American emissions alone (*EPA*, 2006). From both scientific and regulatory points of view, a lower O_3 standard will motivate air quality-control planners to see more accurate and precise attribution of the background O_3 to determine how much domestic emissions must be reduced in order to attain that standard (*Cooper et al.*, 2014).

Surface O_3 in the western U.S. has trended up (0.19-0.51 ppb yr^{-1}) during the past two decades even though surface O_3 in the eastern U.S. has gone down (*Jaffe and Ray*, 2007; *Cooper et al.*, 2012, 2014). Free tropospheric O_3 in the western U.S. has been steadily increasing (0.41 ± 0.27 ppb yr^{-1}) during the same time period (*Cooper et al.*, 2010). PRB O_3 is especially high over the intermountain regions in the western U.S. due to the arid terrain, high elevations, and large-scale subsidence in the region (*Zhang et al.*, 2011). PRB O_3 in the western U.S. is impacted by many factors including biomass burning (*Jaffe et al.*, 2008; *Jaffe*, 2010), lightning (*Zhang et al.*, 2014) and trans-Pacific transport of Asian pollution (*Parrish et al.*, 2009; *Cooper et al.*, 2010).

Long-range transport of air pollution is becoming another major issue as counties at northern mid-latitude strive to meet increasingly stringent air quality standards. Elevated air pollutants levels have been observed in the U.S due to long range transport of Canadian forest fire emission (*Wotawa and Trainer*, 2000), Siberian biomass burning emission (*Jaffe et al.*, 2004; *Oltmans et al.*, 2010) and Asian emission (*Zhang et al.*, 2009). A number of studies have investigated the impact of transpacific pollution on surface O_3 in the WUS. O_3 has a lifetime of days in the boundary layer but weeks in the free troposphere (*Wang et al.*, 1998), enabling transport on the intercontinental scale. Eurasian pollution is typically exported to the Pacific by front lifting in warm conveyor belts (WCBs), convection, and orographic lifting (*Liu et al.*, 2003; *Brock et al.*, 2004; *Liang et al.*, 2004; *Dickerson et al.*, 2007). The transport is most rapid and frequent in spring due to active cyclonic activity and strong westerly winds (*Forster et al.*, 2004; *Liang et al.*, 2004). *Jaffe et al.* (2004) found that the fires in Siberia, 2003 resulted in enhancements in summer background O_3 of 5-9 ppbv at sites in Alaska, Canada and the Pacific Northwest. (*Zhang et al.*, 2008) used an ensemble of aircraft, satellite, sonde, and surface observations during the INTEX-B campaign (April-May 2006) to quantify the transpacific transport of Asian pollution. They concluded that Asian anthropogenic emission increased surface O_3 concentrations by 5-7 ppb in WUS during the INTEX-B period.

Most of the previous studies on the influence of long range transport on surface O_3 have run sensitivity simulations with perturbed emissions using a chemical transport model (*Jacob et al.*, 1999; *Yienger et al.*, 2000; *Wild and Akimoto*, 2001; *Derwent et al.*, 2008; *Duncan et al.*, 2008; *Fiore et al.*, 2009). This source-oriented method is computationally limited in the spatial resolution of the source region that they can achieve. (*Cohan et al.*, 2005) briefly describes the application of sensitivity analysis. The following is from their description. Sensitivity analysis investigates the response of atmospheric concentrations, C(x,t), to perturbations in a sensitivity parameter, p_j(x,t) (a model parameter or input such as an emission rate, initial condition, or boundary condition). Sensitivity coefficients traditionally have been approximated by 'brute force' method. In this method, finite differencing compares concentrations computed by two chemical transport model (CTM) simulations that are identical except for a perturbation in the sensitivity parameter

$$s_j^{(1)} = \frac{C_{+\Delta\epsilon_j} - C_{-\Delta\epsilon_j}}{2\Delta\epsilon_j} \tag{4.1}$$

The fractional perturbation in the parameter is denoted by

$$\Delta\epsilon_j = \epsilon_j - 1 \tag{4.2}$$

The brute force method is simple and ready to be applied in any chemical transport model. However, if we want to compute a large number of sensitivities, the method becomes inefficient , because it requires additional simulations for each perturbation. Although brute force computes exact model response to specific perturbations, the accuracy of scaling these results to other levels of perturbation is unclear in the presence of nonlinearity. In addition, brute force is prone to numerical error for small perturbations.

The adjoint method is a much more computationally efficient approach for the receptor-oriented problem, for example, to calculate the source attribution of O_3 concentration at a given site. A single run of the adjoint model can compute the sensitivity of ozone concentrations at a given location and time (or an average over a spatial domain and time interval)

to the global distribution of sources over the spatial and temporal resolution of the model (*Zhang et al.*, 2009). The adjoint method has been applied in previous studies to investigate long range transport of aerosol to the U.S. (*Henze et al.*, 2009), pollutant transport to Hawaii island (*Vukićević and Hess*, 2000; *Hess and Vukicevic*, 2003) as well as regional sensitivity analyses for O_3 pollution episodes (*Elbern and Schmidt*, 2001; *Hakami et al.*, 2006; *Nester and Panitz*, 2006).

In this study, we used the adjoint model of GEOS-Chem to quantify the impacts of the long-range transport of the Siberian wildfire emissions during the summer of 2008 on surface O_3 on the U.S. west coast. We interpreted model results with the observation at site MBO (Mt. Bachelor Observatory, Oregon). It's a standard reference site for background air entering the United States (*Goldstein et al.*, 2004; *Jaffe et al.*, 2005; *Oltmans et al.*, 2008). It's particularly sensitive to long range influences due to its exposure to the free troposphere (*Jaffe et al.*, 2005; *Weiss-Penzias et al.*, 2006; *Wolfe et al.*, 2007). The GEOS-Chem model and its adjoint is described in Sect.2. We give a description of the observations in Sect.2. Sect. 3 briefly describes the MBO observation. Model evaluation and Hybrid Single-Particle Lagrangian Integrated Trajectory (HYSPLIT) back trajectories analysis are shown in Sect. 4 and 5. We present our simulation results and related discussions in Sect. 6 and 7. Conclusions are given in Sect. 8.

4.2 GEOS-Chem Model and its Adjoint

4.2.1 GEOS-Chem configuration

We use a global 3-D chemical transport model (GEOS-Chem, v8-02-03, available at `http://geos-chem.org`) (*Bey et al.*, 2001) to interpret the CASTNet observations. The model is driven by GEOS-5 data assimilation system (DAS) meteorological fields from the NASA Global Modeling and Assimilation Office (GMAO) with a temporal resolution of 6-hour (3-hour for surface variables and mixing depths) and consists of 47 levels in the vertical up to

0.01 hPa. The lowest model levels are centered at approximately 60, 200, 200, 300, 450, 600, 700, 850, 1000, 1150, 1300, 1450, 1600, 1800 m in GEOS-5. We run the model at 2° latitudes by 2.5° longitude globally.

Tracer advection is calculated using a flux-form semi-Lagrangian method (*Lin and Rood*, 1996) every 15 minutes. Following (*Allen et al.*, 1996a,b), tracer moist convection is computed using GEOS-5 convective, entrainment, and detrainment mass fluxes. Treatment for shallow convection is using (*Hack et al.*, 1994) and parameterization of deep convection follows the relaxed Arakawa-Schubert scheme (*Moorthi and Suarez*, 1992).

GEOS-Chem includes detailed ozone-NO_x-hydrocarbon-aerosol chemistry. Tropospheric O_3 is simulated with about 80 species and over 300 chemical reactions (*Bey et al.*, 2001). Photolysis rates are computed using the fast-J algorithm (*Wild et al.*, 2000). The O_3 simulation over the U.S. has been extensively evaluated (*Wang et al.*, 2009; *Zhang et al.*, 2010; *Walker et al.*, 2010; *Parrington et al.*, 2008). Anthropogenic emissions are as described by (*Zhang et al.*, 2011). Global anthropogenic emissions are from the Emission Database for Global Atmospheric Research (EDGAR) inventory for 2000, superseded by regional emission inventories from the U.S. EPA 2005 National Emission inventory (NEI-05) for the U.S., the European Monitoring and Evaluation Program (EMEP) for Europe, the Canada Criteria Air Contaminates (CAC) emission inventory for Canada, and the Big Ben Regional Aerosol and Visibility Observational (BRAVO) emission inventory for Mexico. Biogenic emissions are based on the Model of Emissions of Gases and Aerosols from Nature (MEGAN) inventory (*Guenther et al.*, 2006).

Lightning NO_x emissions are computed locally in deep convection events (*Price and Rind*, 1992), where flash rates are related to convective cloud top heights. NO_x yields per flash are 260 moles in the tropics and 500 moles in the extra-tropics (*Huntrieser et al.*, 2007, 2008; *Hudman et al.*, 2007; *Ott et al.*, 2010). The vertical distribution of lightning emissions follow (*Pickering et al.*, 1998). In this work, we use the higher density National Lightning Detection Network data (*Christian et al.*, 2003) for the continental U.S. to constrain lightning flash

rates, following (*Zhang et al.*, 2014). NLDN observes cloud-to-ground lightning flashes only, and intra-cloud flashes are estimated to be three times that amount (*Boccippio et al.*, 2001). The constfeferaint largely corrects excessive lightning flash rates and consequently high bias of surface O_3 in the SWUS in previous GEOS-Chem simulations (*Zhang et al.*, 2011, 2014).

Biomass burning emissions are from the daily Global Fire Emission Database version 3 (GFEDv3) (*Giglio et al.*, 2013; *van der Werf et al.*, 2006). GFEDv3 is derived using satellite observations including active fire counts and burned areas in conjunction with the Carnegie-Ames-Stanford-Approach (CASA) biogeochemical model. Carbon emissions are calculated as the product of burned area, fuel loading and combustion completeness. Burned area is derived using the active fire and 500-meter burned area datasets from the Moderate Resolution Imaging Spectroradiometer (MODIS) as described by (*Giglio et al.*, 2013). The NO_x emission factors for extra-tropical forest fires are updated following (*Alvarado et al.*, 2010).

4.2.2 GEOS-Chem adjoint model

Founded in optimal control theory and variational calculus, adjoint methods were initially suggested as approaches to source analysis of atmospheric tracers several decades ago *Lions* (1971); *Marchuk* (1974). By the late 1990s, the method was applied to chemical transport models of the stratosphere (*Fisher and Lary*, 1995) and troposphere (*Elbern et al.*, 1997). The method was used to constrain emissions in an Eulerian air quality model of chemically active species in the troposphere by (*Elbern et al.*, 2000). Subsequent investigations of emissions have been explored with adjoints of chemical transport models such as CHIMERE (*Vautard et al.*, 2000; *Menut*, 2003; *Schmidt and Martin*, 2003), Polair (*Quélo et al.*, 2005), the CIT model (*Martien et al.*, 2006) STEM (*Sandu et al.*, 2005; *Hakami et al.*, 2005), DRAIS (*Nester and Panitz*, 2006), CMAQ (*Hakami et al.*, 2007), IMAGES (*Müller and Stavrakou*, 2005; *Stavrakou and Müller*, 2006; *Stavrakou et al.*, 2008), and GOCART (*Dubovik et al.*, 2004, 2008).

(*Henze et al.*, 2007) provides a full description of the GEOS-Chem adjoint model. In their study, the adjoint of each individual physical and chemical model operator is derived and validated, and pseudo-observations are used to assess the potential inverse modeling performance. Subsequently, the GEOS-Chem adjoint model has been updated to include online calculations of the heterogenous reaction rates (and the corresponding adjoint), and sensitivities with respect to emissions of NO_x from soil and lightning (*Henze et al.*, 2009). The GEOS-Chem adjoint has also been further developed for inverse modeling CO emissions using remote sensing observations (*Kopacz et al.*, 2006). The remainder of this session is from (*Henze et al.*, 2009), which reviewed general approach to adjoint sensitivity analysis.

A chemical transport model can be viewed as a numerical operator, F, acting on a vector of initial concentrations, $\mathbf{c}^0$, and a vector of parameters, $\mathbf{p}$, to yield an estimate of the evolved concentrations at a later time, N,

$$\mathbf{c}^{\mathrm{N}} = F(\mathbf{c}^0, \mathbf{p}), \tag{4.3}$$

where $\mathbf{c}$ is the vector of all K tracer concentrations, $\mathbf{c}=[c_1, ...,c_k, ...,c_K]^T$ at time step n. In practice, F comprises many individual operators representing various physical processes. For the moment, let F n represent a portion of the discrete forward model that advances the concentration vector from time step n to step n+1.

$$\mathbf{c}^{\mathrm{n+1}} = F^{\mathrm{n}}(\mathbf{c}^{\mathrm{n}}, \mathbf{p}), \tag{4.4}$$

The adjoint model is used to calculate the sensitivity of a scalar model response function, J , with respect to the model parameters, $\mathbf{p}$.

$$J = \sum_n J^{\mathrm{n}}(\mathbf{c}^{\mathrm{n}}) + J_{\mathrm{p}}(\mathbf{p}) \tag{4.5}$$

As will become evident, it is first necessary to calculate the sensitivity of the model

response with respect to species concentrations at every time step n in the model,

$$\nabla_{\mathrm{c^n}} J = \frac{\partial J}{\partial c^{\mathrm{n}}} \tag{4.6}$$

The Jacobian matrix of the model operator around any given time step can be written as

$$\frac{\partial \mathbf{c}^{\mathrm{n+1}}}{\partial \mathbf{c}^{\mathrm{n}}} = \frac{\partial F^{\mathrm{n}}(\mathbf{c}^{\mathrm{n}})}{\partial \mathbf{c}^{\mathrm{n}}} \equiv \mathbf{F}_{\mathbf{c}}^{n} \tag{4.7}$$

and similarly,

$$\frac{\partial \mathbf{c}^{\mathrm{n+1}}}{\partial \mathbf{p}} = \frac{\partial F^{\mathrm{n}}(\mathbf{c}^{\mathrm{n}})}{\partial \mathbf{p}} \equiv \mathbf{F}_{\mathbf{p}}^{n} \tag{4.8}$$

Using the chain rule,

$$\begin{aligned} \nabla_{\mathrm{c^n}} J = (\mathbf{F}_{\mathbf{c}}^{n})^{\mathrm{T}} (\mathbf{F}_{\mathbf{c}}{}^{\mathrm{n+1}})^{\mathrm{T}} \cdots (\mathbf{F}_{\mathbf{c}}{}^{\mathrm{N\text{-}1}})^{\mathrm{T}} \frac{\partial J^{N}}{\partial c^{\mathrm{N}}} \\ + (\mathbf{F}_{\mathbf{c}}^{n})^{\mathrm{T}} (\mathbf{F}_{\mathbf{c}}{}^{\mathrm{n+1}})^{\mathrm{T}} \cdots (\mathbf{F}_{\mathbf{c}}{}^{\mathrm{N\text{-}2}})^{\mathrm{T}} \frac{\partial J^{\mathrm{N\text{-}1}}}{\partial c^{\mathrm{N\text{-}1}}} \\ + \cdots + \frac{\partial J^{n}}{\partial c^{\mathrm{n}}} \end{aligned} \tag{4.9}$$

The $\frac{\partial J^n}{\partial c^{\mathrm{n}}}$ terms are referred to as the adjoint forcings as their role in the adjoint model is analogous to that of emissions in the forward model (for further details, see the continuous forward and adjoint model equations in (*Sandu et al.*, 2005)).

4.3 Observations at Mt. Bachelor Observatory (MBO)

4.3.1 MBO instrumentation

Site Mt. Bachelor Observatory (MBO) was established in year 2004 and is a mountaintop site located on the summit of Mt. Bachelor in the Cascades Mountains of central Oregon (*Jaffe et al.*, 2005). Continuous measurements include a suite of chemical (e.g. O_3, CO,

aerosol scattering, mercury) and meteorological (e.g. wind speed/direction, temperature, relative humidity) parameters (*Ambrose et al.*, 2011). Non-continuous measurements (e.g. for specific seasons or studies) include compounds such as nitrogen oxides (NO_x and NO_y) and peroxy acetyl nitrate (PAN) (*Gratz et al.*, 2015).

O_3 is measured using a Dasibi 1008 RS UV Photometric Ozone Analyzer (*Weiss-Penzias et al.*, 2006; *Ambrose et al.*, 2011). The analyzer is calibrated every six months with an O_3 generator referenced to a Washington State Department of Ecology transfer standard, which is calibrated against the EPA Region 9 Standard Reference Photometer (*Gratz et al.*, 2015). The detection limit of the method is 1 ppbv and the estimated total uncertainty is ±2% (*Ambrose et al.*, 2011).

Carbon monoxide was measured during spring 2004 using a Thermo Electron Corporation (TECO) 48C nondispersive infrared analyzer, and thereafter using a TECO 48C Trace Level Enhanced (TLE) analyzer (*Ambrose et al.*, 2011) through April 2012 (*Gratz et al.*, 2015). These analyzers were calibrated every 24 h with a ±2% NIST-traceable working standard of 400e500 ppb referenced to a NOAA-certified breathing air primary standard. Zeroes were performed every two hours. The detection limit was 20 ppbv and the estimated total uncertainty in hourly-averaged mixing ratios was ±6%.

4.3.2 Fire event identification

In the series of studies in Dan Jaffe's group at the University of Washington (*Wigder et al.*, 2013; *Baylon et al.*, 2015), they employed four criteria to identify fire events observed at MBO:

- 5-min ambient aerosol scattering $\sigma_{sp} \geq 20 Mm^{-1}$ for at least two hours.
- 5-min CO ≥150 ppbv for at least two hours.
- Strong correlation ($R^2 \geq 0.70$) between σ_{sp} and CO.
- Consistent backward trajectories indicating transport over known fire locations.

For the fourth criterion, they used the Fire Information for Resource Management System (FIRMS) Web Fire Mapper to identify burning fires (`https://firms.modaps.eosdis.nasa.gov/firemap/`).

4.4 Time series of O_3 and CO at MBO during fire events

During the summer of 2008 to 2010, there are 24 wildfire events identified at MBO observation based on the four criteria we described above. In this study, we analyzed the event with the longest duration, lasting from June 30th, 2008 to July 4th, 2008. Fig.4.1 shows the hourly observed and modeled time series of O_3 (left) and CO (right) at MBO. Surprisingly we found this very good agreement between the measurements and GEOS-Chem simulation at such a high temporal resolution. Model well captures the day-to-day variations of both observed O_3 and CO concentration, especially the significant enhancement in both species during the wildfire event period (between the blue lines). The increase in CO concentration is more evident than that in O_3 due to the fact that CO is emitted directly from wildfire emissions while O_3 is a secondary air pollutant. It takes time for the fire emitted VOCs and NO_x to form O_3 in the presence of sunlight. The mean observed hourly O_3 concentration at MBO is 50±14 ppbv, compared with 49±10 ppbv in the model. As for CO, the mean observed concentration at MBO is 133±71 ppb, compared to 115±52 ppb in the model. The model cannot reproduce the peak CO levels observed at MBO during the wildfire event.

4.5 Description of backward trajectories

(*Wigder et al.*, 2013) identified the approximate fire location for the observed fire event at MBO during June 30th, 2008 to July 4th, 2008 by applying both 10-day backward trajectories with the HYSPLIT model using the 1° resolution Global Data Assimilation System (GDAS) meteorological data and 3-day backward trajectories using the 40 km resolution US Eta Data Assimilation System (EDAS) meteorological data. In their results, this fire event is

attributed to the fires that took place in Northern California. In our study, we also calculated backward trajectories with the HYSPLIT to establish the transport history of the air masses impacting MBO. The result presented in Fig.4.2 is based on back trajectories initialized at July 4th, 15:00 pm from the summit of MBO. These trajectories were calculated using global meteorological data from the GDAS (Global Data Assimilation System) archive, which has a time resolution of 3 hours, a spatial resolution of 1° latitude by 1° longitude, and a vertical resolution of 23 pressure surfaces between 1000 and 20 hPa. Error in HYSPLIT trajectory calculations normal to the direction of flow are 10-30% of the distance traveled after 24 (*Draxler and Hess*, 1998). Fig.4.2 (left) shows the ensemble of the three-day back trajectories and Fig.4.2 (right) shows the ensemble of the ten-day back trajectories. Each member of the trajectory ensemble is calculated by offsetting the meteorological data by a fixed grid factor (one grid meteorological grid point in the horizontal and 0.01 sigma units in the vertical). This results in 27 members for all-possible offsets in X, Y and Z. To our surprise, we found in the ten-day back trajectories that a majority of the ensemble trajectories came from the Siberia regions. The red sparks in the figures are approximate fire locations identified from the FIRMS Web Fire Mapper. For the three-day back trajectory, the ensemble of the paths came across the fire regions in Northern California. While for the ten-day back trajectory, the air mass may bring the fire emission from Siberia before they reach MBO after trans-Pacific transport.

Previous study (*Vivchar*, 2011) has shown that year 2008 is a very strong fire year in Russia with a maximum (33.0 Mha) in total burned areas from wildfires during 2004 to 2010. We also investigated this inter-annual variations of wildfire activities in Siberia. Fig.4.3 shows the GFED3 black carbon (BC) emission in June during 2004 to 2010. Values are summed over the Siberia region. Wildfire emitted BC is the largest in year 2008, compared to the other years investigated here, reaffirming the strong wildfire activities in Siberia in year 2008. Fig.4.4 shows the large amounts of active fire counts during June, 2008 over Siberia. Results are from the FIRMS Web Fire Mapper. In order to investigate how the Siberia wildfire

emission impact surface O_3 in the western U.S. after the long range transport, we conducted adjoint simulation to estimate the source contributions to surface O_3 pollution during the identified fire event at MBO during June 30th, 2008 to July 4th, 2008. The cost function for the adjoint sensitivity calculation is the O_3 concentration at MBO averaged over the fire event period. The forward and backward simulations are performed from May 4th, 2008 to July 4th, 2008, and the cost function is evaluated at every hour throughout the simulation. We calculated two terms using the GEOS-Chem adjoint model: (1) the sensitivity of O_3 concentration at MBO to 3-D O_3 production rates at $2^\circ \times 2.5^\circ$ resolution over the history of air parcels reaching the site (running the model backwards for two months) and (2) the sensitivity of O_3 concentration of MBO to NO_x emission estimates of O_3 precursors such as NO_x (including NO_x emitted from different sources, i.e. biomass burning, lightning, anthropogenic, aircraft, biofuel and soil) and CO (from biomass burning, anthropogenic and biofuel).

4.6 Fine Geographical Source Attribution for MBO O_3 during fire event

Fig.4.5 shows the sensitivities of O_3 concentrations at MBO to the global distribution of O_3 production rates for the previous two months, as inferred from the GEOS-Chem model adjoint. The figure shows the integrals of the production rates over time and over the tropospheric column depths at the $2^\circ \times 2.5^\circ$ horizontal resolution of the model. They show the amount of O_3 produced in each grid square and transported to the receptor site with chemical loss accounted for during transport. Summing these values globally over all $2^\circ \times 2.5^\circ$ grid squares approximates the O_3 concentrations simulated by GEOS-Chem at the receptor site; there is a 10%-15% residual that reflects production in the stratosphere and tropospheric production at time lags larger than two months.

We define four regions as Asia (8°N-50°N, 70°E-152°E), Siberia (50°N-80°N, 80°E-270°E),

North America (15°N-80°N, 232°W-292°W), and the North Pacific (0°N-50°N, 152°E-232°W). We find most of the ozone production contributing to MBO ozone during this episode took place over the North Pacific, about 18 ppb in total, with maxima just off the west coast of the U.S. where subsidence of air masses causes decomposition of PAN (peroxyacetylnitrate, a thermo-unstable NO_x reservoir species) and drives further ozone production (*Kotchenruther et al.*, 2001; *Heald et al.*, 2003; *Hudman et al.*, 2004; *Zhang et al.*, 2008). We also find significant O_3 production of about 12 ppb over East Asia, with maxima over the northeast China plain and Japan. About 8 ppb was produced over North America, with maxima over the fire regions in Northern California. About 7.5 ppb O_3 production was over Siberia, mainly due to the wildfire emissions, which peaks in that region in 2008. It is surprising to see that the amount of O_3 produced over Siberia wildfire regions and transported to MBO after the trans-Pacific transport is comparable to the contribution from fires in northern California which are located much closer to MBO site.

Fig.4.6 shows the time-dependent sensitivities to production over Asia (8°N-50°N, 70°E-152°E), Siberia (50°N-80°N, 80°E-270°E), North America (15°N-80°N, 232°W-292°W), and the North Pacific (0°N-50°N, 152°E-232°W), and Rest of World. Similar sensitivity spectra have been shown by (*Vukićević and Hess*, 2000). Integrating under these curves gives the total contributions of O_3 production in these regions to the O_3 concentrations at the receptor site. Again, the contribution from Asia, North Pacific, Siberia, North America and Rest of World are 12ppb, 18ppb, 7.5 ppb, 8ppb and 12 ppb, respectively. We see that O_3 produced in North America had an immediate impact on MBO, in about 1-2 days. It has a secondary peak at 20-25 days that reflects O_3 produced in the U.S. and transported in the westerly atmospheric circulation. Production over North pacific begins from day 2 and has its maxima on day 4, reflecting the decomposition of PAN in the subsiding air mass as discussed earlier. The impact last until day 25, reflecting significant O_3 production during the plume transport. O_3 production over Asia begins to impact MBO after 6-day time lag and maximum Asian influence is at time lags of 8-11 days, which is consistent with the timescale for trans-pacific

transport(*Yienger et al.*, 2000; *Stohl et al.*, 2002). Similarly, O_3 production over Russia Siberia begins to impact MBO after 8-day time lag and maximum influence is at time lags of 10-14 days.

4.7 Sensitivity of MBO O_3 during fire event to emission estimates of NO_x and CO

We use the adjoint of GEOS-Chem to calculate the sensitivity of O_3 at MBO to emission estimates of different O_3 precoursors. Fig. 4.7 shows the sensitivity of model simulated MBO O_3 to the NO_x emission estimates from biomass burning (top), anthropogenic (middle) and lightning (bottom). The sensitivities shown here have been normalized by dividing the gradient of the cost function by the cost function so that relative influence of the different emission sources can be compared against each other. The largest model O_3 sensitivity is to anthropogenic NO_x emission estimates, centered over western U.S. and northern Mexico. A secondary maximum is located in the emission source regions in east Asia. The influence of anthropogenic emission estimates extends across Europe but the sensitivity is less than one third of the peak values over the main anthropogenic source regions. Biomass burning is the next most significant NO_x emission source, with the peak sensitivity localized to the main biomass burning region in the western U.S. The adjoint simulation also illustrates significant sensitivity of MBO O_3 to biomass burning NO_x emissions over Eastern Siberia, which amounts to about half of the peak values over western U.S. Lastly, the model O_3 shows sensitivity to lightning NO_x emissions which, although smaller in magnitude compared to the anthropogenic and biomass burning sensitivity, cover a large area of southwestern U.S. and Mexico, corresponding the region where most of the lightning activities take place during the North American summer monsoon. The combined sensitivity to NO_x emissions from other sources (i.e. aircraft, biofuel and soil) is considerably lower than that for the anthropogenic, biomass burning and lightning sources. For the CO emissions, shown in Fig.4.8, the largest

O_3 sensitivity is to the biomass burning sources in northern California and Siberia. The peak sensitivity to biomass burning CO emissions is comparable to the peak O_3 sensitivity to anthropogenic NO_x emissions.

Fig. 4.7 and Fig. 4.8 highlight some of the key potential sources of uncertainty in the model O_3 chemistry and their relative contributions. In future study, it is crucial to be able to attribute intercontinental ozone pollution to the actual emissions of ozone precursors, taking advantage of the fine resolution enabled by the adjoint. To quantify the contribution to MBO O_3 from different emission sources, we also need to resolve the non-linearity in O_3 production.

4.8 Conclusion

In this study, we have shown that an adjoint model analysis can provide detailed geographical and temporal information on intercontinental pollution influences at specific receptor sites. Such information can be used to better determine the sources of this intercontinental pollution, down to the scale of individual source countries and urban areas. We also used the GEOS-Chem adjoint model to calculate the sensitivity of O_3 concentration at a receptor site to emission estimates of O_3 precursors (NO_x , CO) from different sources (anthropogenic, biomass burning, lightning, soil, aircraft). For policy purposes it will be important to attribute the long range transport of O_3 pollution to the actual emissions of O_3 precursors, taking advantage of the fine resolution enabled by the adjoint model. This requires us to resolve the non-linearity of the O_3 production in the chemical mechanism in the model, and hence a more elaborate calculation than was presented in this study.

It is also worthwhile to notice that contributions from small fires to carbon emission in Asia and Siberia reach its peak in spring season (*Randerson et al.*, 2012), from March to May, which corresponds with the period when the trans-pacific transport of air pollution is the strongest. We would then expect an increase in background O_3 concentration in the

WUS due to the trans-pacific transport of pollutants from Asian and Siberia during the spring season. Therefore, GEOS-Chem and its adjoint model with biomass burning emission input from GFED-v3 with small fires included could be used to investigate the impact of this intercontinental pollution episode and more detailed analysis should be conducted in the future.

Acknowledgement: This research was supported in part by NASA grants NNX09AF07G and NNX08AF64G from the Atmospheric Chemistry Modeling and Analysis Program (ACMAP) and from the Interdisciplinary Science Program (IDS). The GEOS-Chem model is managed by the Atmospheric Chemistry Modeling group at Harvard University with support from the NASA ACMAP program.

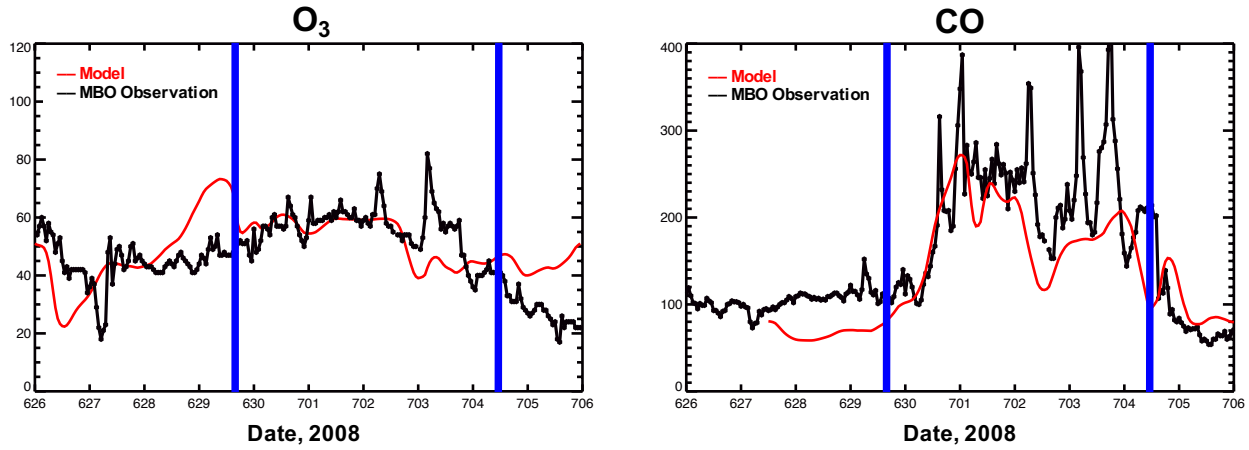

Figure 4.1: Times series of observed (black line) and GEOS-Chem simulated (red line) surface O_3 (ppb, left) and CO (ppb, right) for June 28th - July 6th, 2008 at Mt. Bachelor Observatory (MBO). Values are hourly averages.

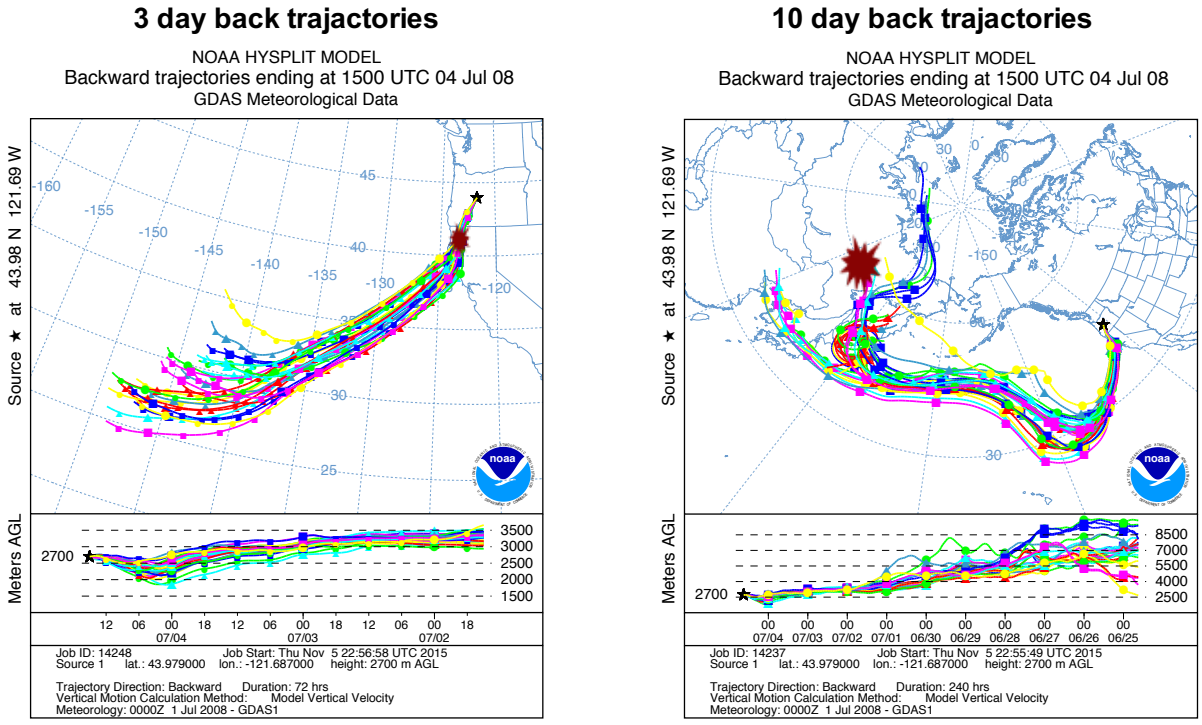

Figure 4.2: Three day (left) and ten day (right) ensemble backward HYSPLIT trajectories initiated at 15:00 pm July 4th, 2008 at Mt. Bachelor Observatory (MBO). Red sparks are showing the approximate fire locations inferred from the FIRMS Web Fire Mapper.

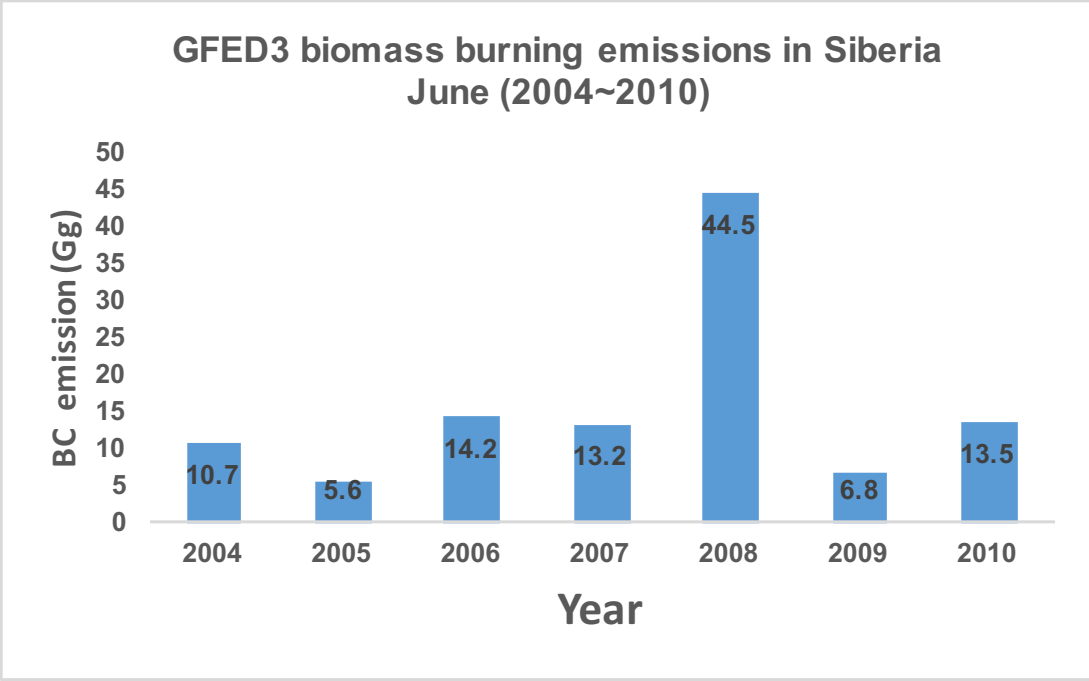

Figure 4.3: GFED3 biomass burning emissions of BC over Siberia (50°N-80°N, 80°E-270°E) in June during year 2004-2010.

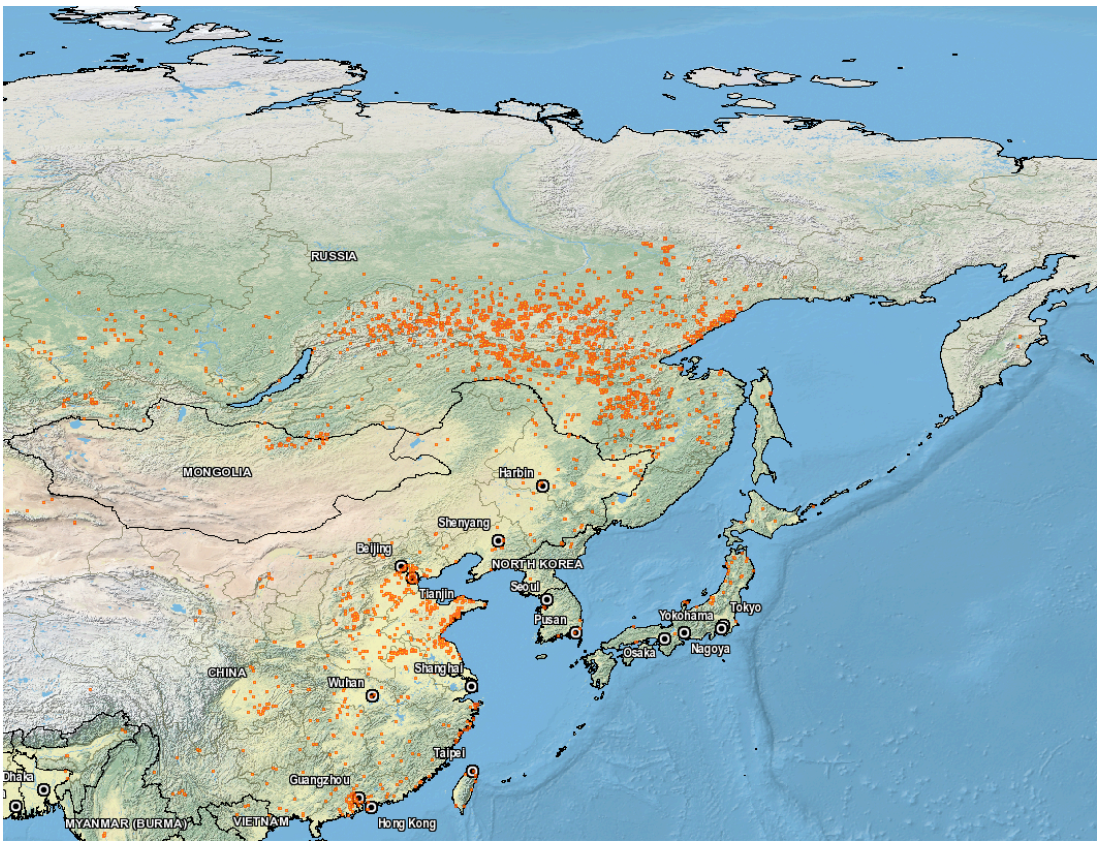

Figure 4.4: Active fire counts from MODIS Fire Information for Resource Management System (FIRMS) Web Fire Mapper during June, 2008 over Siberia (50°N-80°N, 80°E-270°E).

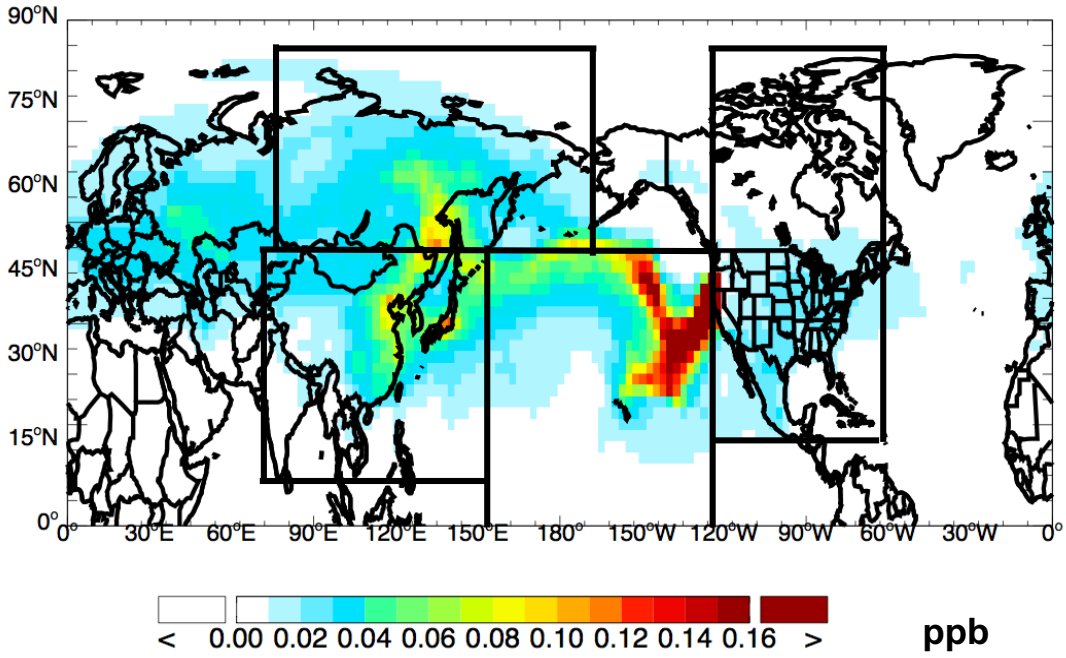

Figure 4.5: Sensitivity of O_3 concentration at Mt. Bachelor Observatory (MBO) to O_3 production worldwide as inferred from the GEOS-Chem adjoint model, integrated in time (two months) , over the depth of the tropospheric column and at the $2° \times 2.5°$ grid resolution of the model.

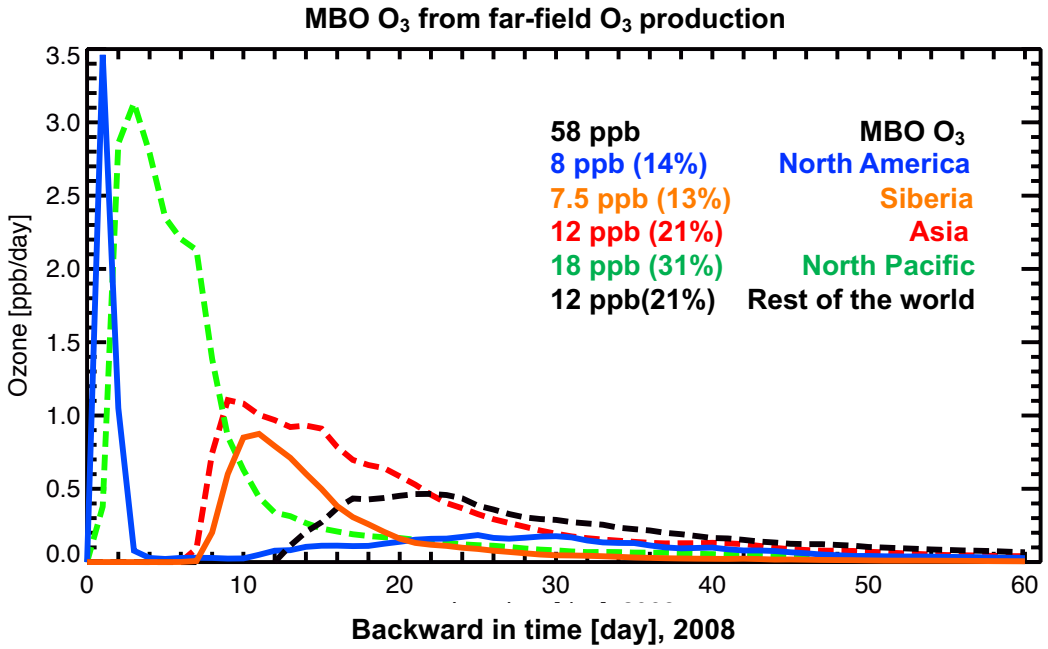

Figure 4.6: The time-dependent sensitivities (going back in time) of O_3 concentration at Mt. Bachelor Observatory (MBO) to O_3 production over Asia (red,8°N-50°N, 70°E-152°E), Siberia (orange, 50°N-80°N, 80°E-270°E), the North Pacific (green, 0°N-50°N, 152°E-232°W), North America (blue, 15°N-80°N, 232°W-292°W) and Rest of World (black), as inferred from the GEOS-Chem adjoint model.

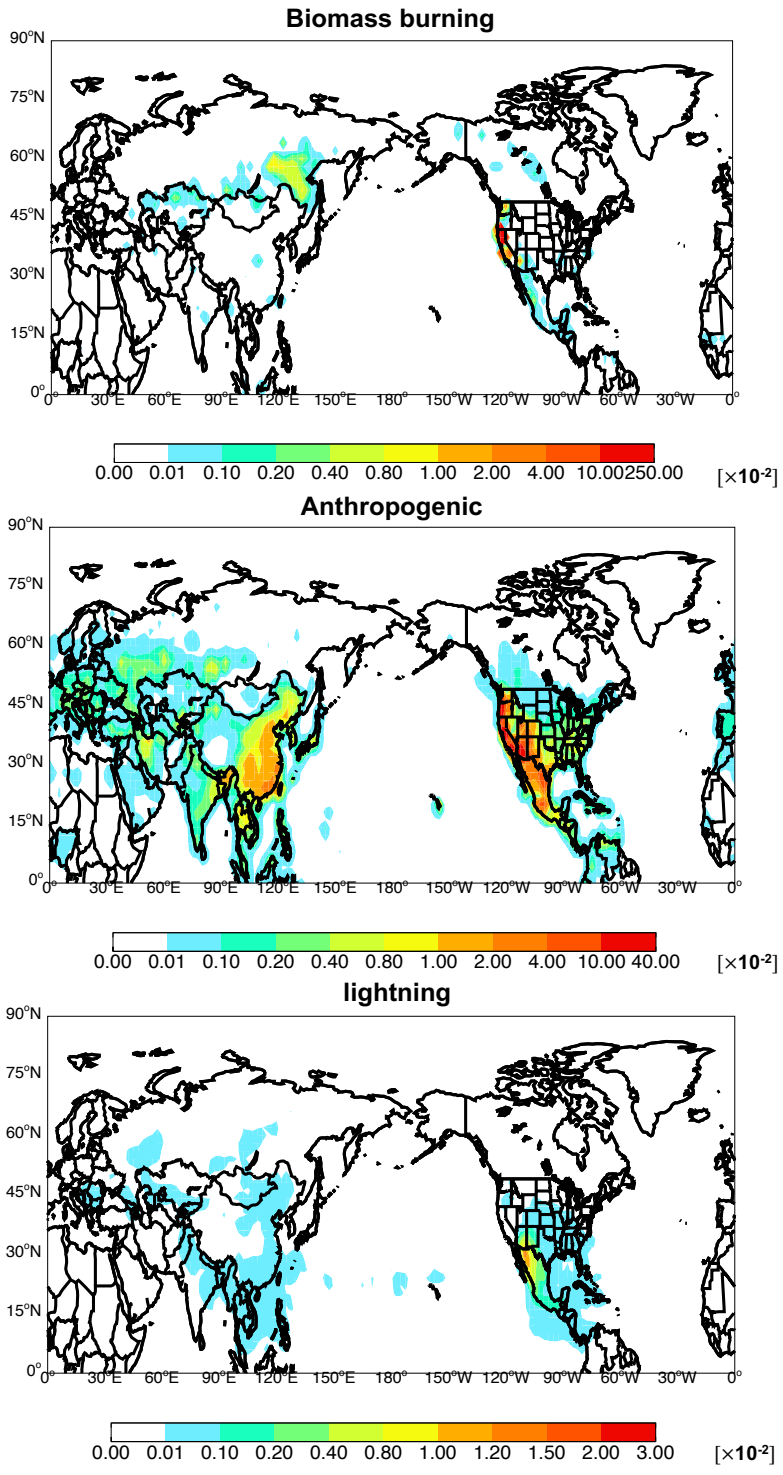

Figure 4.7: Normalised sensitivity of O_3 concentration at Mt. Bachelor Observatory (MBO) to NO_x emissions estimates associated with biomass burning (top), anthropogenic (middle) and lightning (bottom) sources.

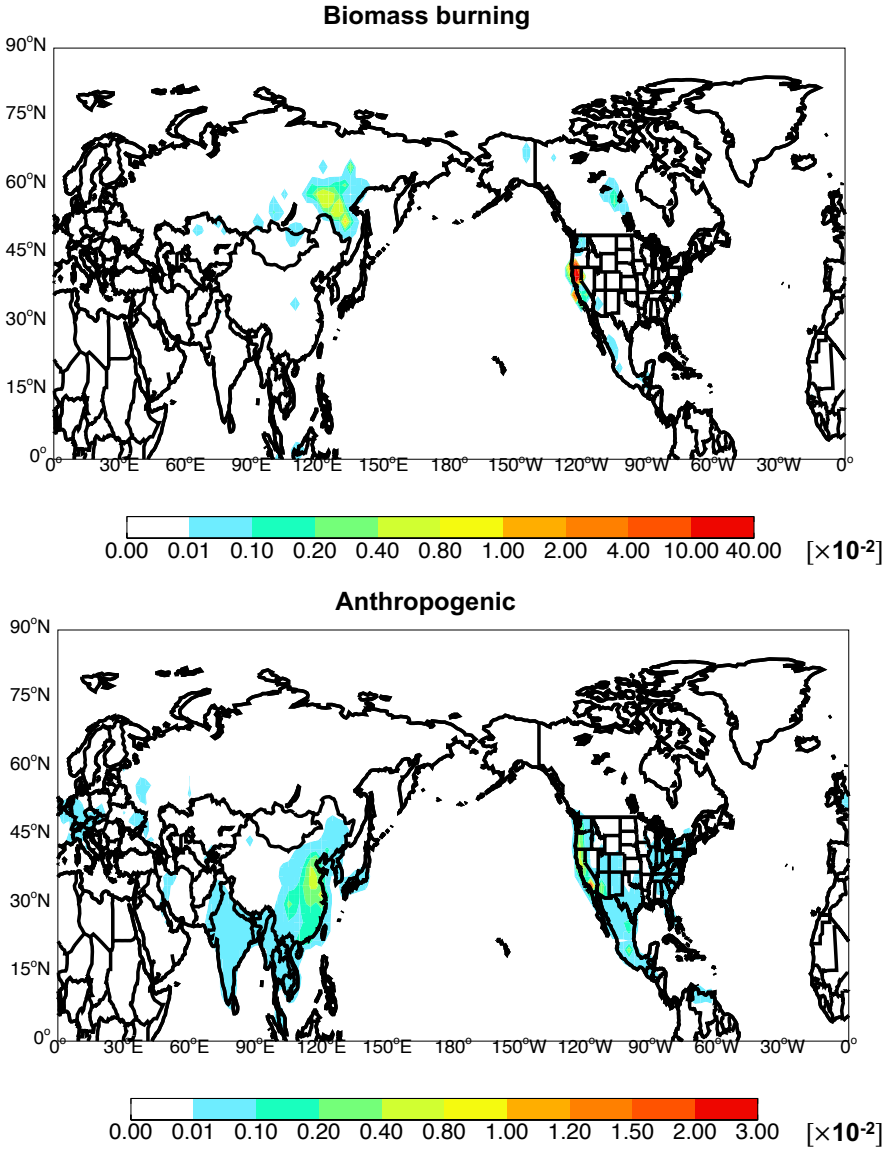

Figure 4.8: Normalised sensitivity of O_3 concentration at Mt. Bachelor Observatory (MBO) to CO emissions estimates associated with biomass burning (top) and anthropogenic (bottom) sources.

CHAPTER 5

Conclusion

5.1 Final conclusions

We analyze the surface ozone observations from the Clean Air Status and Trend Network (CASTNet) using a global chemical transport model (GEOS-Chem) to investigate the impact of biomass burning on surface O_3 in the western U.S. (WUS) mountain ranges during the June-October fire season of 2007, one of the stronger fire years in the WUS in the past decade. GEOS-Chem O_3 captures the observed seasonal, synoptic and daily variations. Model daily afternoon average surface O_3 concentrations at the CASTNet sites are within 2 ppb of the observations, with correlation coefficients of 0.51-0.83 and Taylor scores of 0.64-0.92. Observed maximum daily 8-hour (MAD8) surface O_3 concentrations are 37-58 ppb at the sites, while the corresponding model results are higher by 6 ppb on average. Model results show July-September maximum surface O_3 enhancement of $\sim$9 ppb on average because of biomass burning. Peaks in fire-contributed surface O_3 correspond broadly with high levels of potassium (K), reaffirming a strong fire influence. We find a policy relevant background (PRB) O_3 of 45.6 ppb on average during July-September. Fire-contributed O_3 accounts for up to 30% of the PRB O_3, highest in the intense fire region (Montana, Idaho, and Wyoming) with maxima in August and September.

We examine an unexpected summertime surface O_3 minimum ($\sim$30-45 ppb) in July-August observed throughout the Southwestern U.S. (SWUS) by interpreting observations of O_3 and rainfall from the Clean Air Status and Trends Network (CASTNet) for 2000-11 with a global chemical transport model. The O_3 minimum reflects competing chemical and dy-

namic factors as well as anthropogenic and natural influences. Its occurrence corresponds to the interannual rainfall maximum in North American summer monsoon (NASM) -negative surface O_3 anomalies are accompanied by positive rainfall anomalies at the CASTNet sites (r = -0.5 to -0.7, p <0.05). Relative to June 15-July 15, 2007 (prior to the monsoon onset in the SWUS), increased cloudiness during the maximum rainfall in July 15-August 15 (after the onset) weakens photochemistry, reduces O_3 production from anthropogenic emissions, thereby depresses O_3 at the surface (-5 ppb at Chiricahua, AZ and -3 ppb on average across the SWUS) and throughout the lower troposphere. Largest relative changes (ΔO_3) are seen at rainfall maxima, particularly in the core of the Great Plains low-level jet. The corresponding enhancement in lightning (hence NO_x emissions) augments O_3 production in the middle troposphere and subsequent downward mixing in convective downdrafts, thus increases surface O_3 non-negligibly (+2 ppb at Chiricahua and +1 ppb averaged over the SWUS) and significantly throughout the tropospheric column. The resulting ΔO_3 is largest (+8 ppb) in the anti-cyclonic circulation associated with the upper-level high. Weaker photochemistry dominates the overall ΔO_3 near the surface, while enhanced lightning dominates in much of the free troposphere. Additionally, we find that transport leads to a net export of O_3 throughout the tropospheric column and the influence from stratospheric intrusion is vanishingly small. These competing effects suppress O_3 in the lower troposphere (ΔO_3 up to -5 ppb) while enhance O_3 at higher altitudes (ΔO_3 up to +7 ppb) across the SWUS during the monsoon.

We use the GEOS-Chem 3-D global tropospheric chemical transport model and its adjoint to quantify the source contributions to O_3 pollution observed at Mt. bachelor Observatory (MBO) during the summer of 2008. The adjoint computes the sensitivity of O_3 concentration at the receptor site to O_3 production rates at $2^\circ \times 2.5^\circ$ resolution over the history of air parcels reaching the site. We found that MBO experienced distinct O_3 pollution episodes from Siberia wildfire emissions. During the O_3 pollution episode from June 30th to July 4th in year 2008, 7.5 ppb of MBO O_3 is produced over Siberia, comparable to the amount of O_3

(8ppb) produced over North America. A significant amount of O_3 (18ppb) production took place over the North pacific, with maxima just off the west coast of the U.S. where subsidence of air masses causes decomposition of PAN (peroxyacetylnitrate, a thermo-unstable NO_x reservoir species) and drives further ozone production. We also used the adjoint of GEOS-Chem to show the model O_3 at MBO is largely sensitive to NO_x emissions from biomass burning sources in Siberia and northern California, lightning sources over southwestern U.S. and Mexico, and anthropogenic sources in western U.S. and eastern Asia. For the CO emissions, the largest O_3 sensitivity is to the biomass burning sources in northern California and Siberia. The peak sensitivity to biomass burning CO emissions is comparable to the peak O_3 sensitivity to anthropogenic NO_x emissions.

5.2 Future work

5.2.1 Interannual variability of the impact of wildfire emission on surface O_3 in the western U.S

Our past and ongoing research centered on the seasonal influence of fire contribution to surface O_3 in the WUS mountain ranges. Previous research has shown that the frequency, duration and burned area of wildfires have all been increasing in the WUS in the past a few decades, due to climate changes (*Westerling et al.*, 2006). Figure 2 also indicates very large inter-annual variability of wildfire intensities. Therefore we propose to examine the interannual variability of the impact of wildfire emission on surface O_3 in the WUS.

Because wildfires emit substantial O_3 precursors, we hypothesize that the inter-annual variations in WUS O_3 is related to the variations in wildfire activities. (*Spracklen et al.*, 2007) were able to use GEOS-Chem model to reasonably reproduce the variability in annual mean Organic carbon (OC) and Elemental carbon (EC) concentrations measured by the IMPROVE network averaged over the WUS. Based on our results in Chapter 2, we already quantified the fire contribution to both surface O_3 and PRB O_3 in the WUS for the years 2006

and 2007 using sensitivity analyses with GEOS-Chem. In order to evaluate our hypothesis, we could conduct model simulation for multiple years (e.g. for 2001-2010) to investigate the decadal variations of the influence of wildfires on surface O_3 in the WUS.

We could use fire emission input from GFED-v3, which could provide us with multiple-year fire emission data from 1997 to 2009. Coarse resolution in both GEOS-Chem and GFED-v2 were found to have caused the underestimation of BC surface concentrations during summer fire season in the WUS (*Mao et al.*, 2010). To avoid excessive dispersion of biomass burning emissions, we would conduct NA nested model simulations with high-temporal-resolution GFED-v3 (daily and 3-hourly, $0.5^\circ \times 0.5^\circ$) as fire emission inventory. Model results would be compared with surface observations from both CASTNet and the U.S National Park Service (NPS). Fire-contributed O_3 concentration could be calculated from sensitivity simulations for each year. Time series of the contributions over the past decade could be plotted. We could then analyze how the influence of wildfires on surface O_3 in the WUS has changed in the past decade. Both MODIS fire count data and carbon emission from GFED-v3 will be used as proxy of wildfire intensity. When all these data are ready, we could calculate the correlation of fire intensity proxies and the interannual variations in fire-contributed O_3.

While fires are clearly one important factor to explain the inter-annual variability, other factors, such as large-scale variations in background O_3 may also be important. The question arises as to whether an increase in fire extent is responsible for the positive trend in O_3 in the WUS. We would examine time series of the simulated surface O_3 concentration with fire emission turned off for the past decade. If by removing the influence from fires, the positive trend in surface O_3 in the WUS is significantly reduced, we could then conclude that the increase in fires has largely been responsible for the increase in summertime O_3 reported by (*Jaffe and Ray*, 2007).

5.2.2 Effect of small fires on surface O_3 in the western U.S.

Small fires emission is an important constituent to total biomass burning emission. We should take it into consideration when quantifying the impact of fire emission on surface air quality. However, current inventories for biomass burning emissions significantly underestimate small fire emissions (*Randerson et al.*, 2012). In several biomes, including croplands, wooded savannas, and tropical forests, many small fires occur each year that are well below the detection limit of the current generation of global burned area products derived from moderate resolution surface reflectance imagery. Small fires often occur in agricultural settings where the size of an individual field limits the fire spread (*McCarty et al.*, 2009). In the U.S., for example, agricultural field sizes vary by region, with an average of approximately 16 ha in many southern and eastern regions.

(*Randerson et al.*, 2012) included the small fire emissions in the Global Fire Emissions Database version 3 (GFED-v3) by combining 1km thermal anomalies (active fires) and 500m burned area observations from MODIS. Biomass burning carbon emissions increased by 35% at a global scale when small fires were included in GFED-v3, from 1.9 Pg C/yr to 2.5 Pg C/yr. For regions that could have the most significant impact on surface O_3 in the WUS, including Boreal North America, Temperate North America and Central America, the carbon emissions increased by 9%, 81% and 101%, respectively due to small fires. In termes of burned area, in the continental U.S., the small fires increased the total amount of MODIS burned area by approximately 75% during the same period.

Small fire emissions, including CO, CH_4, NO_x, and comparatively less amount of SO_2, could be an important local and regional contribution of particulate and trace gas emissions that affect both air quality and public health (*Hays et al.*, 2005). In my proposed research, I will conduct sensitivity simulations using GEOS-Chem model with biomass burning emission input from GFED-v3. Emission factors for O_3 precursors from small fires have already been incorporated by Y. Mao (personal communication) into GFED-v3 and implemented in the GEOS-Chem model. By calculating the difference between sensitivity and standard

simulations, we can then quantify the impact of small fire emissions surface O_3 in the WUS.

5.2.3 A regional perspective: The impact of wildfires on regional O_3 air quality in Southern California

Having investigated the impact of wildfire emissions on surface O_3 in the WUS on a continental scale, we would like to zoom in to Southern California and look at the problem from a regional perspective. Wildfires periodically burn large areas of chaparral and woodlands in summer and autumn in Southern California. These fires often occur in conjunction with Santa Ana weather events. Dry Santa Ana winds promote the ignition and rapid spread of wildfires by drying fuels and fanning the flames of fires once they are started (*Westerling et al.*, 2004). One example is the year 2003 in which a large number of fires occurred during Santa Ana events. 12 major fires started between 21 October and 27 October in southern California and another began on 28 October near Ensenada in Baja California, Mexico By the end of November, the fires had burned a total of over 300,000 hectares. The paths of these fires were, in many cases, coincident with some of the most densely populated urban areas in the U.S. Therefore influence of fire emissions on urban air quality may result in severe public health and societal problem. (*Delfino et al.*, 2008) evaluated the relationships of hospital admissions for cardio respiratory outcomes to wildfire-associated PM2.5 using data from the catastrophic wildfires that struck southern California in the autumn of 2003. PM2.5 is the air pollutant with the greatest increase in concentrations during fire events. They found that wildfire-related PM2.5 led to increased respiratory hospital admissions, especially asthma. The average increases of 70-ug/m3 PM2.5 during heavy smoke conditions compared with PM2.5 in the pre-wildfire period were associated with 34% increase in asthma admissions.

WRF-Chem would be the suitable tool for our analysis of the impact of wildfires on regional air quality in southern California. We would use the observations of O_3 and its precursors from California Air Resources Board (CARB, `http://www.arb.ca.gov/homepage.htm`)

sites to validate the WRF-Chem simulation. California's Legislature established the ARB in 1967 to attain and maintain healthy air quality. It has one of the most extensive ambient air monitoring network in the world, consisting of over 250 sites where air pollution levels are monitored and more than 700 monitors used to measure the pollutant levels. The CARB monitoring sites include instruments that measure ambient levels of gaseous and particulate air pollutants, and in some cases, meteorological parameters.

We will conduct model simulations with all the three domains configured in the model, but focusing on Southern California and specifically the L.A. basin. We will run the model for the fire episodes in 2003 and 2007, two of the years when California has experienced the strongest wildfire activities in the past decade. J. Randerson's group at UCI has been developing the high-resolution fire emission (2km $\times$ 2km) based on the GFED approach. We will incorporate this new fire emission inventory in the WRF-Chem model and conduct sensitivity analysis to calculate the contribution of wildfires emissions to the O_3 and PM levels in urban areas in Southern California. If time allows, we will also conduct WRF-Chem adjoint model to quantify source contributions to O_3 pollution in Southern California urban regions.

5.2.4 Impact of wildfires on surface ozone air quality in a future climate

As we enter an era of rapid climate change, how wildfires may impact surface air quality in a future climate needs to be better understood. The long term projections for the impact of fires on surface air quality is a very difficult problem due to the uncertainties in the future emission inventory for both anthropogenic emissions and fire emissions.

In future climate, changes in temperature, atmospheric water vapor, and the presence of stagnant meteorological conditions would all contribute to the changes in O_3 formation in the troposphere. The future climate is expected to be more stagnant, due to a weaker global circulation and a decreasing frequency of mid-latitude cyclone (*Mickley et al.*, 2004). The 4th IPCC report presents mean regional climate projections for the 21st century from an

ensemble of about 20 GCMs. Model results show a strong warming over the northern mid-latitude continents and a slight increase in global precipitation. (*Jacob and Winner*, 2009) summarized previous studies that have examined the effect of climate change on regional O_3 pollution. The results indicate that polluted regions at northern mid-latitude will experience higher surface O_3 as a result of 21st-century climate change. The projected increases are typically in the 1-10 ppb range. (*Steiner et al.*, 2006) investigated the O_3 formation in central California during a 5-day summertime simulation with Community Multistage Air Quality model (CMAQ v4.3). They found that climate changes expected for temperature and atmospheric water vapor each individually cause a 1-5% increase in the daily peak O_3 in central California.

Long-term projections for the impacts of wildfires on surface air quality must account for two factors, future changes in fire emissions and changes in climate. Thus the proposed study would consist of two experiments. In the first experiment, we would assume the future fire emissions are held constant, and quantify the changes in surface O_3 and PM2.5 purely due to climate changes. We could cooperate with Alex Hall's group from UCLA to abtain the future meteorological fields from GCMs. Their results would be particularly useful in our regional study of the impact on air quality in LA basin, because they have applied the state-of-the-art dynamical downscaling techniques to 19 GCMs and projected the mid-21st-century warming in the LA region at 2km (1.2mile) resolution (`http://c-change.la/temperature`). We will conduct sensitivity simulation using both GEOS-Chem and WRF-Chem driven by projected global and regional meteorological fields to quantify the changes in surface O_3 due to changes in future climate.

In the second experiment, we can incorporate future fire emissions in GEOS-Chem model. The current GFED-v3 does not have the emission inventory for future years, but the method used in the paper by (*Spracklen et al.*, 2009) could give us some clue. We could predict future area burned by first regressing observed area burned onto observed meteorological fields and then use future meteorological fields as new input. With the future fire emission

input, we can then conduct sensitivity simulation with GEOS-Chem to quantify the increase in surface O_3 due to increase in future biomass burning emissions. Prediction of wildfire activities' influence on O_3 levels under the climate changing regime would assist us in policy making decisions and fire management strategies.

Bibliography

Adams, D. K., and A. C. Comrie (1997), The north american monsoon, *Bulletin of the American Meteorological Society*, *78*(10), 2197–2213.

Adler, R. F., G. J. Huffman, A. Chang, R. Ferraro, P.-P. Xie, J. Janowiak, B. Rudolf, U. Schneider, S. Curtis, D. Bolvin, et al. (2003), The version-2 global precipitation climatology project (gpcp) monthly precipitation analysis (1979-present), *Journal of hydrometeorology*, *4*(6), 1147–1167.

Agel, L., V. Lopez, M. Barlow, and F. Colby (2011), Regional and large-scale influences on summer ozone levels in southern california, *Journal of Applied Meteorology and Climatology*, *50*(4), 800–805.

Allen, D. J., P. Kasibhatla, A. M. Thompson, R. B. Rood, B. G. Doddridge, K. E. Pickering, R. D. Hudson, and S.-J. Lin (1996a), Transport-induced interannual variability of carbon monoxide determined using a chemistry and transport model, *Journal of Geophysical Research: Atmospheres (1984–2012)*, *101*(D22), 28,655–28,669.

Allen, D. J., R. B. Rood, A. M. Thompson, and R. D. Hudson (1996b), Three-dimensional radon 222 calculations using assimilated meteorological data and a convective mixing algorithm, *Journal of Geophysical Research: Atmospheres (1984–2012)*, *101*(D3), 6871–6881.

Alvarado, M., J. Logan, J. Mao, E. Apel, D. Riemer, D. Blake, R. Cohen, K.-E. Min, A. Perring, E. Browne, et al. (2010), Nitrogen oxides and pan in plumes from boreal fires during arctas-b and their impact on ozone: an integrated analysis of aircraft and satellite observations, *Atmospheric Chemistry and Physics*, *10*(20), 9739–9760.

Ambrose, J., D. Reidmiller, and D. Jaffe (2011), Causes of high o 3 in the lower free tropo-

sphere over the pacific northwest as observed at the mt. bachelor observatory, *Atmospheric Environment*, *45*(30), 5302–5315.

Barlow, M., S. Nigam, and E. H. Berbery (1998), Evolution of the north american monsoon system, *Journal of Climate*, *11*(9), 2238–2257.

Baumgardner, R. (1998), Clean air status and trends network (castnet) deposition, summary report (1987–1995). technical report, *Tech. rep.*, QST Environmental, Inc., Gainesville, FL (United States); Environmental Protection Agency, Atmospheric Research and Exposure Assessment Lab., Research Triangle Park, NC (United States).

Baylon, P., D. Jaffe, N. Wigder, H. Gao, and J. Hee (2015), Ozone enhancement in western us wildfire plumes at the mt. bachelor observatory: The role of no x, *Atmospheric Environment*, *109*, 297–304.

Bey, I., D. J. Jacob, R. M. Yantosca, J. A. Logan, B. D. Field, A. M. Fiore, Q. Li, H. Y. Liu, L. J. Mickley, and M. G. Schultz (2001), Global modeling of tropospheric chemistry with assimilated meteorology: Model description and evaluation.

Boccippio, D. J., K. L. Cummins, H. J. Christian, and S. J. Goodman (2001), Combined satellite-and surface-based estimation of the intracloud-cloud-to-ground lightning ratio over the continental united states, *Monthly Weather Review*, *129*(1), 108–122.

Bordoni, S., P. E. Ciesielski, R. H. Johnson, B. D. McNoldy, and B. Stevens (2004), The low-level circulation of the north american monsoon as revealed by quikscat, *Geophysical Research Letters*, *31*(10).

Brock, C. A., P. K. Hudson, E. R. Lovejoy, A. Sullivan, J. B. Nowak, L. G. Huey, O. R. Cooper, D. J. Cziczo, J. De Gouw, F. C. Fehsenfeld, et al. (2004), Particle characteristics following cloud-modified transport from asia to north america, *Journal of Geophysical Research: Atmospheres (1984–2012)*, *109*(D23).

Carleton, A. M., D. A. Carpenter, and P. J. Weser (1990), Mechanisms of interannual variability of the southwest united states summer rainfall maximum, *Journal of Climate*, *3*(9), 999–1015.

Change, I. P. O. C. (2007), Climate change 2007: The physical science basis, *Agenda*, *6*(07), 333.

Chen, H., A. Karion, C. Rella, J. Winderlich, C. Gerbig, A. Filges, T. Newberger, C. Sweeney, and P. Tans (2013), Accurate measurements of carbon monoxide in humid air using the cavity ring-down spectroscopy (crds) technique, *Atmospheric Measurement Techniques*, *6*, 1031–1040.

Chen, Y., Q. Li, J. Randerson, E. Lyons, R. Kahn, D. Nelson, and D. Diner (2009), The sensitivity of co and aerosol transport to the temporal and vertical distribution of north american boreal fire emissions, *Atmospheric Chemistry and Physics*, *9*(17), 6559–6580.

Christian, H. J., R. J. Blakeslee, D. J. Boccippio, W. L. Boeck, D. E. Buechler, K. T. Driscoll, S. J. Goodman, J. M. Hall, W. J. Koshak, D. M. Mach, et al. (2003), Global frequency and distribution of lightning as observed from space by the optical transient detector, *Journal of Geophysical Research: Atmospheres (1984–2012)*, *108*(D1), ACL–4.

Clarke, J., E. Edgerton, and B. Martin (1997), Dry deposition calculations for the clean air status and trends network, *Atmospheric Environment*, *31*(21), 3667–3678.

Cohan, D. S., A. Hakami, Y. Hu, and A. G. Russell (2005), Nonlinear response of ozone to emissions: Source apportionment and sensitivity analysis, *Environmental Science & Technology*, *39*(17), 6739–6748.

Cook, B., and R. Seager (2013), The response of the north american monsoon to increased greenhouse gas forcing, *Journal of Geophysical Research: Atmospheres*, *118*(4), 1690–1699.

Cooper, O., A. Stohl, M. Trainer, A. Thompson, J. Witte, S. Oltmans, G. Morris, K. Pickering, J. Crawford, G. Chen, et al. (2006), Large upper tropospheric ozone enhancements

above midlatitude north america during summer: In situ evidence from the ions and mozaic ozone measurement network, *Journal of Geophysical Research: Atmospheres (1984–2012)*, *111*(D24).

Cooper, O., M. Trainer, A. Thompson, S. Oltmans, D. Tarasick, J. Witte, A. Stohl, S. Eckhardt, J. Lelieveld, M. Newchurch, et al. (2007), Evidence for a recurring eastern north america upper tropospheric ozone maximum during summer, *Journal of Geophysical Research: Atmospheres (1984–2012)*, *112*(D23).

Cooper, O., D. Parrish, A. Stohl, M. Trainer, P. Nédélec, V. Thouret, J. Cammas, S. Oltmans, B. Johnson, D. Tarasick, et al. (2010), Increasing springtime ozone mixing ratios in the free troposphere over western north america, *Nature*, *463*(7279), 344–348.

Cooper, O. R., R.-S. Gao, D. Tarasick, T. Leblanc, and C. Sweeney (2012), Long-term ozone trends at rural ozone monitoring sites across the united states, 1990–2010, *Journal of Geophysical Research: Atmospheres (1984–2012)*, *117*(D22).

Cooper, O. R., D. Parrish, J. Ziemke, N. Balashov, M. Cupeiro, I. Galbally, S. Gilge, L. Horowitz, N. Jensen, J.-F. Lamarque, et al. (2014), Global distribution and trends of tropospheric ozone: An observation-based review, *Elementa: Science of the Anthropocene*, *2*(1), 000,029.

Crimmins, M. (2006), Arizona and the north american monsoon system.

Cynthia Lin, C.-Y., D. J. Jacob, J. W. Munger, and A. M. Fiore (2000), Increasing background ozone in surface air over the united states.

DeCaria, A. J., K. E. Pickering, G. L. Stenchikov, and L. E. Ott (2005), Lightning-generated nox and its impact on tropospheric ozone production: A three-dimensional modeling study of a stratosphere-troposphere experiment: Radiation, aerosols and ozone (sterao-a) thunderstorm, *Journal of Geophysical Research: Atmospheres (1984–2012)*, *110*(D14).

Delfino, R. J., S. Brummel, J. Wu, H. Stern, B. Ostro, M. Lipsett, A. Winer, D. H. Street, L. Zhang, T. Tjoa, et al. (2008), The relationship of respiratory and cardiovascular hospital admissions to the southern california wildfires of 2003, *Occupational and Environmental Medicine*.

Derwent, R., D. Stevenson, R. Doherty, W. Collins, and M. Sanderson (2008), How is surface ozone in europe linked to asian and north american nox emissions?, *Atmospheric Environment*, *42*(32), 7412–7422.

Dickerson, R., C. Li, Z. Li, L. Marufu, J. Stehr, B. McClure, N. Krotkov, H. Chen, P. Wang, X. Xia, et al. (2007), Aircraft observations of dust and pollutants over northeast china: Insight into the meteorological mechanisms of transport, *Journal of Geophysical Research: Atmospheres (1984–2012)*, *112*(D24).

Draxler, R. R., and G. Hess (1998), An overview of the hysplit_4 modelling system for trajectories, *Australian meteorological magazine*, *47*(4), 295–308.

Dubovik, O., T. Lapyonok, Y. J. Kaufman, M. Chin, P. Ginoux, L. Remer, and B. N. Holben (2004), Inversion of global distribution of aerosol sources using modis and aeronet data, *Optica Pura y Aplicada*, *37*, 3349–3358.

Dubovik, O., T. Lapyonok, Y. Kaufman, M. Chin, P. Ginoux, R. Kahn, and A. Sinyuk (2008), Retrieving global aerosol sources from satellites using inverse modeling, *Atmospheric Chemistry and Physics*, *8*(2), 209–250.

Duncan, B., J. West, Y. Yoshida, A. Fiore, and J. Ziemke (2008), The influence of european pollution on ozone in the near east and northern africa, *Atmospheric Chemistry and Physics*, *8*(8), 2267–2283.

Elbern, H., and H. Schmidt (2001), Ozone episode analysis by four-dimensional variational chemistry data assimilation, *Journal of Geophysical Research: Atmospheres (1984–2012)*, *106*(D4), 3569–3590.

Elbern, H., H. Schmidt, and A. Ebel (1997), Variational data assimilation for tropospheric chemistry modeling, *Journal of Geophysical Research: Atmospheres (1984–2012)*, *102*(D13), 15,967–15,985.

Elbern, H., H. Schmidt, O. Talagrand, and A. Ebel (2000), 4d-variational data assimilation with an adjoint air quality model for emission analysis, *Environmental Modelling & Software*, *15*(6), 539–548.

EPA, U. (2003), Latest findings on national air quality: 2002 status and trends report, *EPA, Research Triangle Park*, *EPA-OAQPS*, 454/K–03–001.

EPA, U. (2004), The o3 report: Measuring progress through 2003, *EPA, Research Triangle Park*, pp. 454/K–04–001.

EPA, U. (2006), Air quality criteria for o3 and other photochemical oxidants, *EPA, Office of Air Quality Planning and Standards*, *I*, 600/R–05/004aF.

EPA, U. (2008), Clean air status and trends network (castnet) fact sheet, *EPA, available at: www.epa.gov/castnet/library/facts*.

EPA, U. (2010), Castnet quality assurance, 3rd quarterly report.

Fiore, A., D. J. Jacob, H. Liu, R. M. Yantosca, T. D. Fairlie, and Q. Li (2003), Variability in surface ozone background over the united states: Implications for air quality policy, *Journal of Geophysical Research: Atmospheres (1984–2012)*, *108*(D24).

Fiore, A., F. Dentener, O. Wild, C. Cuvelier, M. Schultz, P. Hess, C. Textor, M. Schulz, R. Doherty, L. Horowitz, et al. (2009), Multimodel estimates of intercontinental source-receptor relationships for ozone pollution, *Journal of Geophysical Research: Atmospheres (1984–2012)*, *114*(D4).

Fiore, A. M., D. J. Jacob, I. Bey, R. M. Yantosca, B. D. Field, A. C. Fusco, and J. G. Wilkinson (2002), Background ozone over the united states in summer: Origin, trend,

and contribution to pollution episodes, *Journal of Geophysical Research: Atmospheres (1984–2012)*, *107*(D15), ACH–11.

Fisher, M., and D. Lary (1995), Lagrangian four-dimensional variational data assimilation of chemical species, *Quarterly Journal of the Royal Meteorological Society*, *121*(527), 1681–1704.

Forster, C., O. Cooper, A. Stohl, S. Eckhardt, P. James, E. Dunlea, D. K. Nicks, J. S. Holloway, G. Hübler, D. D. Parrish, et al. (2004), Lagrangian transport model forecasts and a transport climatology for the intercontinental transport and chemical transformation 2002 (itct 2k2) measurement campaign, *Journal of Geophysical Research: Atmospheres (1984–2012)*, *109*(D7).

Garreaud, R., and J. M. Wallace (1997), The diurnal march of convective cloudiness over the americas, *Monthly Weather Review*, *125*(12), 3157–3171.

Giglio, L., G. Van der Werf, J. Randerson, G. Collatz, and P. Kasibhatla (2006), Global estimation of burned area using modis active fire observations, *Atmospheric Chemistry and Physics*, *6*(4), 957–974.

Giglio, L., J. T. Randerson, and G. R. Werf (2013), Analysis of daily, monthly, and annual burned area using the fourth-generation global fire emissions database (gfed4), *Journal of Geophysical Research: Biogeosciences*, *118*(1), 317–328.

Goldstein, A. H., D. B. Millet, M. McKay, L. Jaegle, L. Horowitz, O. Cooper, R. Hudman, D. J. Jacob, S. Oltmans, and A. Clarke (2004), Impact of asian emissions on observations at trinidad head, california, during itct 2k2, *Journal of Geophysical Research: Atmospheres (1984–2012)*, *109*(D23).

Gratz, L., D. Jaffe, and J. Hee (2015), Causes of increasing ozone and decreasing carbon monoxide in springtime at the mt. bachelor observatory from 2004 to 2013, *Atmospheric Environment*, *109*, 323–330.

Guenther, A., T. Karl, P. Harley, C. Wiedinmyer, P. Palmer, and C. Geron (2006), Estimates of global terrestrial isoprene emissions using megan (model of emissions of gases and aerosols from nature), *Atmospheric Chemistry and Physics Discussions*, *6*(1), 107–173.

Hack, J. J., B. Boville, J. Kiehl, P. Rasch, and D. Williamson (1994), Climate statistics from the national center for atmospheric research community climate model ccm2, *Journal of Geophysical Research: Atmospheres (1984–2012)*, *99*(D10), 20,785–20,813.

Hakami, A., D. Henze, J. Seinfeld, T. Chai, Y. Tang, G. Carmichael, and A. Sandu (2005), Adjoint inverse modeling of black carbon during the asian pacific regional aerosol characterization experiment, *Journal of Geophysical Research: Atmospheres (1984–2012)*, *110*(D14).

Hakami, A., J. H. Seinfeld, T. Chai, Y. Tang, G. R. Carmichael, and A. Sandu (2006), Adjoint sensitivity analysis of ozone nonattainment over the continental united states, *Environmental science & technology*, *40*(12), 3855–3864.

Hakami, A., D. K. Henze, J. H. Seinfeld, K. Singh, A. Sandu, S. Kim, D. Byun, and Q. Li (2007), The adjoint of cmaq, *Environmental science & technology*, *41*(22), 7807–7817.

Harrington Jr, J. A., R. S. Cerveny, and R. C. Balling Jr (1992), Impact of the southern oscillation on the north american southwest monsoon, *Physical Geography*, *13*(4), 318–330.

Hays, M. D., P. M. Fine, C. D. Geron, M. J. Kleeman, and B. K. Gullett (2005), Open burning of agricultural biomass: physical and chemical properties of particle-phase emissions, *Atmospheric Environment*, *39*(36), 6747–6764.

Heald, C. L., D. J. Jacob, A. M. Fiore, L. K. Emmons, J. C. Gille, M. N. Deeter, J. Warner, D. P. Edwards, J. H. Crawford, A. J. Hamlin, et al. (2003), Asian outflow and trans-pacific transport of carbon monoxide and ozone pollution: An integrated satellite, aircraft, and model perspective, *Journal of Geophysical Research: Atmospheres (1984–2012)*, *108*(D24).

Helfand, H. M., and S. D. Schubert (1995), Climatology of the simulated great plains low-level jet and its contribution to the continental moisture budget of the united states, *Journal of Climate*, *8*(4), 784–806.

Henze, D. K., A. Hakami, and J. H. Seinfeld (2007), Development of the adjoint of geos-chem, *Atmospheric Chemistry and Physics*, *7*(9), 2413–2433.

Henze, D. K., J. H. Seinfeld, and D. T. Shindell (2009), Inverse modeling and mapping us air quality influences of inorganic pm 2.5 precursor emissions using the adjoint of geos-chem, *Atmospheric Chemistry and Physics*, *9*(16), 5877–5903.

Hess, P., and T. Vukicevic (2003), Intercontinental transport, chemical transformations, and baroclinic systems, *Journal of Geophysical Research: Atmospheres (1984–2012)*, *108*(D12).

Higgins, R., Y. Yao, E. Yarosh, J. Janowiak, and K. Mo (1997), Influence of the great plains low-level jet on summertime precipitation and moisture transport over the central united states, *Journal of Climate*, *10*(3), 481–507.

Hudman, R., D. J. Jacob, O. Cooper, M. Evans, C. Heald, R. Park, F. Fehsenfeld, F. Flocke, J. Holloway, G. Hübler, et al. (2004), Ozone production in transpacific asian pollution plumes and implications for ozone air quality in california, *Journal of Geophysical Research: Atmospheres (1984–2012)*, *109*(D23).

Hudman, R., D. J. Jacob, S. Turquety, E. M. Leibensperger, L. T. Murray, S. Wu, A. Gilliland, M. Avery, T. Bertram, W. Brune, et al. (2007), Surface and lightning sources of nitrogen oxides over the united states: Magnitudes, chemical evolution, and outflow, *Journal of Geophysical Research: Atmospheres (1984–2012)*, *112*(D12).

Hudman, R., L. T. Murray, D. J. Jacob, S. Turquety, S. Wu, D. Millet, M. Avery, A. Goldstein, and J. Holloway (2009), North american influence on tropospheric ozone and the

effects of recent emission reductions: Constraints from icartt observations, *Journal of Geophysical Research: Atmospheres (1984–2012)*, *114*(D7).

Huntrieser, H., H. Schlager, A. Roiger, M. Lichtenstern, U. Schumann, C. Kurz, D. Brunner, C. Schwierz, A. Richter, and A. Stohl (2007), Lightning-produced no x over brazil during troccinox: airborne measurements in tropical and subtropical thunderstorms and the importance of mesoscale convective systems, *Atmospheric Chemistry and Physics*, *7*(11), 2987–3013.

Huntrieser, H., U. Schumann, H. Schlager, H. Höller, A. Giez, H.-D. Betz, D. Brunner, C. Forster, O. Pinto Jr, and R. Calheiros (2008), Lightning activity in brazilian thunderstorms during troccinox: implications for no x production, *Atmospheric Chemistry and Physics*, *8*(4), 921–953.

Jacob, D. J., and D. A. Winner (2009), Effect of climate change on air quality, *Atmospheric Environment*, *43*(1), 51–63.

Jacob, D. J., J. A. Logan, and P. P. Murti (1999), Effect of rising asian emissions on surface ozone in the united states, *Geophysical Research Letters*, *26*(14), 2175–2178.

Jaffe, D. (2010), Relationship between surface and free tropospheric ozone in the western us, *Environmental science & technology*, *45*(2), 432–438.

Jaffe, D., and J. Ray (2007), Increase in surface ozone at rural sites in the western us, *Atmospheric Environment*, *41*(26), 5452–5463.

Jaffe, D., I. Bertschi, L. Jaeglé, P. Novelli, J. S. Reid, H. Tanimoto, R. Vingarzan, and D. L. Westphal (2004), Long-range transport of siberian biomass burning emissions and impact on surface ozone in western north america, *Geophysical Research Letters*, *31*(16).

Jaffe, D., E. Prestbo, P. Swartzendruber, P. Weiss-Penzias, S. Kato, A. Takami, S. Hatakeyama, and Y. Kajii (2005), Export of atmospheric mercury from asia, *Atmospheric Environment*, *39*(17), 3029–3038.

Jaffe, D., D. Chand, W. Hafner, A. Westerling, and D. Spracklen (2008), Influence of fires on o3 concentrations in the western us, *Environmental science & technology*, *42*(16), 5885–5891.

Jianping, L., and Z. Qingcun (2003), A new monsoon index and the geographical distribution of the global monsoons, *Advances in Atmospheric Sciences*, *20*(2), 299–302.

Jourdain, L., S. Kulawik, H. Worden, K. Pickering, J. Worden, and A. Thompson (2010), Lightning no x emissions over the usa constrained by tes ozone observations and the geos-chem model, *Atmospheric Chemistry and Physics*, *10*(1), 107–119.

Kaynak, B., Y. Hu, R. Martin, A. Russell, Y. Choi, and Y. Wang (2008), The effect of lightning no x production on surface ozone in the continental united states, *Atmospheric Chemistry and Physics*, *8*(17), 5151–5159.

Kopacz, M., D. Jacob, D. Henze, C. Heald, D. Streets, and Q. Zhang (2006), A comparison of analytical and adjoint bayesian inversion methods for constraining asian sources of co using satellite (mopitt) measurements of co columns, in *AGU Fall Meeting Abstracts*, vol. 1, p. 0875.

Kotchenruther, R. A., D. A. Jaffe, and L. Jaeglé (2001), Ozone photochemistry and the role of pan in the springtime northeastern pacific troposphere: Results from the phobea campaign, *J. Geophys. Res*, *106*(28), 731–28.

Koumoutsaris, S., I. Bey, S. Generoso, and V. Thouret (2008), Influence of el niño–southern oscillation on the interannual variability of tropospheric ozone in the northern midlatitudes, *Journal of Geophysical Research: Atmospheres (1984–2012)*, *113*(D19).

Langford, A. (1999), Stratosphere-troposphere exchange at the subtropical jet: Contribution to the tropospheric ozone budget at midlatitudes, *Geophysical research letters*, *26*(16), 2449–2452.

Lefohn, A. S., S. J. Oltmans, T. Dann, and H. B. Singh (2001), Present-day variability of background ozone in the lower troposphere, *Journal of Geophysical Research: Atmospheres (1984–2012)*, *106*(D9), 9945–9958.

Lelieveld, J., and P. J. Crutzen (1994), Role of deep cloud convection in the ozone budget of the troposphere, *Science*, *264*(5166), 1759–1761.

Liang, J., and M. Z. Jacobson (2000), Effects of subgrid segregation on ozone production efficiency in a chemical model, *Atmospheric Environment*, *34*(18), 2975–2982.

Liang, Q., L. Jaeglé, D. A. Jaffe, P. Weiss-Penzias, A. Heckman, and J. A. Snow (2004), Long-range transport of asian pollution to the northeast pacific: Seasonal variations and transport pathways of carbon monoxide, *Journal of Geophysical Research: Atmospheres (1984–2012)*, *109*(D23).

Lin, C.-Y. C., D. J. Jacob, and A. M. Fiore (2001), Trends in exceedances of the ozone air quality standard in the continental united states, 1980–1998, *Atmospheric Environment*, *35*(19), 3217–3228.

Lin, M., A. M. Fiore, L. W. Horowitz, A. O. Langford, S. J. Oltmans, D. Tarasick, and H. E. Rieder (2015), Climate variability modulates western us ozone air quality in spring via deep stratospheric intrusions, *Nature communications*, *6*.

Lin, S.-J., and R. B. Rood (1996), Multidimensional flux-form semi-lagrangian transport schemes, *Monthly Weather Review*, *124*(9), 2046–2070.

Lions, J. L. (1971), *Optimal control of systems governed by partial differential equations*, vol. 170, Springer Verlag.

Liu, H., D. J. Jacob, I. Bey, R. M. Yantosca, B. N. Duncan, and G. W. Sachse (2003), Transport pathways for asian pollution outflow over the pacific: Interannual and seasonal variations, *Journal of Geophysical Research: Atmospheres (1984–2012)*, *108*(D20).

Mao, Y., Q. Li, L. Zhang, Y. Jin, Y. Chen, and J. Randerson (2010), Wildfire contribution to black carbon in the western us mountain ranges, in *AGU Fall Meeting Abstracts*, vol. 1, p. 0068.

Marchuk, G. (1974), Numerical solution of the problems of the dynamics of the atmosphere and ocean, gigrometeoizdat.

Martien, P. T., R. A. Harley, and D. G. Cacuci (2006), Adjoint sensitivity analysis for a three-dimensional photochemical model: Implementation and method comparison, *Environmental science & technology*, *40*(8), 2663–2670.

Martin, R. V., B. Sauvage, I. Folkins, C. E. Sioris, C. Boone, P. Bernath, and J. Ziemke (2007), Space-based constraints on the production of nitric oxide by lightning, *Journal of Geophysical Research: Atmospheres (1984–2012)*, *112*(D9).

McCarty, J. L., S. Korontzi, C. O. Justice, and T. Loboda (2009), The spatial and temporal distribution of crop residue burning in the contiguous united states, *Science of the Total Environment*, *407*(21), 5701–5712.

McDonald-Buller, E. C., D. T. Allen, N. Brown, D. J. Jacob, D. Jaffe, C. E. Kolb, A. S. Lefohn, S. Oltmans, D. D. Parrish, G. Yarwood, et al. (2011), Establishing policy relevant background (prb) ozone concentrations in the united states, *Environmental science & technology*, *45*(22), 9484–9497.

Menut, L. (2003), Adjoint modeling for atmospheric pollution process sensitivity at regional scale, *Journal of Geophysical Research: Atmospheres (1984–2012)*, *108*(D17).

Mickley, L. J. (2007), A future short of breath? possible effects of climate change on smog, *Environment: Science and Policy for Sustainable Development*, *49*(6), 32–43.

Mickley, L. J., D. J. Jacob, B. Field, and D. Rind (2004), Effects of future climate change on regional air pollution episodes in the united states, *Geophysical Research Letters*, *31*(24).

Mo, K. C., and E. H. Berbery (2004), Low-level jets and the summer precipitation regimes over north america, *Journal of Geophysical Research: Atmospheres (1984–2012)*, *109*(D6).

Mo, K. C., M. Chelliah, M. L. Carrera, R. W. Higgins, and W. Ebisuzaki (2005), Atmospheric moisture transport over the united states and mexico as evaluated in the ncep regional reanalysis, *Journal of Hydrometeorology*, *6*(5), 710–728.

Moorthi, S., and M. J. Suarez (1992), Relaxed arakawa-schubert. a parameterization of moist convection for general circulation models, *Monthly Weather Review*, *120*(6), 978–1002.

Müller, J.-F., and T. Stavrakou (2005), Inversion of co and no x emissions using the adjoint of the images model, *Atmospheric Chemistry and Physics*, *5*(5), 1157–1186.

Murazaki, K., and P. Hess (2006), How does climate change contribute to surface ozone change over the united states?, *Journal of Geophysical Research: Atmospheres (1984–2012)*, *111*(D5).

Murray, L., J. Logan, D. Jacob, R. Hudman, and W. Koshak (2012), Spatial and interannual variability in lightning constrained by lis/otd satellite data for 1998–2006: implications for tropospheric ozone and oh, to be submitted to j, *Geophys. Res.*

Nassar, R., J. A. Logan, I. A. Megretskaia, L. T. Murray, L. Zhang, and D. Jones (2009), Analysis of tropical tropospheric ozone, carbon monoxide, and water vapor during the 2006 el niño using tes observations and the geos-chem model, *Journal of Geophysical Research: Atmospheres (1984–2012)*, *114*(D17).

Nester, K., and H.-J. Panitz (2006), Sensitivity analysis by the adjoint chemistry transport model draisfor an episode in the berlin ozone (berlioz) experiment, *Atmospheric Chemistry and Physics*, *6*(8), 2091–2106.

Neu, J. L., T. Flury, G. L. Manney, M. L. Santee, N. J. Livesey, and J. Worden (2014), Tropospheric ozone variations governed by changes in stratospheric circulation, *Nature Geoscience*, *7*(5), 340–344.

Oltmans, S., A. Lefohn, J. Harris, D. Tarasick, A. Thompson, H. Wernli, B. Johnson, P. Novelli, S. Montzka, J. Ray, et al. (2010), Enhanced ozone over western north america from biomass burning in eurasia during april 2008 as seen in surface and profile observations, *Atmospheric Environment*, *44*(35), 4497–4509.

Oltmans, S. J., A. S. Lefohn, J. M. Harris, and D. S. Shadwick (2008), Background ozone levels of air entering the west coast of the us and assessment of longer-term changes, *Atmospheric Environment*, *42*(24), 6020–6038.

Ott, L. E., K. E. Pickering, G. L. Stenchikov, D. J. Allen, A. J. DeCaria, B. Ridley, R.-F. Lin, S. Lang, and W.-K. Tao (2010), Production of lightning nox and its vertical distribution calculated from three-dimensional cloud-scale chemical transport model simulations, *Journal of Geophysical Research: Atmospheres (1984–2012)*, *115*(D4).

Pachauri, R. K., M. Allen, V. Barros, J. Broome, W. Cramer, R. Christ, J. Church, L. Clarke, Q. Dahe, P. Dasgupta, et al. (2014), Climate change 2014: Synthesis report. contribution of working groups i, ii and iii to the fifth assessment report of the intergovernmental panel on climate change.

Parrington, M., D. Jones, K. Bowman, L. Horowitz, A. Thompson, D. Tarasick, and J. Witte (2008), Estimating the summertime tropospheric ozone distribution over north america through assimilation of observations from the tropospheric emission spectrometer, *Journal of Geophysical Research: Atmospheres (1984–2012)*, *113*(D18).

Parrish, D., D. Millet, and A. Goldstein (2009), Increasing ozone in marine boundary layer inflow at the west coasts of north america and europe, *Atmospheric Chemistry and Physics*, *9*(4), 1303–1323.

Parrish, D., K. S. Law, J. Staehelin, R. Derwent, O. Cooper, H. Tanimoto, A. Volz-Thomas, S. Gilge, H.-E. Scheel, M. Steinbacher, et al. (2013), Lower tropospheric ozone at northern midlatitudes: Changing seasonal cycle, *Geophysical Research Letters*, *40*(8), 1631–1636.

Pfister, G., L. Emmons, P. Hess, J.-F. Lamarque, A. Thompson, and J. Yorks (2008), Analysis of the summer 2004 ozone budget over the united states using intercontinental transport experiment ozonesonde network study (ions) observations and model of ozone and related tracers (mozart-4) simulations, *Journal of Geophysical Research: Atmospheres (1984–2012)*, *113*(D23).

Pickering, K. E., A. M. Thompson, W.-K. Tao, and T. L. Kucsera (1993), Upper tropospheric ozone production following mesoscale convection during step/emex, *Journal of Geophysical Research: Atmospheres (1984–2012)*, *98*(D5), 8737–8749.

Pickering, K. E., Y. Wang, W.-K. Tao, C. Price, and J.-F. Müller (1998), Vertical distributions of lightning nox for use in regional and global chemical transport models, *Journal of Geophysical Research: Atmospheres (1984–2012)*, *103*(D23), 31,203–31,216.

Price, C., and D. Rind (1992), A simple lightning parameterization for calculating global lightning distributions, *Journal of Geophysical Research: Atmospheres (1984–2012)*, *97*(D9), 9919–9933.

Quélo, D., V. Mallet, and B. Sportisse (2005), Inverse modeling of nox emissions at regional scale over northern france: Preliminary investigation of the second-order sensitivity, *Journal of Geophysical Research: Atmospheres (1984–2012)*, *110*(D24).

Ramaswamy, V., O. Boucher, J. Haigh, D. Hauglusataine, J. Haywood, G. Myhre, T. Nakajima, G. Shi, and S. Solomon (2001), Atmospheric chemistry and greenhouse gases, *IPCC Third Assessment-Climate Change*.

Randerson, J., Y. Chen, G. Werf, B. Rogers, and D. Morton (2012), Global burned area and biomass burning emissions from small fires, *Journal of Geophysical Research: Biogeosciences (2005–2012)*, *117*(G4).

Randerson, J. T., H. Liu, M. G. Flanner, S. D. Chambers, Y. Jin, P. G. Hess, G. Pfister,

M. Mack, K. Treseder, L. Welp, et al. (2006), The impact of boreal forest fire on climate warming, *science*, *314*(5802), 1130–1132.

Russell, A. G., G. R. Cass, and J. H. Seinfeld (1986), On some aspects of nighttime atmospheric chemistry, *Environmental science & technology*, *20*(11), 1167–1172.

Sandu, A., D. N. Daescu, G. R. Carmichael, and T. Chai (2005), Adjoint sensitivity analysis of regional air quality models, *Journal of Computational Physics*, *204*(1), 222–252.

Sauvage, B., R. Martin, A. v. Donkelaar, X. Liu, K. Chance, L. Jaeglé, P. Palmer, S. Wu, and T.-M. Fu (2007a), Remote sensed and in situ constraints on processes affecting tropical tropospheric ozone, *Atmospheric Chemistry and Physics*, *7*(3), 815–838.

Sauvage, B., R. V. Martin, A. Van Donkelaar, and J. Ziemke (2007b), Quantification of the factors controlling tropical tropospheric ozone and the south atlantic maximum, *Journal of Geophysical Research: Atmospheres (1984–2012)*, *112*(D11).

Schmidt, H., and D. Martin (2003), Adjoint sensitivity of episodic ozone in the paris area to emissions on the continental scale, *Journal of Geophysical Research: Atmospheres (1984–2012)*, *108*(D17).

Seager, R., and G. A. Vecchi (2010), Greenhouse warming and the 21st century hydroclimate of southwestern north america, *Proceedings of the National Academy of Sciences*, *107*(50), 21,277–21,282.

Sheppard, P. R., A. C. Comrie, G. D. Packin, K. Angersbach, and M. K. Hughes (1999), *The climate of the Southwest*, Institute for the Study of Planet Earth.

Spracklen, D. V., J. A. Logan, L. J. Mickley, R. J. Park, R. Yevich, A. L. Westerling, and D. A. Jaffe (2007), Wildfires drive interannual variability of organic carbon aerosol in the western us in summer, *Geophysical Research Letters*, *34*(16).

Spracklen, D. V., L. J. Mickley, J. A. Logan, R. C. Hudman, R. Yevich, M. D. Flannigan, and A. L. Westerling (2009), Impacts of climate change from 2000 to 2050 on wildfire activity and carbonaceous aerosol concentrations in the western united states, *Journal of Geophysical Research: Atmospheres (1984–2012)*, *114*(D20).

Stavrakou, T., and J.-F. Müller (2006), Grid-based versus big region approach for inverting co emissions using measurement of pollution in the troposphere (mopitt) data, *Journal of Geophysical Research: Atmospheres (1984–2012)*, *111*(D15).

Stavrakou, T., J.-F. Müller, K. Boersma, I. De Smedt, and R. van der A (2008), Assessing the distribution and growth rates of nox emission sources by inverting a 10-year record of no2 satellite columns, *Geophysical Research Letters*, *35*(10).

Steiner, A. L., S. Tonse, R. C. Cohen, A. H. Goldstein, and R. A. Harley (2006), Influence of future climate and emissions on regional air quality in california, *Journal of Geophysical Research: Atmospheres (1984–2012)*, *111*(D18).

Stohl, A., S. Eckhardt, C. Forster, P. James, and N. Spichtinger (2002), On the pathways and timescales of intercontinental air pollution transport, *Journal of Geophysical Research: Atmospheres (1984–2012)*, *107*(D23), ACH–6.

Tang, M., and E. R. Reiter (1984), Plateau monsoons of the northern hemisphere: A comparison between north america and tibet, *Monthly Weather Review*, *112*(4), 617–637.

Tanner, R. L., W. J. Parkhurst, M. L. Valente, K. L. Humes, K. Jones, and J. Gilbert (2001), Impact of the 1998 central american fires on pm 2.5 mass and composition in the southeastern united states, *Atmospheric Environment*, *35*(36), 6539–6547.

Taylor, K. E. (2000), *Summarizing multiple aspects of model performance in a single diagram*, Program for Climate Model Diagnosis and Intercomparison, Lawrence Livermore National Laboratory, University of California.

Taylor, K. E., R. J. Stouffer, and G. A. Meehl (2012), An overview of cmip5 and the experiment design, *Bulletin of the American Meteorological Society*, *93*(4), 485–498.

Trainer, M., D. Parrish, M. Buhr, R. Norton, F. Fehsenfeld, K. Anlauf, J. Bottenheim, Y. Tang, H. Wiebe, J. Roberts, et al. (1993), Correlation of ozone with noy in photochemically aged air, *Journal of Geophysical Research: Atmospheres (1984–2012)*, *98*(D2), 2917–2925.

van der Werf, G. R., J. T. Randerson, L. Giglio, G. J. Collatz, P. S. Kasibhatla, and A. F. Arellano Jr (2006), Interannual variability in global biomass burning emissions from 1997 to 2004, *Atmospheric Chemistry and Physics*, *6*(11), 3423–3441.

Vautard, R., M. Beekmann, and L. Menut (2000), Applications of adjoint modelling in atmospheric chemistry: sensitivity and inverse modelling, *Environmental Modelling & Software*, *15*(6), 703–709.

Vivchar, A. (2011), Wildfires in russia in 2000–2008: estimates of burnt areas using the satellite modis mcd45 data, *Remote Sensing Letters*, *2*(1), 81–90.

Vukićević, T., and P. Hess (2000), Analysis of tropospheric transport in the pacific basin using the adjoint technique, *Journal of Geophysical Research: Atmospheres (1984–2012)*, *105*(D6), 7213–7230.

Walker, T., R. Martin, A. v. Donkelaar, W. Leaitch, A. MacDonald, K. Anlauf, R. Cohen, T. Bertram, L. Huey, M. Avery, et al. (2010), Trans-pacific transport of reactive nitrogen and ozone to canada during spring, *Atmospheric Chemistry and Physics*, *10*(17), 8353–8372.

Wang, H., D. J. Jacob, P. Le Sager, D. G. Streets, R. J. Park, A. B. Gilliland, and A. Van Donkelaar (2009), Surface ozone background in the united states: Canadian and mexican pollution influences, *Atmospheric Environment*, *43*(6), 1310–1319.

Wang, L., M. Newchurch, A. Pour-Biazar, S. Kuang, M. Khan, X. Liu, W. Koshak, and K. Chance (2013), Estimating the influence of lightning on upper tropospheric ozone using nldn lightning data and cmaq model, *Atmospheric Environment*, *67*, 219–228.

Wang, Y., J. A. Logan, and D. J. Jacob (1998), Global simulation of tropospheric o3-no x-hydrocarbon chemistry: 2. model evaluation and global ozone budget, *Journal of Geophysical Research: Atmospheres (1984–2012)*, *103*(D9), 10,727–10,755.

Wang, Y., Y. Zhang, J. Hao, and M. Luo (2011), Seasonal and spatial variability of surface ozone over china: contributions from background and domestic pollution, *Atmospheric Chemistry and Physics*, *11*(7), 3511–3525.

Wang, Y. X., M. B. McElroy, D. J. Jacob, and R. M. Yantosca (2004), A nested grid formulation for chemical transport over asia: Applications to co, *Journal of Geophysical Research: Atmospheres (1984–2012)*, *109*(D22).

Weiss-Penzias, P., D. A. Jaffe, P. Swartzendruber, J. B. Dennison, D. Chand, W. Hafner, and E. Prestbo (2006), Observations of asian air pollution in the free troposphere at mount bachelor observatory during the spring of 2004, *Journal of Geophysical Research: Atmospheres (1984–2012)*, *111*(D10).

Westerling, A. L., D. R. Cayan, T. J. Brown, B. L. Hall, and L. G. Riddle (2004), Climate, santa ana winds and autumn wildfires in southern california, *Eos, Transactions American Geophysical Union*, *85*(31), 289–296.

Westerling, A. L., H. G. Hidalgo, D. R. Cayan, and T. W. Swetnam (2006), Warming and earlier spring increase western us forest wildfire activity, *science*, *313*(5789), 940–943.

Wigder, N., D. Jaffe, and F. Saketa (2013), Ozone and particulate matter enhancements from regional wildfires observed at mount bachelor during 2004–2011, *Atmospheric Environment*, *75*, 24–31.

Wild, O., and H. Akimoto (2001), Intercontinental transport of ozone and its precursors in a three-dimensional global ctm, *Journal of Geophysical Research: Atmospheres (1984–2012)*, *106*(D21), 27,729–27,744.

Wild, O., X. Zhu, and M. J. Prather (2000), Fast-j: Accurate simulation of in-and below-cloud photolysis in tropospheric chemical models, *Journal of Atmospheric Chemistry*, *37*(3), 245–282.

Wise, E. K., and A. C. Comrie (2005), Extending the kolmogorov–zurbenko filter: application to ozone, particulate matter, and meteorological trends, *Journal of the Air & Waste Management Association*, *55*(8), 1208–1216.

Wolfe, G., J. Thornton, V. F. Mcneill, D. Jaffe, D. Reidmiller, D. Chand, J. Smith, P. Swartzendruber, F. Flocke, and W. Zheng (2007), Influence of trans-pacific pollution transport on acyl peroxy nitrate abundances and speciation at mount bachelor observatory during intex-b, *Atmospheric Chemistry and Physics*, *7*(20), 5309–5325.

Wotawa, G., and M. Trainer (2000), The influence of canadian forest fires on pollutant concentrations in the united states, *Science*, *288*(5464), 324–328.

Xie, P., J. E. Janowiak, P. A. Arkin, R. Adler, A. Gruber, R. Ferraro, G. J. Huffman, and S. Curtis (2003), Gpcp pentad precipitation analyses: An experimental dataset based on gauge observations and satellite estimates, *Journal of Climate*, *16*(13), 2197–2214.

Xu, J., and E. E. Small (2002), Simulating summertime rainfall variability in the north american monsoon region: The influence of convection and radiation parameterizations, *Journal of Geophysical Research: Atmospheres (1984–2012)*, *107*(D23), ACL–22.

Yang, Y., H. Liao, and J. Li (2014), Impacts of the east asian summer monsoon on interannual variations of summertime surface-layer ozone concentrations over china, *Atmospheric Chemistry and Physics*, *14*(13), 6867–6879.

Yienger, J. J., M. Galanter, T. A. Holloway, M. J. Phadnis, S. K. Guttikunda, G. R. Carmichael, W. J. Moxim, and H. Levy (2000), The episodic nature of air pollution transport from asia to north america, *Journal of Geophysical Research: Atmospheres (1984–2012)*, *105*(D22), 26,931–26,945.

Zeng, G., and J. A. Pyle (2005), Influence of el nino southern oscillation on stratosphere/troposphere exchange and the global tropospheric ozone budget, *Geophysical research letters*, *32*(1).

Zhang, G. J., and N. A. McFarlane (1995), Sensitivity of climate simulations to the parameterization of cumulus convection in the canadian climate centre general circulation model, *Atmosphere-Ocean*, *33*(3), 407–446.

Zhang, L., D. J. Jacob, K. Boersma, D. Jaffe, J. Olson, K. Bowman, J. Worden, A. Thompson, M. Avery, R. Cohen, et al. (2008), Transpacific transport of ozone pollution and the effect of recent asian emission increases on air quality in north america: an integrated analysis using satellite, aircraft, ozonesonde, and surface observations.

Zhang, L., D. J. Jacob, M. Kopacz, D. K. Henze, K. Singh, and D. A. Jaffe (2009), Intercontinental source attribution of ozone pollution at western us sites using an adjoint method, *Geophysical Research Letters*, *36*(11).

Zhang, L., D. J. Jacob, X. Liu, J. A. Logan, K. Chance, A. Eldering, and B. R. Bojkov (2010), Intercomparison methods for satellite measurements of atmospheric composition: application to tropospheric ozone from tes and omi, *Atmospheric Chemistry and Physics*, *10*(10), 4725–4739.

Zhang, L., D. J. Jacob, N. V. Downey, D. A. Wood, D. Blewitt, C. C. Carouge, A. van Donkelaar, D. B. Jones, L. T. Murray, and Y. Wang (2011), Improved estimate of the policy-relevant background ozone in the united states using the geos-chem global model with

1/2× 2/3 horizontal resolution over north america, *Atmospheric Environment*, *45*(37), 6769–6776.

Zhang, L., D. J. Jacob, X. Yue, N. Downey, D. Wood, and D. Blewitt (2014), Sources contributing to background surface ozone in the us intermountain west, *Atmospheric Chemistry and Physics*, *14*(11), 5295–5309.